THE UNIVERSITY OF MICHIGAN

COLLEGE OF ENGINEERING
Department of Chemical and Metallurical Engineering

Technical Report

PHOTOCHEMICAL CHLORINATION OF SULFUR DIOXIDE UTILIZING A PLASMA LIGHT SOURCE

George J. Quarderer

Project Directors

R. H. Kadlec
S. W. Churchill

ORA Project 07658

supported by:

NATIONAL SCIENCE FOUNDATION
GRANT NO. GK-632
WASHINGTON, D.C.

Administered through:

OFFICE OF RESEARCH ADMINISTRATION ANN ARBOR

April 1967

This report was also a dissertation submitted in partial fulfillment of the requirements for the degree of Doctor of Philosophy in The University of Michigan, 1967.

ACKNOWLEDGMENTS

The author wishes to express his appreciation to all those persons who have aided in this investigation.

In particular, he wishes to acknowledge the interest, guidance, and criticism offered by Professor Robert H. Kadlec, chairman of the doctoral committee. The assistance of Dr. D. E. Harmer, of the Dow Chemical Company, and Professors S. W. Churchill, J. D. Goddard, and T. M. Dunn was also appreciated.

The author wishes to express his gratitude to the shop personnel of the Department of Chemical and Metallurgical Engineering, Pete, John, Fanny, Doug, Al, and Bob, who were most cooperative and helpful.

The author is also indepted to his wife and his parents for their encouragement and aid, and to the Dow Chemical Company and the National Science Foundation for their financial assistance.

TABLE OF CONTENTS

TABLE OF CONTENTS (Concluded)

LIST OF TABLES

LIST OF FIGURES

LIST OF FIGURES (Continued)

LIST OF FIGURES (Continued)

LIST OF FIGURES (Continued)

LIST OF FIGURES (Concluded)

PHOTOCHEMICAL CHLORINATION OF SULFUR DIOXIDE UTILIZING A PLASMA LIGHT SOURCE

George J. Quarderer

Two aspects of the photochemical chlorination of sulfur dioxide were investigated experimentally. The first objective was to study the applicability of a plasma light source as a device with which to promote photochemical reactions of a low quantum yield. The second, in a flow system, was to investigate the parameters affecting the photochlorination of sulfur dioxide, a low quantum yield reversible photochemical reaction.

The photochemical reactor was a vortex-stabilized arc radiation source and an annular, triple-walled, fused-silica reaction chamber aligned on a common axis. The inner wall of the reaction chamber was sealed to the two water cooled conical electrodes of the light source forming a transparent envelope for the arc. Argon was introduced into this envelope tangential to the inside circumference of the fused silica cylinder, forming a vortex exhausting through a centrally drilled hole at the anode tip. Aqueous inorganic solutions, providing selective wavelength filtration, were circulated through the inner annular region. The outer annular oxide and chlorine were passed.

Argon plasma gas at a pressure of one atmosphere was circulated through the arc at flowrates from 12.1 to 22.5 gm/min with power inputs to the plasma of 3.84 to 11.2 kw. The spectral output of the light source was characterized as a function of wavelength, arc-gas flowrate, power input to the arc, and position along the arc. For power inputs of 3.84 and 8.45 kw there were, respectively, 0.314 and 0.862 gmol equivalents of photons emitted per hour in the 2500 to 5000 Å wavelength region.

The dependence of the reaction on wavelength from 2500 to 5000 Å was investigated by circulating selective filter solutions, e.g., 1.5 normal potassium nitrate and 0.05 normal potassium iodide through the inner annulus. Reaction gas inlet temperatures of 15 to 45°C and pressures from 1 to 2 atm were used at reactant flowrates of 1.0 to 12.0 gmol/hr. The fraction of sulfur dioxide in the mixture varied from 1/6 to 2/3.

The photochemical rate of formation of sulfuryl chloride is best described by the rate expression:

$$\frac{d[SO_2Cl_2]}{dt} = J - k_o e^{-\frac{E}{RT}} \sqrt{J/[SO_2]} \quad [SO_2Cl_2]$$

where J is the volumetric rate of light absorption and where k_o and E have values of 0.0542 $(sec)^{1/2}$ and -2.6 kcal/gmol, respectively.

1. INTRODUCTION

Within the last few years plasma light sources have been introduced which possess the ability to produce high intensity levels of ultraviolet light. To the chemist or the chemical engineer then, this device suggests itself as a powerful tool with which to conduct investigations of photochemical reactions possessing a low quantum yield.

This thesis describes an experimental investigation of the kinetics of the photochemical chlorination of sulfur dioxide utilizing a plasma light source to provide high intensity levels of ultraviolet radiation.

The primary purpose of this investigation was to study the applicability of the plasma light source as a catalytic tool with which to promote photochemical reactions of a low quantum yield. The secondary goal of this work was to investigate in a flow system the parameters affecting the photochemical chlorination of sulfur dioxide, a photochemical reaction known to possess a low quantum yield.

Spectrographic measurements were made to characterize the ultraviolet radiation emitted by the plasma light source. Utilizing the spectral output of the light source, the photochemical chlorination was investigated as a function of such reaction parameters as rate of light absorption, flowrate, concentration, temperature, pressure, and wavelength of the absorbed radiation.

As a result it was possible to postulate and verify a mathematical rate equation describing the photochemical reaction as well as to determine the means of energy transfer during the reaction.

2. SURVEY OF PREVIOUS WORK

2.1 LIGHT SOURCE

Only a limited amount of published information pertaining to the construction, operation, and performance of plasma light sources (or vortex stabilized arc radiation sources as they are known elsewhere) is presently available in the literature.

Papp[1-3] reported that a plasma light source operating at 25 kw power input with argon as the arc gas and with an arc pressure of 17 atm had a total radiant output of 7.68 kw representing a 31% efficiency in conversion of electrical power to radiant energy. Of these 7.68 kw, 2.6 kw were found in the 2000 to 4000 Å wavelength range. Papp also indicated that as power inputs increased the fraction of the total radiant energy found in the ultraviolet region increased.

Anderson, et al.,[4] reported on an extensive investigation of a vortex-stabilized arc radiation source. Both total radiance and spectral distribution were measured as functions of the arc current, arc length, gas pressure in the arc, arc gas flowrate, and nozzle diameter. The authors also studied the effect of using a variety of different gases as the arc gas and reported that argon had the highest total radiance.

The authors investigated the effect of lengthening the arc and observed a greater than 60% conversion of electrical energy to radiant energy with an arc length of approximately 12 cm. This corresponded

to a radiant energy flux of 18 kw. The authors substantiate Papp's observation that as power inputs to the light source increased, the fraction of energy converted to ultraviolet radiation increased faster than that of the infrared radiation.

2.2 PHOTOCHEMICAL FORMATION OF SULFURYL CHLORIDE

In 1839 Regnault[5,6] reported that when a flask containing a mixture of dry sulfur dioxide and chlorine was exposed to the light of the June sun part of the mixture combined to form sulfuryl chloride.

More recently, the photochemical formation of sulfuryl chloride was investigated by Schumacher and Schott[7] at 2 and 30°C. The investigations were performed according to a statistical method in a quartz container.

Their light source had a spectral output centered between 3500 and 4500 Å with the peak intensity located at approximately 4000 Å. In this wavelength region the light was absorbed only by chlorine. Over the temperature range investigated, the reaction took place with a quantum yield less than 1. The activation energy for the reaction was negative between 2 and 30°C.

The reaction was strongly influenced by the wall which made it difficult to reproduce the experiments. By cleaning the quartz reaction tube in hot nitric acid, the authors state that the reaction could practically be stopped.

The reaction velocity was almost proportional to the first power

of light intensity. Within the low experimental precision of the investigation, the rate was independent of the chlorine concentration, the total pressure (400 to 1200 mm Hg), and the presence of large amounts of oxygen, while sulfur dioxide had an accelerating effect and the presence of sulfuryl chloride had a strong inhibiting influence on the reaction.

Londergan[8] studied the reaction at 70°C in a pyrex reaction vessel with a circulating gas mixture. The quantum yield was observed to be 1.2±.2 for 4358 Å light. The reaction velocity was first order with respect to the chlorine concentration.

An approximate value of 1.0 was given for the quantum yield by Bonhoeffer[9] who used light with a wavelength of approximately 4200 Å for the determination.

LeBlanc, Andrich, and Kangro[10] manometrically studied the reaction at generally low initial pressures and at 55, 105, and 125°C. The temperature dependence of the formation reaction, using light that was only absorbed by chlorine, was low. The authors suggested that the reaction velocity depended on a small water vapor content. Trautz[11] measured the rate of formation of sulfuryl chloride in a quartz container at 291 and 372°K and at various concentrations. The reaction was observed to proceed via a second order mechanism. A temperature increase of 80°K lowered the reaction rate according to a coefficient of 0.88 for a 10°K increase in temperature.

2.3 PHOTOCHEMICAL DECOMPOSITION OF SULFURYL CHLORIDE

The photochemical decomposition of sulfuryl chloride was investi-

gated by Schumacher and Schott[7] at 110 and 130°C. According to a previous investigation the thermal decomposition is not appreciable in this temperature region.

The investigation was carried out using a quartz reaction vessel. Gas phase mixtures of sulfuryl chloride, sulfur dioxide, and chlorine were exposed to radiation from the 436, 405, and 365 mμ mercury lines, which was absorbed only by chlorine.

The overall reaction was believed to be a chain reaction proceeding according to the rate expression:

$$\frac{d(SO_2Cl_2)}{dt} = -k \sqrt{\frac{J}{(SO_2)P}} (SO_2Cl_2) \qquad (2.1)$$

where J is the intensity of the absorbed radiation, P is the total pressure, and k is a rate constant having values of $15\pm1\times10^{-3}$ and $50\pm2\times10^{-3}$ mm of mercury/minute at 110 and 130°C, respectively.

The temperature coefficient for a 10°C rise in temperature was 1.83, which indicates an apparent activation energy of 18 kcal/gmol. The quantum yield at 110°C and at from 150 to 200 mm of mercury total pressure was approximately 100.

Investigations made without the addition of sulfur dioxide often showed a short induction period. The influence of total pressure up to 1200 mm of mercury was examined through the addition of CF_2Cl_2 (Freon-12). The presence of oxygen did not influence the reaction.

Schumacher and Schott suggest that the following reaction scheme takes into account the experimental findings:

(1) $Cl_2+h\nu \rightarrow Cl\cdot + Cl\cdot$ (2.2)

(2) $Cl\cdot + SO_2 \rightleftarrows SO_2Cl\cdot$ (thermal equilibrium) (2.3)

(3) $SO_2Cl\cdot + Cl\cdot \xrightarrow{[M]} SO_2Cl_2$ (2.4)

(4) $SO_2Cl_2 + Cl\cdot \rightarrow SO_2Cl\cdot + Cl_2$ (2.5)

For Q_2, the dissociation energy of $SO_2Cl\cdot$, the authors suggest a value of 10 to 15 kcal/gmol.

LeBlanc, Andrich, and Kangro[10] investigated the reaction by illuminating samples of sulfuryl chloride with light in the wavelength region 2500 to 2400 Å, a region in which the light is absorbed only by sulfuryl chloride. Illumination for 30 hr resulted in the almost quantitative destruction of sulfuryl chloride. The decomposition reaction proceeded, at constant light intensity, with a constant velocity unrelated to the sulfuryl chloride concentration.

LeBlanc, Ardrich, and Kangro also investigated the reaction using light that was absorbed only by chlorine. They state that the reaction was of an entirely different type. At 105°C and with 65 mm of mercury starting pressure, the reaction velocity reached a maximum after 30 min and then decreased gradually to zero after 50 to 60% of the starting mixture had been decomposed.

3. DISCUSSION OF PREVIOUS WORK

3.1 GENERAL

As a general observation, the published investigations regarding plasma light sources are of a uniform high quality, while those regarding the photochlorination of sulfur dioxide tend to be of a somewhat lower quality.

3.2 LIGHT SOURCE

The papers by Papp[1-3] concerning light sources were of considerable importance during the earlier design stage of this investigation; while the paper by Anderson, et al.,[4] which was published somewhat later, provided a check on many of the observations and assumptions made in connection with this investigation.

3.3 PHOTOCHEMICAL FORMATION OF SULFURYL CHLORIDE

Investigators of the photochlorination reaction tend to contradict each other on several points. For example, Schumacher and Schott[7] state that the reaction is independent of the chlorine concentration while sulfur dioxide has an accelerating effect. Londergan[8] reports that the reaction is first order with respect to the chlorine concentration. A third researcher, Trautz,[11] reports that the reaction is first order in both chlorine and sulfur dioxide.

These and other anomalies among the various sets of data presented, involving the effects of such parameters as water vapor concentration,

wall surface area, and temperature have caused a certain amount of suspicion as to the validity of much of the data.

3.4 PHOTOCHEMICAL DECOMPOSITION OF SULFURYL CHLORIDE

Considerable doubt exists as to the validity of the reaction scheme suggested by Schumacher and Schott[7] for the photochemical decomposition of sulfuryl chloride. A careful analysis of their data suggests that a more plausible reaction scheme would be:

$$(1)\quad Cl_2 + h\nu \xrightarrow{J} Cl\cdot + Cl\cdot \tag{3.1}$$

$$(1')\quad Cl\cdot + Cl\cdot \xrightarrow{k_i'[M]} Cl_2 \tag{3.2}$$

$$(2)\ \&\ (2')\quad SO_2 + Cl\cdot \underset{k_2'}{\overset{k_2}{\rightleftharpoons}} SO_2Cl\cdot \text{ (thermal equilibrium)} \tag{3.3}$$

$$(3)\quad SO_2Cl\cdot + Cl\cdot \xrightarrow{k_3} SO_2Cl_2 \tag{3.4}$$

$$(4)\quad SO_2Cl_2 + Cl\cdot \xrightarrow{k_4} SO_2Cl\cdot + Cl_2 \tag{3.5}$$

where M represents an effective third body for the recombination reaction, in this case CF_2Cl_2.

Making the standard Bodenstein assumption relative to the concentrations of intermediate species (see Benson,[12] Chapter III), the above mechanism yields the rate of decomposition of sulfuryl chloride:

$$-\frac{d[SO_2Cl_2]}{dt} = \frac{k_4[SO_2Cl_2]I^{1/2}}{\sqrt{k_i'[M]+k_3K_2[SO_2]}} \tag{3.6}$$

or letting $k' = k_4/(k_i')^{1/2}$ and $k'' = k_3K_2/k_i'$:

$$-\frac{d[SO_2Cl_2]}{dt} = \frac{k'[SO_2Cl_2]I^{1/2}}{\sqrt{M+k''[SO_2]}} \tag{3.7}$$

The data reported were processed according to this rate expression, and the consistency of the results was compared to the internal consistency of the analysis made by Schumacher and Schott. The comparison indicates that the reaction scheme presented above provides a significantly better description of the physical system than the scheme suggested by Schumacher and Schott.

Graphically, this can be seen by comparing the information presented in Figs. 1 and 2. For a series of the experiments reported by Schumacher and Schott, Fig. 1 presents the values of the rate constant k obtained when the data were analyzed according to the rate expression suggested by the authors. In Fig. 2 are presented the values of the rate constant k' obtained when the data were analyzed according to the rate expression suggested above while using a value of 13.94 for k". The abscissa in both graphs is amount of sulfuryl chloride decomposed expressed in millimeters of mercury.

In Fig. 1 the value of k varies strongly with the extent of the reaction, while in Fig. 2 the value of k', within the limits of experimental error, is independent of the extent of the reaction.

It is also possible, from semi-theoretical considerations, to compare the rate of recombination of chlorine atoms with the rate for the combination reaction of Cl· atoms and SO_2Cl· free radicals. From the above development, the two rates will be equal when:

$$\frac{[M]}{[SO_2]} = \frac{k_3 K_2}{k_1'} \qquad (3.8)$$

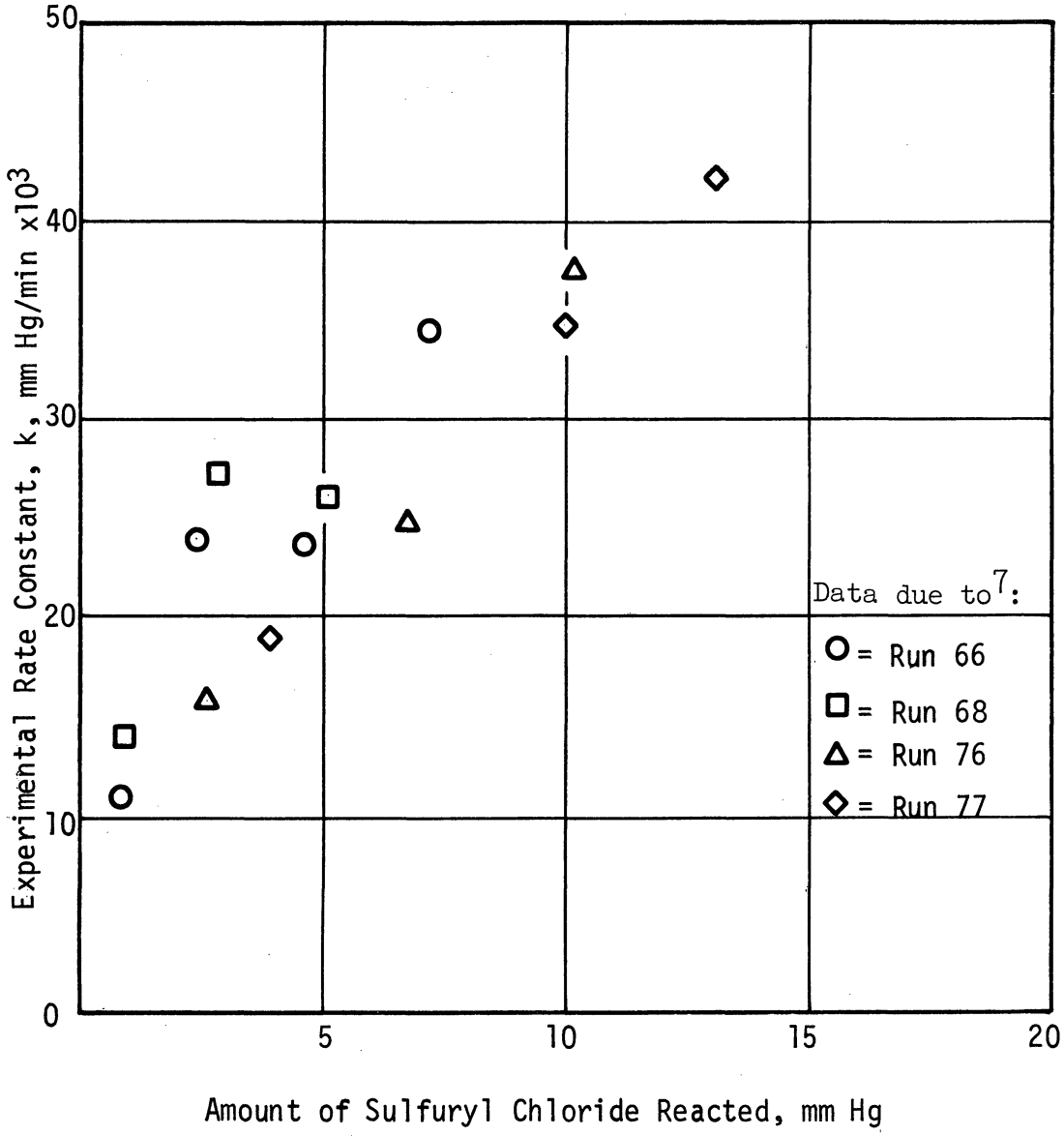

Fig. 1. Calculated rate constant k as a function of the extent of the photochemical reaction.

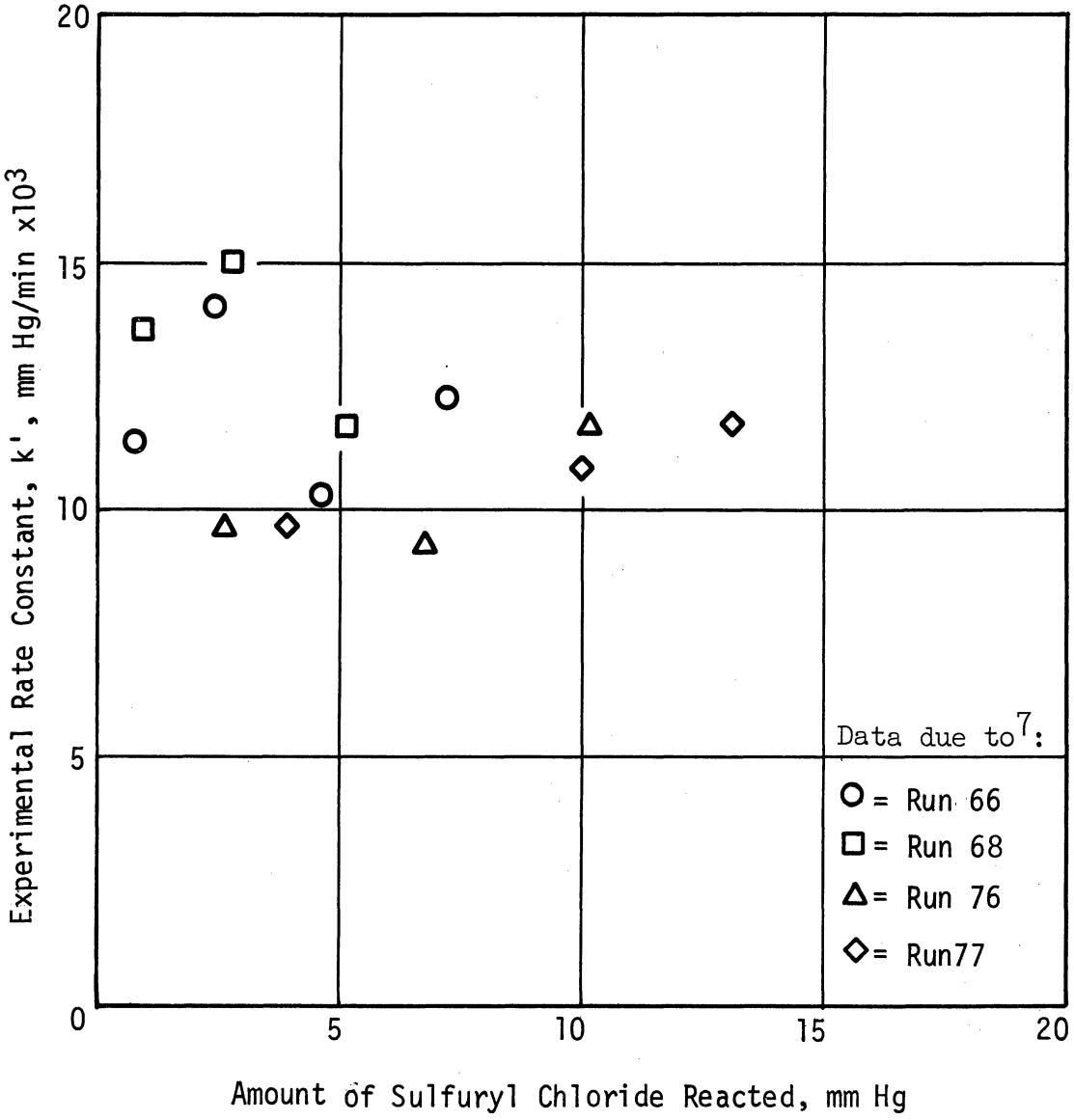

Fig. 2. Calculated rate constant k' as a function of the extent of the photochemical reaction.

The value of k_3, the rate constant for the bimolecular recombination of Cl· and SO_2Cl· free radicals, may be estimated to be 10^8 liters/gmol/sec (see Benson,[12] Chapter XII). Similarly k_1', the rate constant for the termolecular recombination of chlorine atoms, may be estimated to be $10^{11.3}$ $(liters)^2/(gmol)^2/sec$.[13,14]

The value of the equilibrium constant K_2 may be calculated from the thermodynamic information presented in Appendix III. It is a strong function of temperature, having a value of $10^{4.75}$ liters/gmol at 110°C, the temperature at which Schumacher and Schott carried out most of their experimental runs.

Inserting these values into the above expression, it is predicted that, at 110°C, the two rates will be equal when $(M)/(SO_2) = 28.2$. This value may be compared with 13.94, the value of k", which was obtained from an analysis of the data published by Schumacher and Schott. The agreement between the two values is remarkable and this fact supports the reaction scheme suggested above.

The only other published information on the photochemical decomposition of sulfuryl chloride, due to LeBlanc, Andrich, and Kangro,[10] is not of a quantitative nature and as such is not subject to further discussion.

4. PERTINENT THEORY AND MATHEMATICAL MODEL

4.1 PHOTOCHEMICAL REACTIONS

The occurrence of a photochemical reaction may be ascribed to the absorption of quanta of radiation, each molecule requiring one quanta, $h\nu$, of a frequency ν, characteristic of the absorbing molecule. The absorption of a quantum of radiation is the primary stage in a photochemical reaction. This acquisition of energy may or may not be accompanied by the dissociation of the absorbing molecule.

The primary process may be succeeded by further processes, involving the atoms, radicals, and excited molecules generated in this manner, to yield the net observed photo-reaction. The secondary processess will, in general, be entirely independent of the light action, being determined by purely thermodynamic considerations.

4.2 BEER'S LAW

At a given wavelength, the intensity of a beam of light passing through d cm of an absorbing medium is related to the incident intensity I_o according to the familiar Beer's Law relationship:

$$\log_{10} \frac{I}{I_o} = -\epsilon \cdot c \cdot d \qquad (4.1)$$

where ϵ is known as the molecular extinction coefficient of the absorbing material, having units of liters/gmol/cm, and where c is the concentration of the absorbing medium expressed in gmol/liter.

The molecular extinction coefficient indicates the degree to which a material absorbs light and is a function of the absorbing medium, the wavelength of the light used, and of the temperature.

4.3 PRIMARY PROCESSES

In the wavelength region of interest, 2500 to 5000 Å, both chlorine and sulfur dioxide absorb strongly. At wavelengths shorter than 4785 Å chlorine shows unstructured absorption, while sulfur dioxide exhibits two absorption bands extending downward from 3900 Å.

For chlorine, absorption in the continuous absorption region involves dissociation of the molecule into two atoms, one in the normal ground state, the other in an electronically excited state.[15] At the convergence limit, 4785 Å, the two atoms separate with negligibly small kinetic energy, while within the continuous absorption region, the energy in excess of that required for the dissociation emerges as the kinetic energy of the two atoms. A plot of the extinction coefficient of chlorine as a function of the wavelength is presented in Fig. 3.

Between 2500 and 5000 Å, sulfur dioxide has two overlapping absorption bands. The first band is a very weak one, originating at 3880 Å and extending downward to 3400 Å with an absorption maximum at 3740 Å. Due to the weakness of this band it was not significant in this work.

The second absorption band originates at about 3400 Å and extends down below 2600 Å. This band is structured and is much stronger than the first. A smoothed plot of its extinction coefficient versus wave-

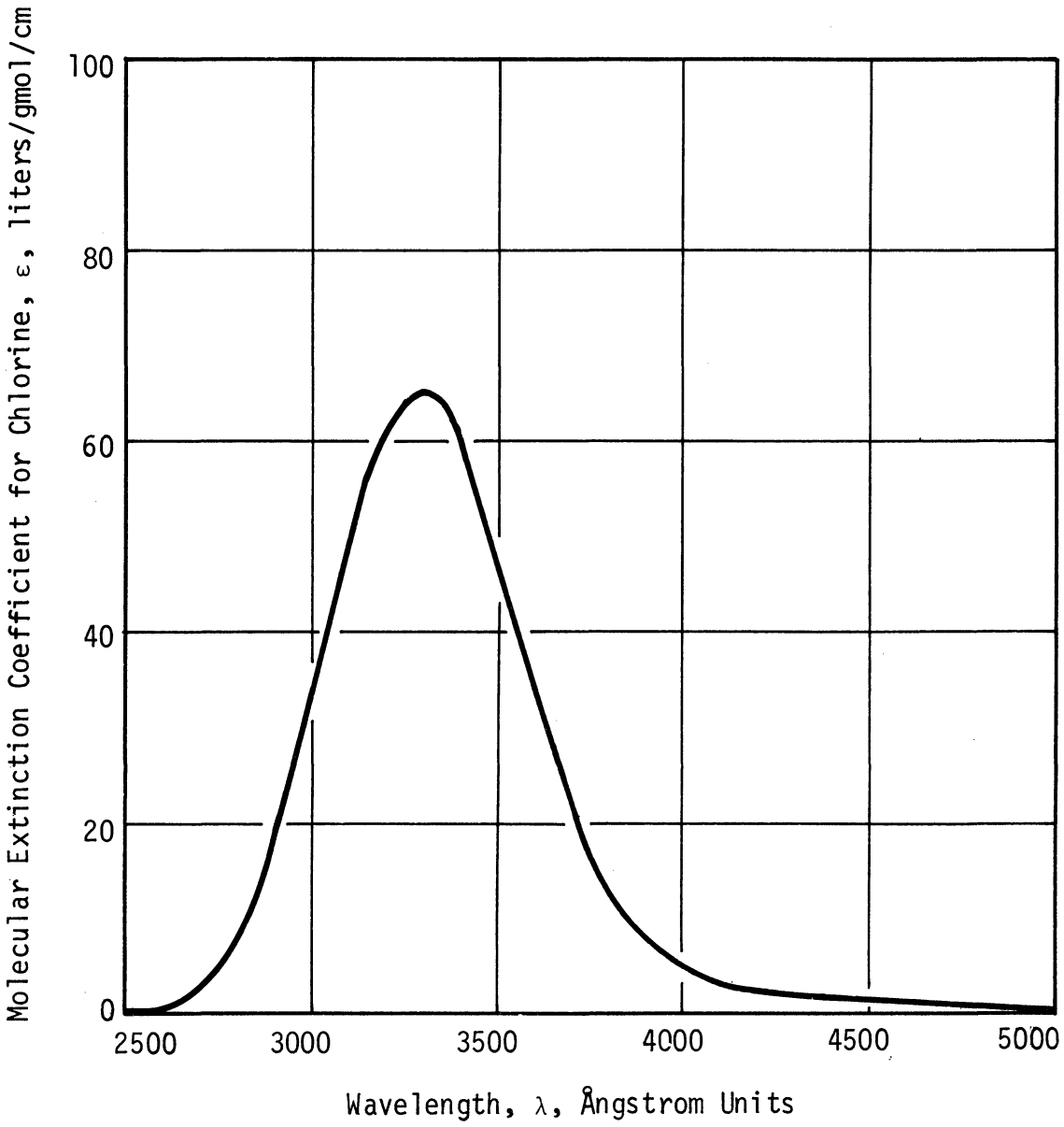

Fig. 3. Molecular extinction coefficient of chlorine as a function of wavelength.

length is presented in Fig. 4. The nature of the electronic states involved has been considered by Walsh[16] and Mulliken.[17] Unless the excited sulfur dioxide molecule is deactivated by means of a collision, it will return to the ground state by fluorescing. The integrated absorption of the band suggests a natural radiative lifetime of 2×10^{-7} sec.[18]

4.4 REACTION MECHANISM

Before entering into a discussion of potential reaction mechanisms, it is of value to recall the unwritten law of chemical kinetics that all proposed mechanisms are inherently suspect. In the words of an old adage, "A mechanism may be disproven but never proven."

As mentioned earlier, the net observed photochemical reaction is a combination of one or more primary processes involving the absorption of quanta of radiation followed by one or more secondary thermal reactions involving the atoms, radicals and excited molecules generated by the primary processes.

A convenient starting point for modeling the photochemical reaction is the reaction scheme, as modified above, suggested by Schumacher and Schott.[7] This scheme considers the reaction when only chlorine is involved in the primary process:

$$(1) \quad Cl_2 + h\nu \rightarrow Cl\cdot + Cl\cdot \tag{4.2}$$

$$(1') \quad Cl\cdot + Cl\cdot \xrightarrow{k_1'[M]} Cl_2 \tag{4.3}$$

$$(2) \ \& \ (2') \quad SO_2 + Cl\cdot \underset{k_2'}{\overset{k_2}{\rightleftharpoons}} SO_2Cl\cdot \tag{4.4}$$

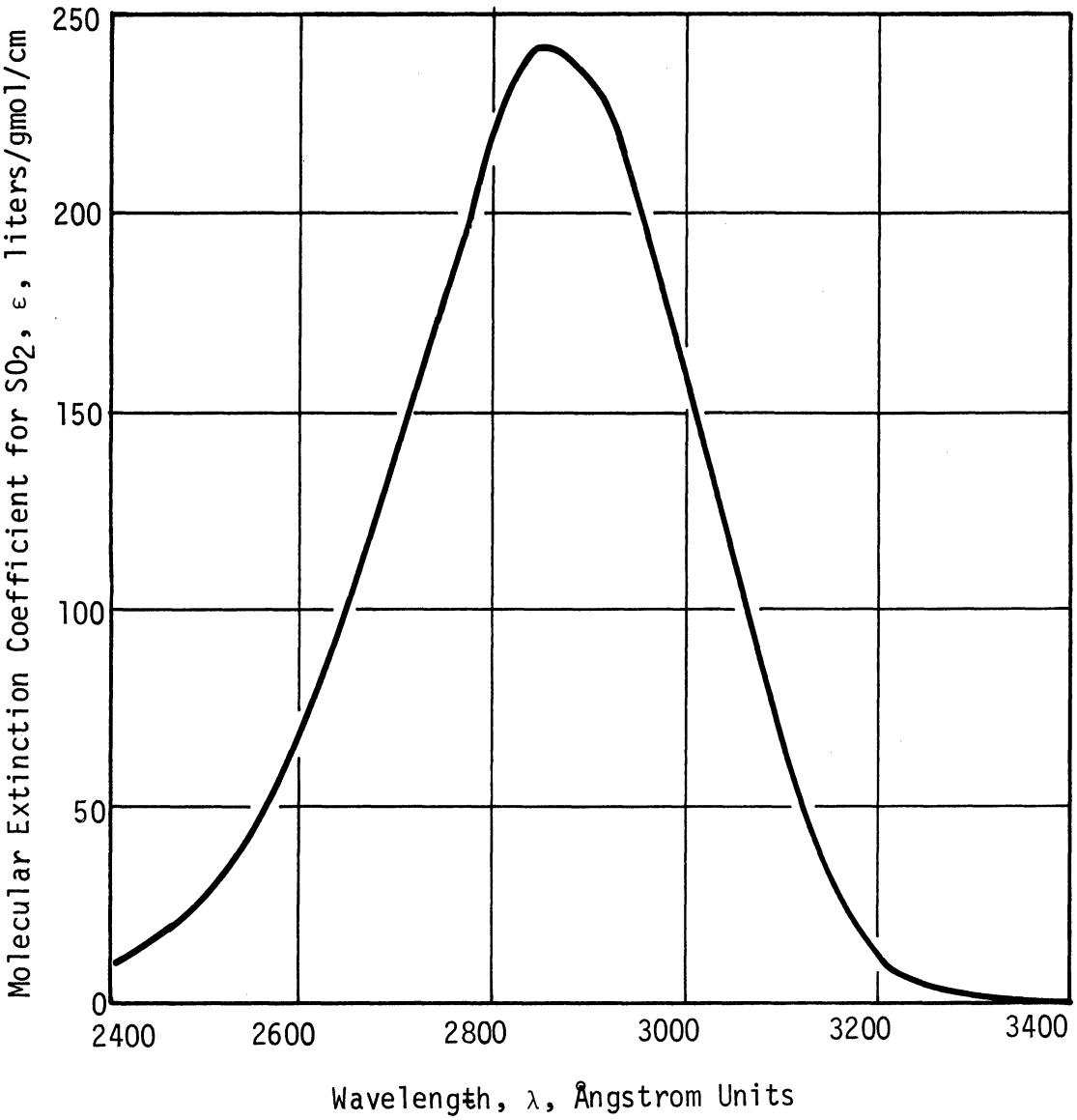

Fig. 4. Molecular extinction coefficient of sulfur dioxide as a function of wavelength.

$$(3)\quad SO_2Cl\cdot + Cl\cdot \xrightarrow{k_3} SO_2Cl_2 \qquad (4.5)$$

$$(4)\quad SO_2Cl_2 + Cl\cdot \xrightarrow{k_4} SO_2Cl\cdot + Cl_2 \qquad (4.6)$$

During this investigation, no effective third body for the recombination of chlorine was included in the reactant mixture. This suggests that reaction (1') was not significant, and thus may be deleted from any postulated reaction scheme.

Previous researchers have indicated that the quantum yield for the overall reaction is of the order of one. This indicates that the actual reaction scheme is of closed sequence, i.e., does not involve a chain reaction. This means that the potential chain propogation reaction:

$$(4')\quad SO_2Cl\cdot + Cl_2 \rightarrow SO_2Cl_2 + Cl\cdot \qquad (4.7)$$

does not enter into the reaction scheme.

When sulfur dioxide enters into the primary process:

$$(5)\quad SO_2 + h\nu \rightarrow SO_2^* \qquad (4.8)$$

deactivation of the excited molecule can occur via one of several different routes:

$$(5')\quad SO_2^* \rightarrow SO_2 + h\nu \qquad (4.9)$$

$$(6)\quad SO_2^* + M \rightarrow SO_2 + M \qquad (4.10)$$

$$(7)\quad SO_2^* + Cl_2 \rightarrow SO_2 + Cl\cdot + Cl\cdot \qquad (4.11)$$

As mentioned above the fluorescence process described by reaction (5') occurs with a natural radiative lifetime of 2×10^{-7} sec. At 25°C and 1 atm total pressure, a sulfur dioxide molecule undergoes approximately 250 collisions during this time span. If the collision processes described by reactions (6) and (7) are at all efficient it will be anticipated that reaction (5') does not enter into the actual reaction scheme.

If reaction (7) occurs to the exclusion of reaction (6), the quantum yield will be independent of the composition of the reaction mixture. However, if the reverse is true, the quantum yield for the overall reaction will be a strong function of the sulfur dioxide concentration. Thus it is relatively simple to experimentally determine whether reaction (6) or reaction (7) predominates.

If for the present it is assumed that reaction (7) predominates, the rate of generation of chlorine radicals is the sum of the rates of light absorption by chlorine and sulfur dioxide;

$$\frac{d(Cl\cdot)}{dt} = 2J_{Cl_2} + 2J_{SO_2} = 2J \qquad (4.12)$$

where J is the total rate at which light is absorbed by the reactant mixture expressed in gmol/liter-hr.

The rate of formation of sulfuryl chloride is the difference between the rate of reaction (3) and the rate of reaction (4):

$$\frac{d(SO_2Cl_2)}{dt} = k_3(SO_2Cl\cdot)(Cl\cdot) - k_4(SO_2Cl_2)(Cl\cdot) \qquad (4.13)$$

Using the Bodenstein steady-state hypothesis the rate of production of free radicals is equated to their rate of destruction:

$$2J = 2k_3(SO_2Cl\cdot)(Cl\cdot) \qquad (4.14)$$

Making, as Schumacher and Schott suggest, the further assumption that reactions (2) and (2') are in thermal equilibrium;

$$\frac{(SO_2Cl\cdot)}{(SO_2)(Cl\cdot)} = K_2 \qquad (4.15)$$

the following rate expression can be written for the formation of sulfuryl chloride:

$$\frac{d(SO_2Cl_2)}{dt} = J - \frac{k_4}{(k_3K_2)^{1/2}} \sqrt{\frac{J}{(SO_2)}}\ (SO_2Cl_2) \qquad (4.16)$$

The effective rate constant for the reverse reaction is $k_4/(k_3K_2)^{1/2}$ The effective activation energy for the reverse reaction is given by:

$$E = E_4 - \frac{\Delta H_2}{2} - \frac{E_3}{2} \qquad (4.17)$$

Goldfinger[25] states that, for abstraction reactions of strongly bound chlorine atoms, published information indicates that the activation energy is practically constant and about 4 to 5 kcal/gmol. The activation energy for reaction (4) is thus assumed to be 4.5 kcal/gmol. The heat of reaction for reaction (2), as discussed above, is approximately 18.1 kcal/gmol.

Using the above information and assuming that the activation energy for reaction (3), a free-radical recombination is zero, the effec-

tive activation energy predicted for the decomposition reaction is 13.6 kcal/gmol. This number is in reasonable agreement with the value 18 kcal/gmol which was obtained experimentally by Schumacher and Schott.

4.5 WALL EFFECTS

Noyes has considered the effect of wall terminations on photochemical reactions.[26] He has shown that there is an effective thickness r_w over which the wall exerts an appreciable effect. Noyes finds that:

$$r_w \cong 0.9\, D^{1/2}/(k_i k_{t2})^{1/4} \qquad (4.18)$$

where D is the diffusion coefficient, k_i is the volumetric rate of initiation of radicals, and k_{t2} is the rate constant for homogeneous second order termination of radicals. Within the shell thickness r_w near the wall, it may be assumed, if the surface is an efficient radical trap, that the concentration of radicals is essentially zero while outside this shell the concentration of radicals may be assumed to correspond to that which is unperturbed by the walls.

For this study r_w is equal to approximately 0.002 cm, which is a negligibly small fraction of the total volume of the reactor. This result eliminates wall influenced reactions from consideration during the remainder of this investigation.

5. EXPERIMENTAL APPARATUS

5.1 GENERAL

The experimental system used in this investigation consisted of a plasma light source, an argon delivery and cooling water system, a dye solution recirculation system, a reactant delivery system, a safety interlock system, an ultraviolet spectrographic analysis system and an infrared spectrographic analysis system. A schematic diagram of the experimental apparatus is presented in Fig. 5.

5.2 PHOTOCHEMICAL REACTION SYSTEM

The photochemical reaction system used in this investigation is shown schematically in Fig. 6. It was fabricated in the machine, welding, and glass fabrication shops of the Department of Chemical and Metallurgical Engineering. The system consisted of a direct current, vortex stabilized arc radiation source, and an annular triple walled fused silica reaction chamber aligned on a common axis. The system could be operated in any attitude and could be easily disassembled.

The anode surface was fabricated from copper while a 1% thoriated tungsten rod served as the cathode tip. The main body of each of the two electrodes was constructed of brass. Each was held in position by a laminated plastic "Micarta" end piece which provided electrical insulation between electrodes. The length of the arc was determined by adjusting the position of the tungsten rod relative to the main body of

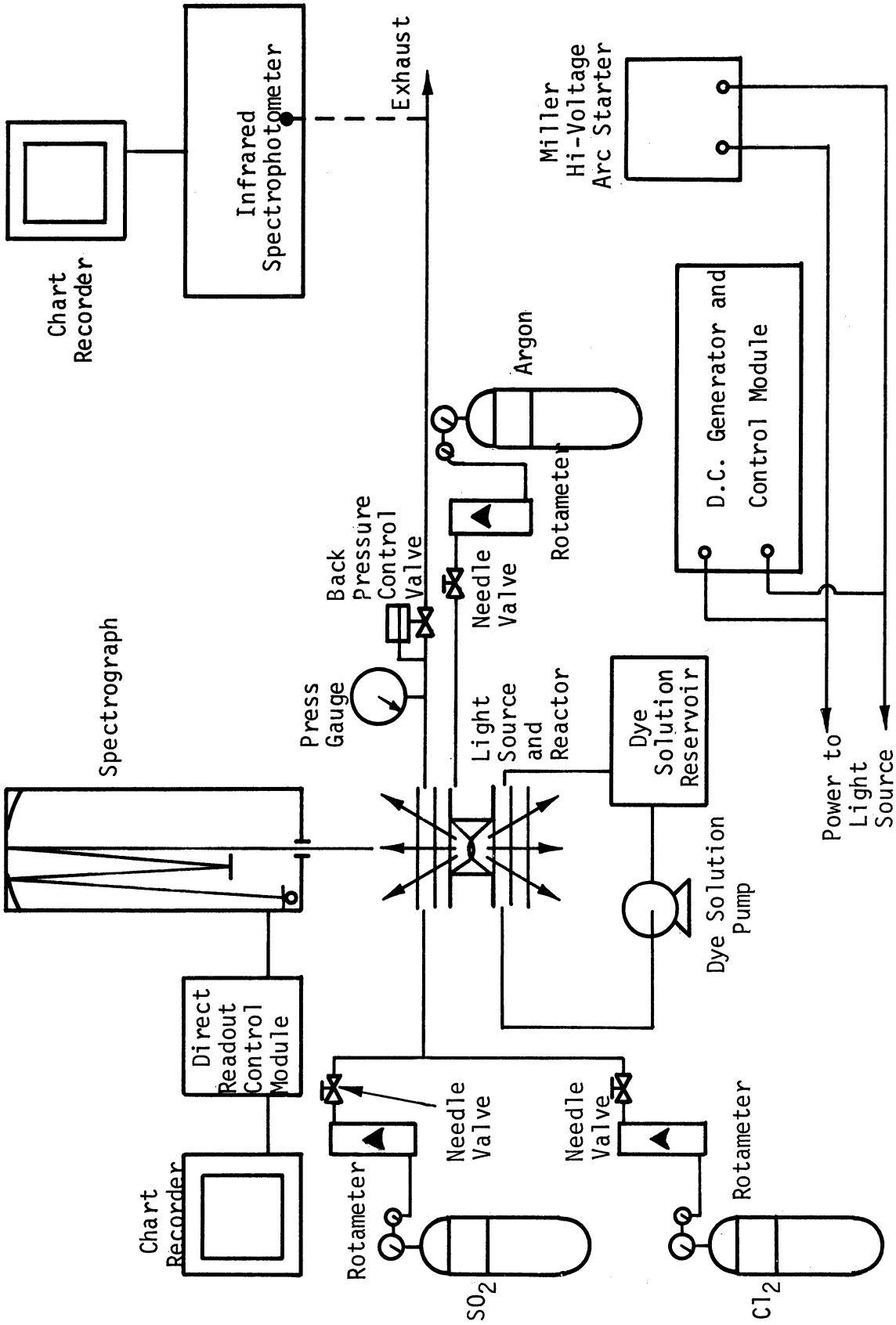

Fig. 5. Schematic diagram of experimental apparatus.

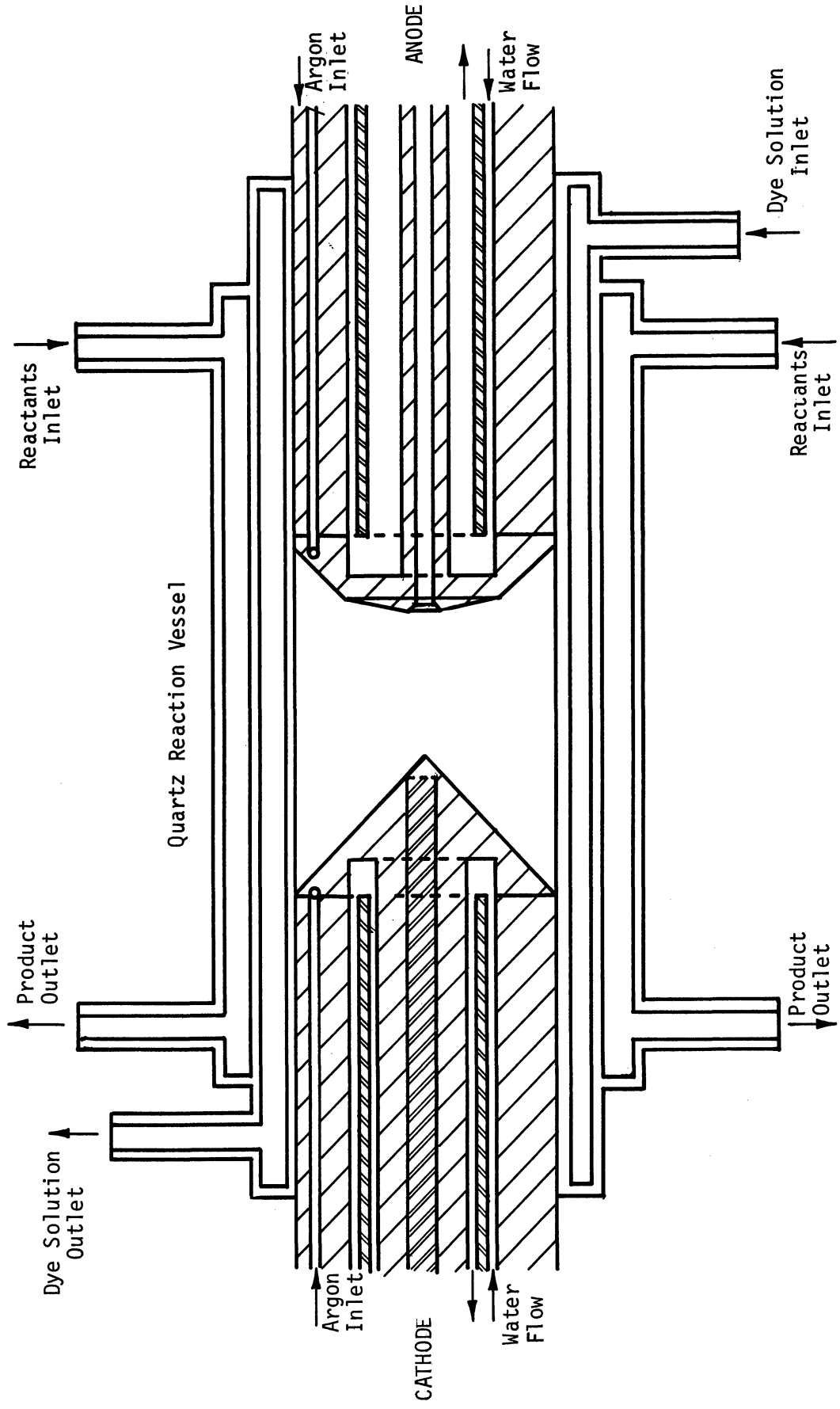

Fig. 6. Schematic diagram of photochemical reaction system.

the cathode. Separate cooling water passages were built into both of the electrodes, with metal-to-metal seals being provided by "O"-rings.

The inner wall of the annular reaction chamber was sealed to the main body of each of the electrodes of the light source by means of "O"-ring seals, forming a transparent envelope for the arc. The argon arc gas was introduced into this envelope tangential to the inside circumference of the fused silica cylinder, forming a vortex as it spun to the central axis, exhausting through a drilled hole at the anode tip.

The vortex flow fixed the dimensions and the location of the arc. It also served to centrifuge the hotter argon atoms to the center of the column of plasma, thus keeping the inside quartz wall of the arc envelope relatively cool.

As mentioned earlier, the reaction chamber was an annular triple-walled vessel. Water soluble inorganic dyes, which provided selective wavelength filtration and which cooled the inner quartz wall, were circulated through the inner of the two annular regions. The outer annulus of the quartz chamber served as the actual reactor volume. The reactant gases entered one end of the annulus through two glass nipples, passed through the annular region, and then exited via two more nipples. Two inlet and exit nipples were provided for the reactant gas flow in order to insure an essentially linear flow profile as the reactant mixture traveled down the annulus.

5.3 SUPPORT EQUIPMENT

The dc power for the radiation source was provided by a Plasmatron P-200 series dc power supply. The power generator was rated at 40 kw with a maximum output of 60 kw. The rated current load was 1000 amp.

The power unit was essentially a 3-phase transformer with 3-phase full-wave bridge rectification, utilizing a saturable reactor current control device. The power supply control system also monitored the voltage and current and provided for automatic stopping of the generator in case of a loss of pressure by the cooling water or the arc gas.

The plasma arc column was initiated by using a Miller (No. HF-20-2) high-frequency arc starter to effect partial ionization of the arc gas.

The dye solution recirculated through the inner annulus was either distilled water, a potassium iodide solution, or a potassium nitrate solution. The dye solution was stored in a 5-gallon glass vessel and was recirculated by a positive displacement gear pump. Before returning the dye solution to the storage vessel, it was cooled by heat exchange with tap water.

Air bubbles which were introduced into the dye solution during the recirculation cycle collected in the inner annulus. To avoid this problem, the aerated dye solution was passed, from top to bottom, through a 4-1/2-ft length of 3-inch O.D. copper pipe before it was introduced into the annulus. The hold-up time of the section of pipe was sufficient to effect separation of the air bubbles from the dye solution.

The bubbles which collected at the top of the pipe were vented periodically.

The argon for the plasma was supplied through a calibrated Fischer-Porter rotameter. As the gas exited from the anode it was first cooled by passing it through a small heat exchanger and was then vented to the atmosphere.

The reactant gases, sulfur dioxide, and chlorine, were supplied to the reactor through calibrated Fischer-Porter "Tri-Flat" flowmeters. The pressure in the reactor was measured with a calibrated pressure gauge and was controlled by a needle valve downstream from the reactor.

During the experimental runs for which the temperature of the gas entering the reactor was different from the ambient temperature, the dye solution was heated or cooled to the desired temperature and then it and the reactant gas mixture were passed through a co-current heat exchanger before they entered separate annuli of the quartz reaction vessel.

Tap water was used to cool both of the electrodes and the arc gas heat exchanger. The tap water was supplied to the cooling channels by a positive displacement gear pump. The various cooling water flowrates were measured with calibrated Fischer-Porter rotameters.

Calibrated iron-constantan thermocouples were used in all gas and water streams. The outputs from the various thermocouples could be switch-selected and were measured on a Honeywell potentiometer.

5.4 INFRARED SPECTROPHOTOMETER

All infrared absorption measurements were performed using a Baird Associates Double-Beam Infrared Recording Spectrophotometer. The instrument was of standard design and was so constructed that infrared spectrograms giving the percent transmission and the wavelength in microns on a linear scale were obtained by direct recording. The apparatus was so constructed that samples of gases, solids, and liquids could be analyzed. A gas cell with a 5-cm optical path length having two removable rock salt plates as windows, was used during all absorption measurements.

5.5 SPECTROGRAPHIC EQUIPMENT

The radiation emitted by the light source was analyzed with a 3.4 m focal length Ebert Mark IV stigmatic plane grating spectrograph manufactured by the Jarrell-Ash Company. The spectrograph was equipped with a grating ruled with 15,000 lines/in. which gave a first-order linear dispersion of 5.1 Å/mm at the focal plane. The useful range of the grating was from 2100 to 7500 Å. The entrance slit of the spectrograph was adjustable in width from 4 to 400 μ and in height from 1 to 15 mm.

The scanning and condensing system (Jarrell-Ash No. 18-022) could scan and bring selected areas of an extended source into focus on the spectrograph slit. The system of 6 front surfaced mirrors and 2 quartz-lithium fluoride acromatic doublet lenses automatically maintained focus and alignment with the optical axis of the spectrograph. The lenses

effected a 2.28 to 1 reduction in image size between the light source and the spectrographic slit.

The plasma was scanned horizontally (along the plasma axis of symmetry) by turning a screw drive mechanism which moved the mirror assembly. The horizontal scan permitted accurate positioning along the plasma column perpendicular to its axis of symmetry.

The spectrograph was equipped with a sine bar wavelength drive (Jarrell-Ash No. 70-005) which rotated the grating in a manner such that the wavelength seen by the center of the focal plane corresponded to the number recorded on a wavelength counter. The sine bar wavelength drive permitted twelve rates of scan ranging from 1 to 500 Å/min.

The spectra were recorded by an RCA 1P28 multiplier phototube located at the center of the focal plane. The tube was operated with a supply voltage of 1000 vdc. It was driven with a Furst Electronics (No. 710-PR) dc power supply having a continuously adjustable voltage output (0-1500 v). The current output of the multiplier phototube was passed through a variable precision resistor. The resulting voltage was amplified by a variable range Leeds and Northrup (No. 9835-A) stabilized dc μv amplifier. The (0-10 mv) output of the amplifier was monitored with a Leeds and Northrup Speedomax H strip chart recorder.

The 118 vac power used by the spectrograph and related direct readout equipment was supplied through a Sola type CVS voltage regulator. The supply voltage for the multiplier phototube was monitored by a DigiTec Model 201 dc digital voltmeter with an absolute accuracy of ±1 v and a reproducibility of ±.1 v.

6. EXPERIMENTAL PROCEDURES

6.1 START-UP PROCEDURES

The operation of the plasma light source was initiated with the intraelectrode distance set at approximately 1/4 in. During start-up of the light source, the argon, cooling water and dye solution flows were initiated and then the arc starter was turned on. If everything appeared satisfactory, the dc power supply was then engaged. As soon as the dc power supply was in operation the arc starter was turned off and the arc was stretched to its normal operating length of 1 in. by adjustment of the tungsten cathode.

6.2 ANALYSIS OF REACTION PRODUCTS

In preparation for an experimental run a glass sample tube was placed in the product gas stream in parallel with a by-pass line. During the run the product stream was diverted from the by-pass line, the sample tube was flushed, and a sample of product gas was obtained.

Using a gas manifold system, part of the gas sample was transferred to a 5-cm path length infrared cell equipped with sodium chloride windows. An infrared spectrogram of the gas sample was then made using a Baird Associates Recording Infrared Spectrophotometer.

The infrared spectrogram was analyzed by comparing the strength of the sulfuryl chloride absorption peak at 7.06 μ with the strength of the sulfur dioxide absorption peak at 4.00 μ.

6.3 PRECAUTIONARY SAFETY MEASURES

Due to the high-intensity level of the ultraviolet light emitted by the light source, there were three potential physiological hazards which had to be considered.

The light source was sufficiently intense to cause reversible or even permanent eye damage if viewed without appropriate eye protection. The plasma column was observed directly only through a standard design electrical welding helmet. A set of oxyacetylene welding goggles were worn during work which was related to the light source but which did not involve direct observation of the plasma. Appropriate warning lights were installed at all laboratory exits to avoid having visitors enter the laboratory without proper eye protection.

When uncovered skin was exposed to the light source for any length of time it took on a cherry red glow which in time turned into a painful burn analogous to a sunburn. With sufficient exposure time it was possible to observe this effect on skin which was covered with a light layer of clothing. This problem was avoided by wearing heavier clothing during operation of the light source.

During extended operation of the light source there was some danger of respiratory damage due to the external buildup of ozone. A laboratory exhaust fan minimized this problem.

6.4 EVOLUTION OF ANODE DESIGN

In designing and testing the light source, a difficult problem

presented itself. The problem involved the selection of the physical shape of and the construction material for the anode.

In technical writing it is not a customary procedure to discuss experimental difficulties encountered, however, experience in the construction and operation of arc-type plasma generation devices has shown that such information is invaluable to the succeeding experimentalists. It is the opinion of the author that said persons require all the help that they can get.

The evolution of the design of the anode tip is depicted in Fig. 7. In all the configurations tested, cooling water under pressure was pumped against the inner face of the electrode via cooling water passages sealed into the main body of the electrode.

Design A (Fig. 7) was the first anode configuration tested. It was constructed entirely of brass. This configuration operated successfully at current levels below approximately 200 amp. When the current level exceeded this value melting occurred at the electrode face. The flow of argon swept the molten brass into the argon exit line where it solidified, halting the operation of the vortex. The loss of vortex flow resulted in additional damage to the electrodes and the surrounding quartz glass.

In design B (Fig. 7), a tantalum insert was shrunk fit into the main body of the electrode so that it served as the anode tip. Tantalum possess a thermal conductivity equivalent to that of brass, however, its melting point is approximately 2000°C higher than the melting point

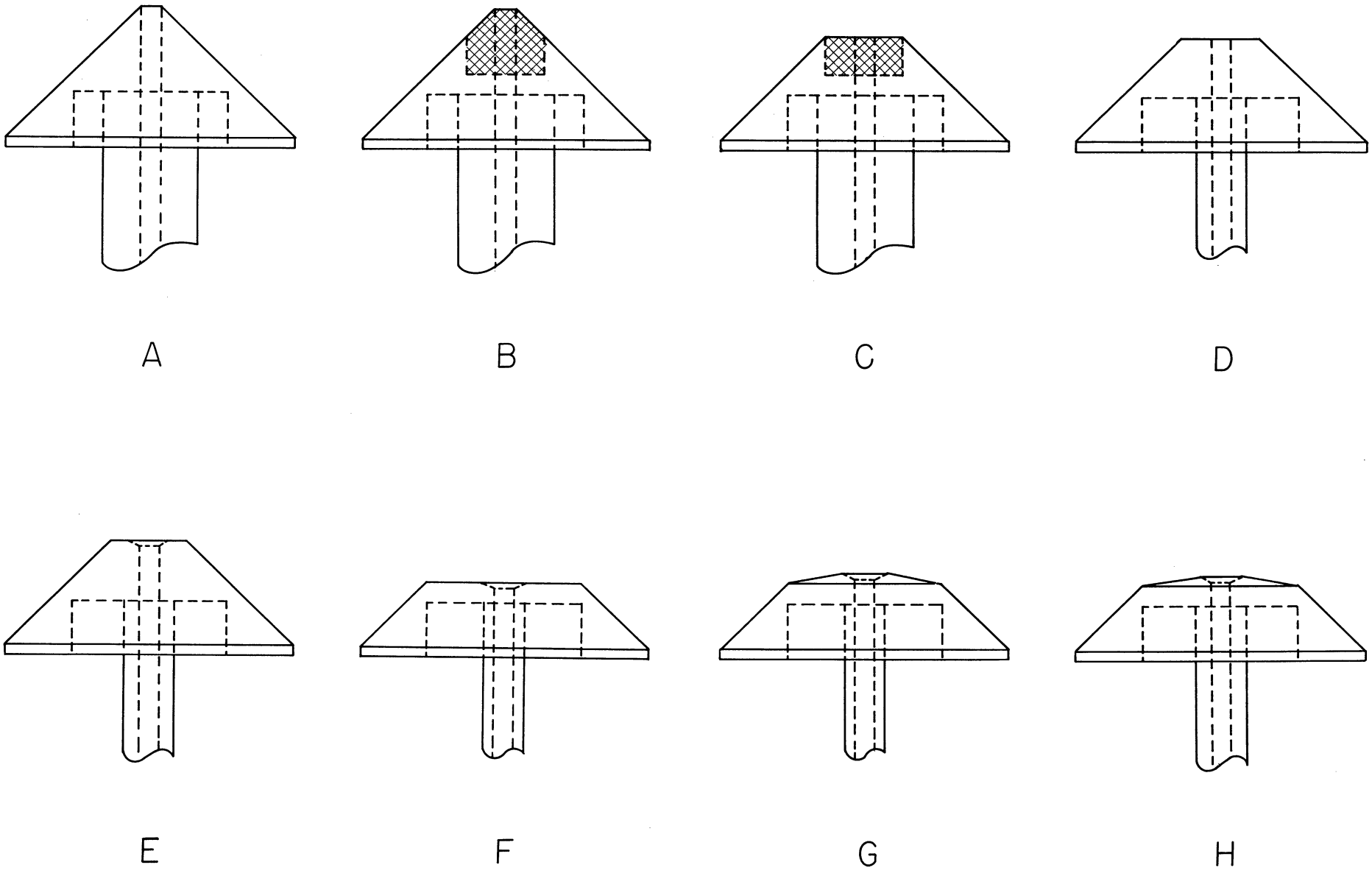

Fig. 7. Evolution of anode design.

of brass. When this configuration was tested in the light source it performed in a manner analogous to design A (Fig. 7).

In order to have the anode surface closer to the cooling water channel, design B (Fig. 7) was modified to yield design C (Fig. 7). This design decreased the distance from the anode to the cooling water and also spread the heating process over a much larger surface area. However, in operation, no improvement in performance was obtained.

In design D (Fig. 7) the material of construction was changed to copper, and the outer diameter of the electrode step was decreased from 5/8 in. to 5/16 in. A definite improvement in the operating characteristics of the light source was realized with this design. After a period of operation, however, the anode tip began to erode around the argon exit line. The eventual shape of the erosion was anticipated and incorporated into design E (Fig. 7). Design E (Fig. 7) operated successfully at current levels below approximately 400 amp, however, when the current level exceeded this value it failed in a manner analogous to previous designs.

In the next configuration tested, design F (Fig. 7), the outside diameter of the electrode stem was further reduced to 1/4 in. and the distance between the cooling surface and the electrode face was decreased to 5/32 in. This configuration was tested successfully at current levels in excess of 600 amp, with no appreciable damage to the anode face. However, during repeated operation several difficulties were encountered. The more serious problem arose when the 5/32 in. thickness of copper

did not provide sufficient structural strength to maintain the "O"-ring water seals during operation, resulting in a water leak directly into the arc. When an attempt was made to compress the "O"-rings by applying additional tension to the electrode stem, the anode face bowed noticeably.

The second problem was that even at high vortex flowrates, the arc would not locate itself at the center of the anode surface, but rather would move about the surface in a random fashion. This difficulty was increased by the bowing of the anode face.

Both of these problems were eliminated by providing the anode face with a 10° rise as shown in design G (Fig. 7). The rise not only increased the structural strength of the anode but also provided a "nearest point" to which the arc could strike. This configuration operated successfully for many hours at a wide range of power settings. Eventually, however, it failed when the electrode stem broke due to repeated heating and cooling. The final configuration was obtained when the outer diameter of the electrode stem was increased to 5/16 in., as shown in design H (Fig. 7). This design provided satisfactory performance under all operating conditions investigated.

6.5 SPECTROGRAPHIC MEASUREMENTS

As discussed previously, the current output of the multiplier phototube was passed through a variable precision resistor, with the resulting voltage being amplified by a variable range Leeds and Northrup sta-

bilized direct current microvolt amplifier. The amplifier output was then monitored with a Leeds and Northrup Speedomax H strip chart recorder.

The specifications for the amplifier and the chart recorder indicate, respectively, a 3- and a 1-sec response time for approach to within 1% of balance. Since a typical argon line is of the order of 1 to 5 Å wide at half height, even a moderate scan rate causes appreciable attenuation of the true signal.

Figure 8 depicts this droop in amplifier output as a function of the spectrographic scan rate when the 3650 Å mercury line was observed spectrographically at various scan rates. It was noted that considerable attenuation of the signal resulted when scan rates of 10 Å/min or higher were employed.

Since it was necessary to scan a 2500 Å wavelength region it was not feasible to utilize such a low scan rate.

All spectra prepared during this investigation were scanned at 100 Å/min. At this scan rate the peak heights recorded were approximately 36% of the true peak heights. For this reason, only continuum radiation was considered in calculations pertaining to the spectral output of the light source while keeping in mind that a considerable amount of radiation was in the form of line radiation. This suggests that calculated values of the available light were on the low side of the true value, especially in areas of the spectrum where the line radiation of argon was the strongest. The argon line radiation was not appreciable

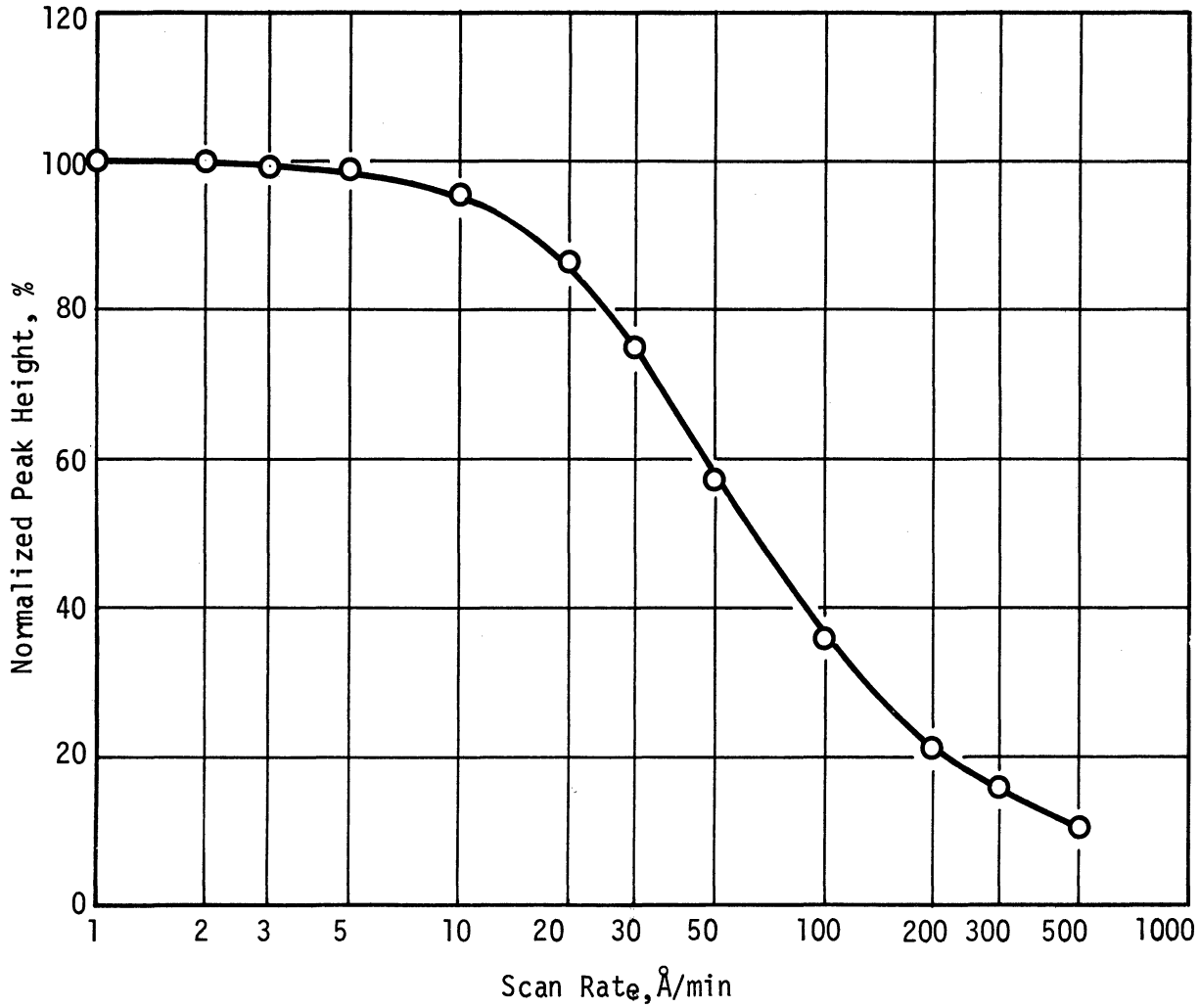

Fig. 8. Photomultiplier response as a function of the spectrographic scan rate.

below approximately 3450 Å, however, above this wavelength it was a significant fraction of the total spectral contribution.

It was not possible to calculate what fraction of the total radiant output was due to line radiation, however, it may be crudely estimated that approximately 25% of the total radiation in the 3450 to 5000 Å wavelength region is due to line radiation.

Using an FM tape recorder and an analog computer, an experimental attempt was made to measure the fraction of the total radiant output which was attributable to line radiation. The results of these measurements were inconclusive. If a reasonable signal to noise ratio was used when scanning continuum radiation the amplifiers of the analog computer were saturated when a line was passed. Conversely if the peak heights for the major argon lines were kept on scale by decreasing the sensitivity of the computer, no quantitative results could be obtained due to the high signal to noise ratio over the continuous region of the spectrum.

6.6 MEASUREMENT OF REACTANT INLET TEMPERATURE

Difficulties were encountered in monitoring the temperature of the reactant mixture along the reactor length. Two different phenomena contributed to the problems encountered.

The mean linear velocity of the reactants as they passed through the reactor was in the range 1 to 10 cm/sec. Using available correlations it can be estimated that the film heat transfer coefficient for a

thermocouple immersed in the reactant gas stream is approximately 5 Btu/hr-°F-ft^2.[27]

For this value of the heat transfer coefficient, the response time for a 1 mm diam iron-constantan thermocouple bead would be in excess of 30 sec. At best, this large response time made measurement of the gas stream temperature time consuming as well as making the measurements insensitive to temperature changes in the gas stream.

During operation of the light source the temperature of thermocouples exposed to the radiation increased markedly. Due to space limitations in the quartz reactor it was not possible to provide a light shield for the thermocouples. This made it impossible to measure accurately the temperature of the reactant gas mixture during its exposure to the light source. Even when the thermocouple was not directly exposed to the radiation, reflected light increased the temperature of the thermocouple.

For experimental runs carried out with feed temperature different from the ambient temperature, an indirect method was used for the measurement and control of the inlet gas temperature. The dye solution was heated or cooled to the desired temperature and then it and the reactant gas mixture were passed co-currently through a heat exchanger before they entered the separate annuli of the quartz reaction vessel. Heat transfer calculations indicate that the two streams left the heat exchanger with an approach of less than 0.5°C.[27] Thus the inlet temperature of the reactant gas mixture was assumed to be equal to the inlet

temperature of the dye solution, a quantity which was relatively simple to measure experimentally.

6.7 DYE SOLUTION EVALUATION

Relative to the operation of the continuous flow optical filtration system, the light absorption properties of numerous inorganic and organic compounds were investigated.

In order to possess the desired absorption properties a compound, or a mixture of compounds, had to absorb light selectively over the wavelength region of interest, 2500 to 5000 Å. The ideal light absorbing medium would possess the following properties:

1. It would absorb strongly at wavelengths shorter than some wavelength L_o, but would be completely transparent at wavelengths longer than L_o.

2. L_o would be at a point of interest in the wavelength interval.

3. The material would not decompose photolytically when it absorbed light.

4. The compound would itself be useable as a heat transfer fluid or, alternatively, a sufficient amount of the compound could be dissolved in water.

5. The compound would not react chemically with the pump, the heat exchanger or other items in the light filtration system.

For purposes of this investigation two values of L_o were of interest. The lower, 2600 Å, would pass all light that could be absorbed by

sulfur dioxide and chlorine but would filter wavelengths that would be absorbed by sulfuryl chloride. The second value of L_o, 3300 Å, would filter light that could be absorbed by sulfur dioxide and sulfuryl chloride but would pass a large percentage of the light which could be absorbed by chlorine.

No single compound or group of compounds completely satisifed all of the requirements listed above. The nitrates and the iodides of the alkali metals came the closest to fulfilling all the requirements.

The percentage of incident light transmitted by 0.579 cm of a 1.5 normal aqueous solution of potassium nitrate is shown in Fig. 9 as a function of the wavelength of the incident light. The "cut-off" region (wavelength region in which percent transmission increases from 10 to 90%) was 3260 to 3450 Å. The only major drawback of the potassium nitrate solutions was that they decomposed slowly as they absorbed light.

The photochemical decomposition of potassium nitrate has been investigated by Villars.[29] His work demonstrated that there is a strong relationship between the pH of the nitrate solution and the quantum yield of the photolytic reaction.

Using Villars' results, the nitrate solutions used in this investigation were buffered at a pH of 5.0 using an acetic acid-sodium acetate mixture. According to Villars, this reduces the expected quantum yield for the photolytic decomposition to a value less than 0.01.

Figure 10 shows the percentage of incident light transmitted by 0.579 cm of a 0.05 normal aqueous solution of potassium iodide as a

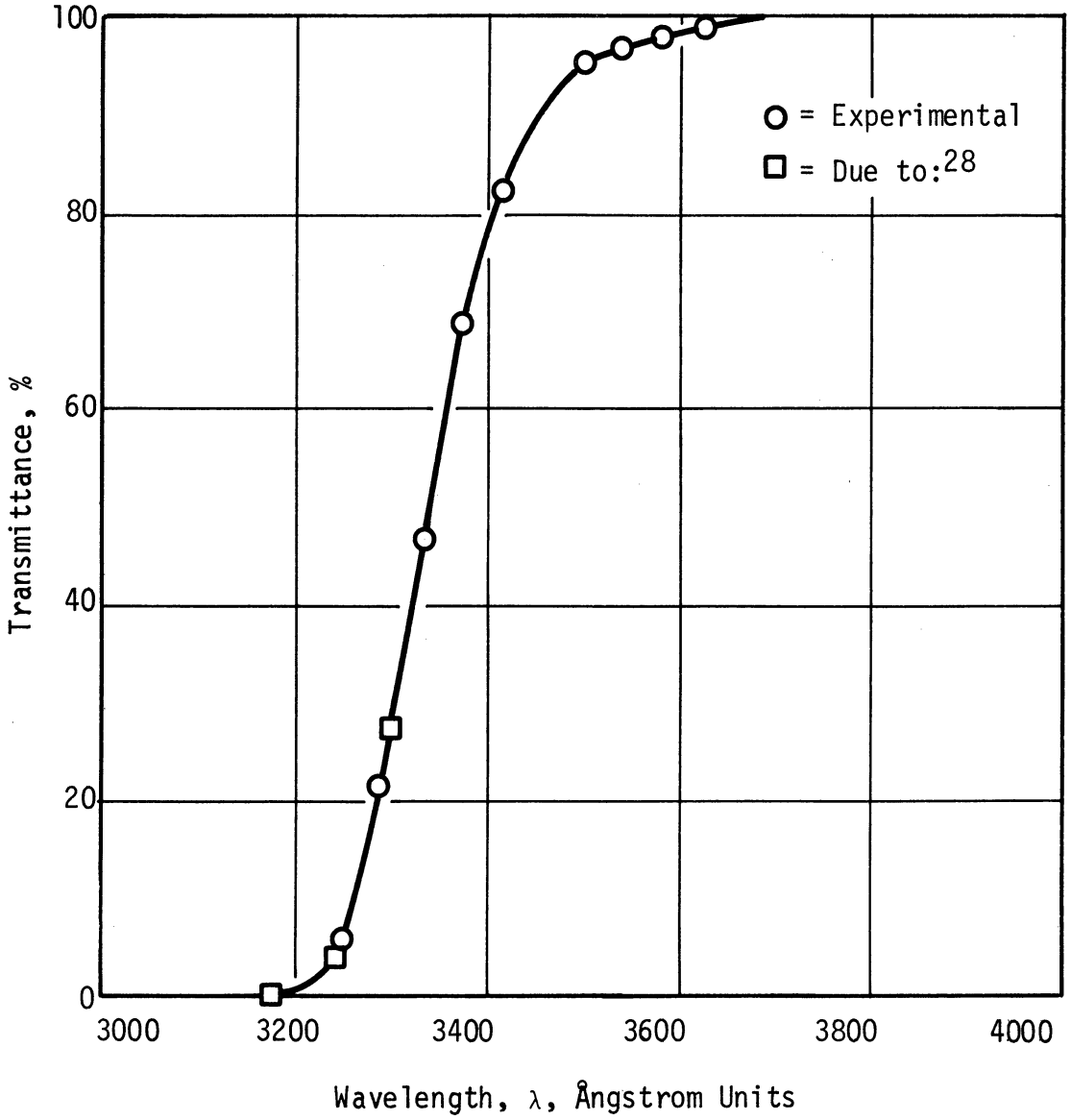

Fig. 9. Percent of incident light transmitted by .579 cm of 1.5N potassium nitrate.

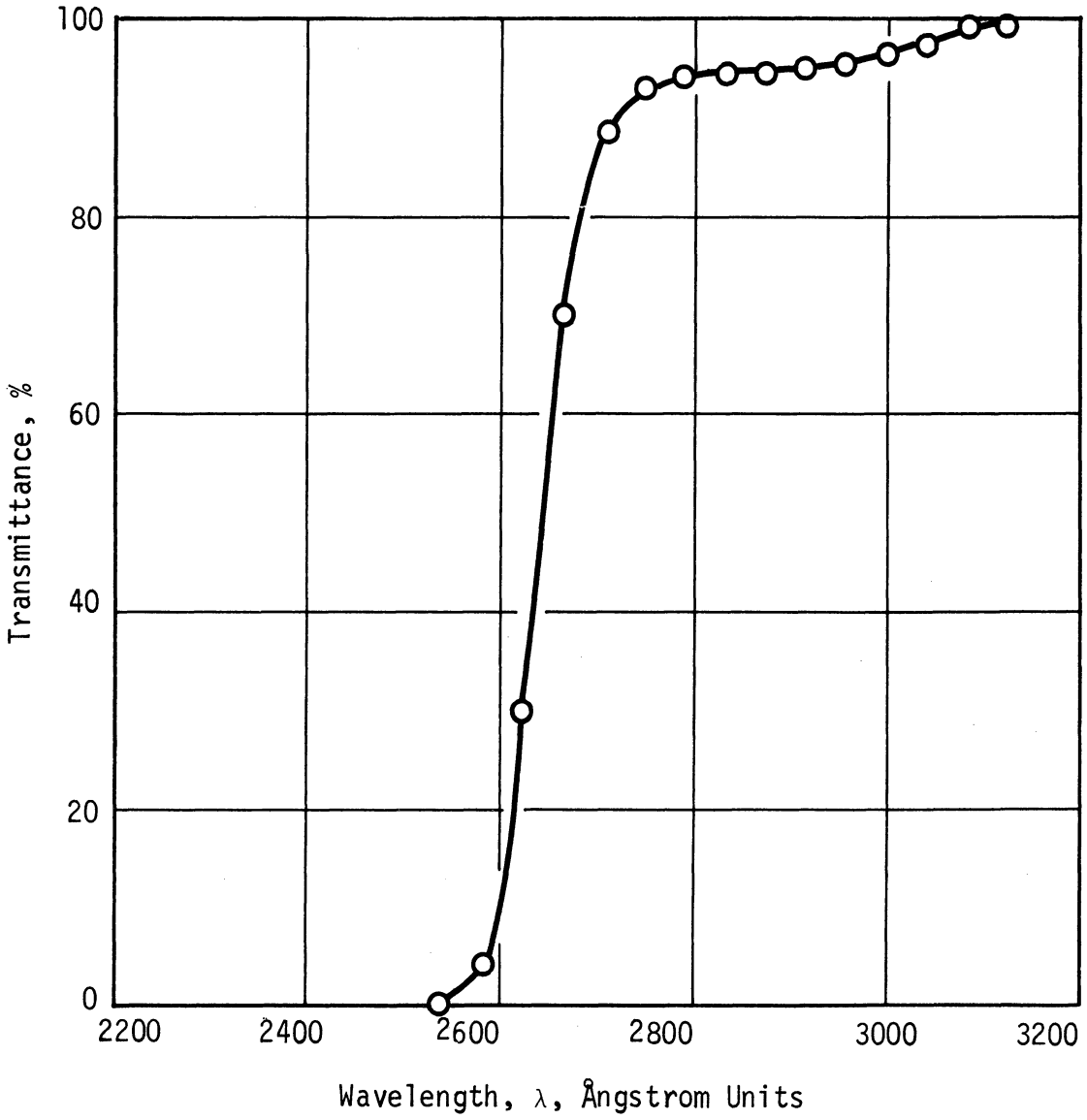

Fig. 10. Percent of incident light transmitted by .579 cm of .05N potassium iodide.

function of the wavelengths of the incident light. "Cut-off" occurs between 2600 and 2715 Å. As in the case of the nitrates, iodide solutions decompose slowly as they absorb light.

The photochemical decomposition of iodide solutions has been investigated by Jortner and co-workers.[30] As in the case of nitrate solutions the quantum yield for the reaction was strongly dependent upon the solution pH. Jortner observed that the quantum yield decreased with increasing pH value up to approximately a pH of 6.0.

The iodide solutions used in this investigation were kept at a pH greater than 6.0. This reduced the expected quantum yield for the photochemical decomposition reaction to less than 0.03.

Some difficulty was experienced with the iodide solutions due to the solutions reacting with the components of the recirculation system. As operation proceeded over a period of hours the solutions took on a pale yellow color. It is believed that the reaction involved the solder used to form the various seals in the recirculation system. Difficulties due to this phenomenon were minimized by changing the iodide solution in the recirculation system at regular intervals during operation of the light source.

6.8 ANALYSIS OF SPECTROGRAPHIC MEASUREMENTS

Such light intensity units as the candlepower and the monochromatic emissive power were not relevant to the work done during this investigation. Due to this situation two new light intensity units will be "de-

fined" and used throughout this report. The units are the "spectral radiance," Q, of the arc expressed in gram-mole equivalents of photons emitted per hour per Ångstrom unit of wavelength per centimeter of arc length and the "spectral output" of the arc expressed in gram-mole equivalents of photons emitted per hour per Ångstrom unit of wavelength. The spectral output of the arc is equal to the spectral radiance integrated over the length of the arc.

The photomultiplier tube and the optical system of the spectrograph were calibrated by spectrographically observing a luminous tungsten ribbon filament and a hydrogen lamp, standard sources whose spectral radiances were calculable. The current output of the photomultiplier tube as a function of wavelength was then compared with the calculated spectral radiance of the standard source. The ratio of the spectral radiance to the photomultiplier current output, designated by $R(\lambda)$, represents the spectral-response characteristic function for the photomultiplier tube and the optical system. Details involved in the calculation of $R(\lambda)$ are discussed in Appendix I.

The analysis of spectrographic measurements was simplified considerably by assuming that the arc column could be represented as a linear radiation source rather than considering it as an extended source. Discussion of and justification for this assumption are presented in Appendix II.

The calibration factor used for all spectrographic measurements, $R(\lambda)$, had units of gram-mole equivalents of photons per hour per Ång-

strom unit per square centimeter per steradian per ampere, where the square centimeter term in the denominator refers to the area of the radiation source observed by the slit of the spectrograph. During calibration, the area of the source subtended by the slit was:

$$S = H_c \cdot W_c / M^2 \qquad (6.1)$$

with M being the overall image magnification effected by the lenses in the scanning and condensing system, and H_c and W_c being the slit height and slit width during calibration.

The magnification factor for the lens system, M, was calculated by considering the spatial location of the components of the optical scanning-condensing system and the focal lengths of the two quartz-lithium fluoride acromatic doublet lenses. The calculated value of M is 0.4386.

During this investigation, the quantity of interest was the spectral radiance, Q. Integrating over the solid angle dependence, Q can be expressed as:

$$Q = \frac{4\pi \cdot R(\lambda) \cdot A(\lambda) \cdot H_c \cdot W_c}{W \cdot M} \qquad (6.2)$$

where $A(\lambda)$ is the current output of the photomultiplier as a function of wavelength and W is the slit width.

7. PERFORMANCE CHARACTERISTICS OF THE LIGHT SOURCE

7.1 GENERAL

The spectral radiance of the light source was studied as a function of the arc gas flowrate, position along the arc, and as a function of the power input to the arc column.

7.2 EFFECT OF ARGON FLOWRATE

Over the gas flowrate range investigated, which spanned the entire range of stable operation, the spectral radiance varied only slightly with changing argon flowrate. Figure 11 shows the dependence of spectral radiance on argon flowrate for light having a wavelength of 3000 Å and for a power input to the arc of the light source of 8.10 kw. Under these conditions a 90% increase in argon flowrate resulted in only a 2.1% increase in the 3000 Å spectral radiance of the light source.

During the remainder of the investigation the effect of argon flowrate on the spectral radiance was neglected. The only criteria used in selecting the argon flowrate was that the light source operate in a stable manner.

7.3 EFFECT OF POWER INPUT AND POSITION ALONG ARC

The spectral radiance of the light source was investigated extensively as a function of the power input to the arc, the wavelength of the radiation, and the axial position in the arc. For reasons discussed previously, only continuum radiation was considered during calculations

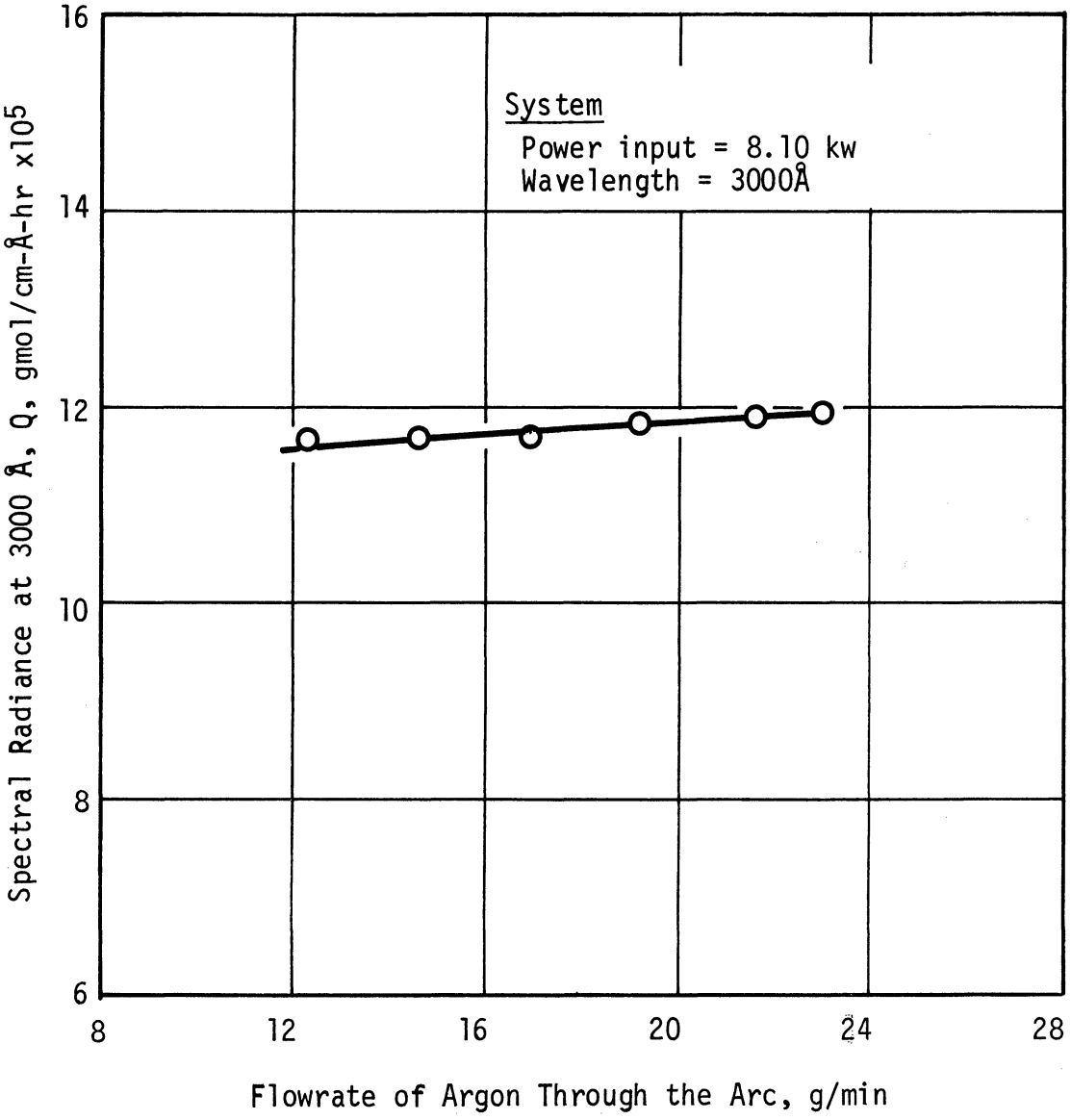

Fig. 11. Effect of argon flowrate on the spectral radiance of the arc.

involving these measurements. The experimental observations are presented in Figs. 12 to 25.

As a matter of convenience, the arc of the light source was subdivided into 25 regions, measuring from the vicinity of the tungsten cathode to the vicinity of the anode. Each region was 0.127 cm (0.05 in.) wide. Spectrographically the arc was observed at the 24 points which subdivided the arc.

The continuum radiation of the source is shown in Figs. 12 and 13 as a function of axial position along the arc for several values of the wavelength. Figure 12 corresponds to operation at 3.84 kw while Fig. 13 represents operation at 8.45 kw.

It can be seen from Figs. 12 and 13 that the tungsten cathode tip is located at position no. 3 while the copper anode is at position no. 22. This indicates that the arc length is 2.413 cm (0.95 in.) long, a value confirmed by physical measurement.

In both cases the spectral radiance at all wavelengths went through a maximum near the tungsten cathode and then decreased as the anode was approached. This drop off in spectral radiance with position was much more pronounced in the case of operation at 3.84 kw (160 amp) than it was for operation at 8.45 kw (320 amp). It is anticipated that, for higher current inputs to the arc, the spectral radiance will become constant with respect to position across the arc.

In Figs. 14 and 15 are shown the spectral outputs of the light source as

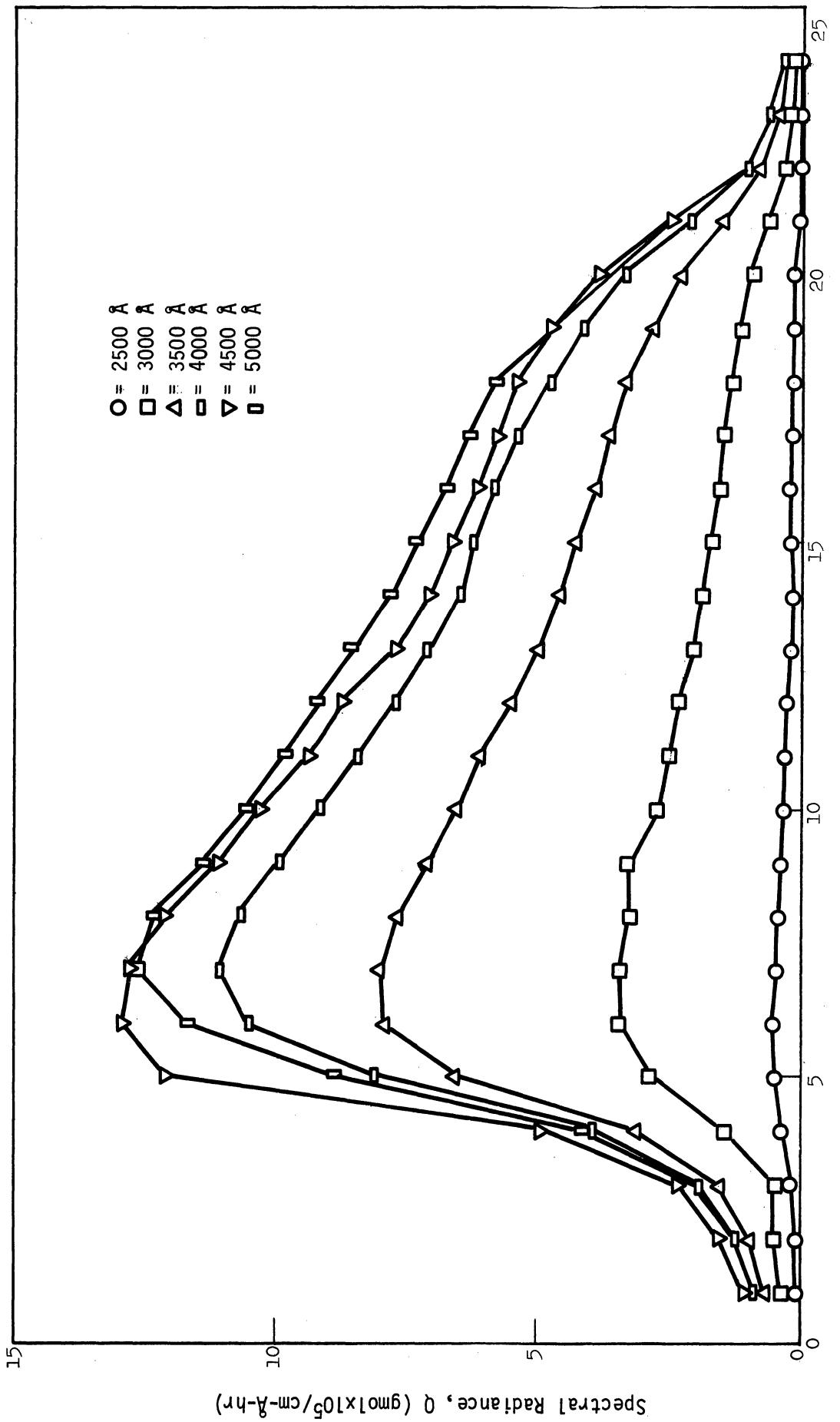

Fig. 12. Spectral radiance of the arc operating at 160 amp vs. axial position along arc for several wavelengths.

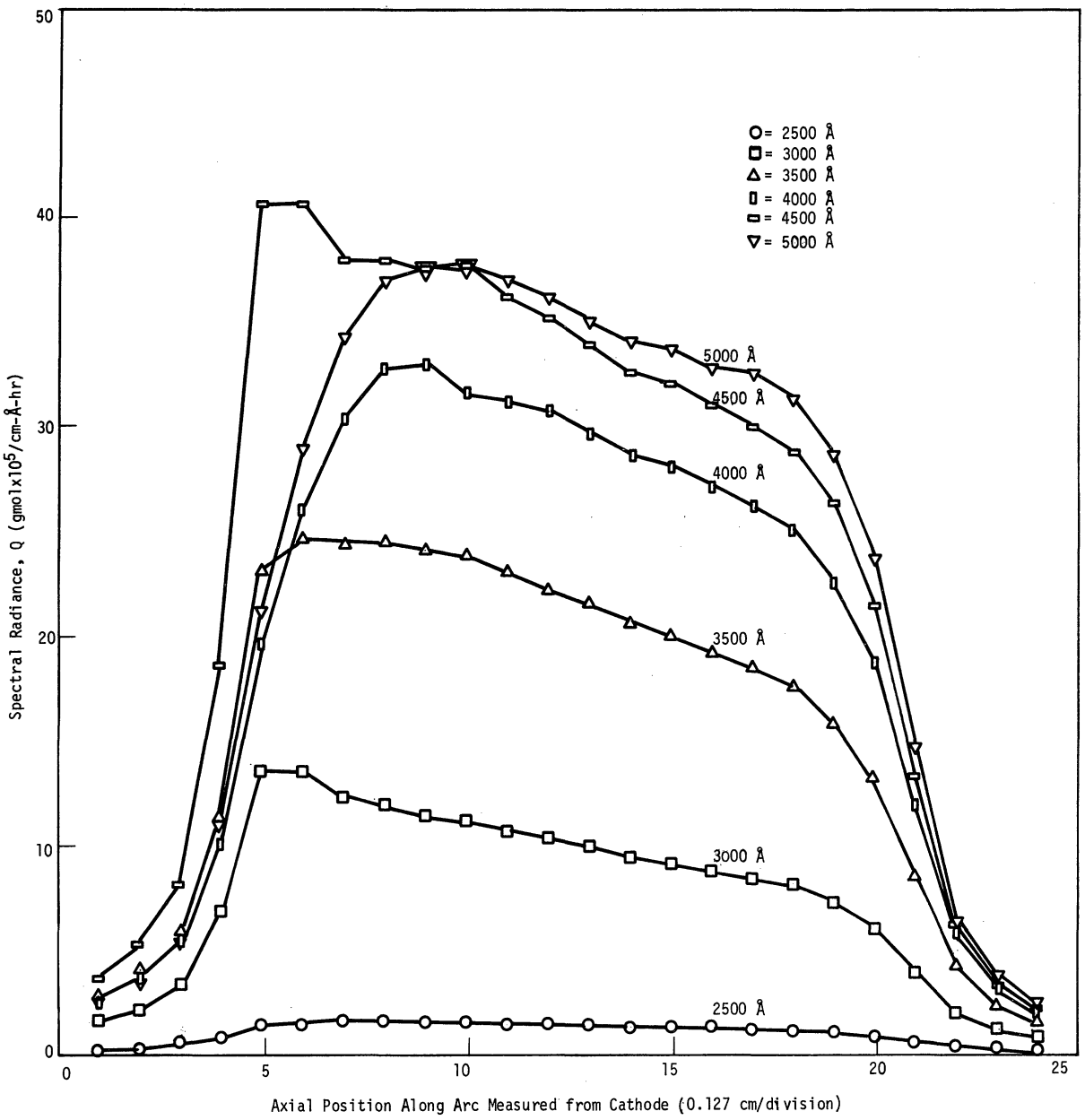

Fig. 13. Spectral radiance of the arc operating at 320 amp vs. axial position along arc for several wavelengths.

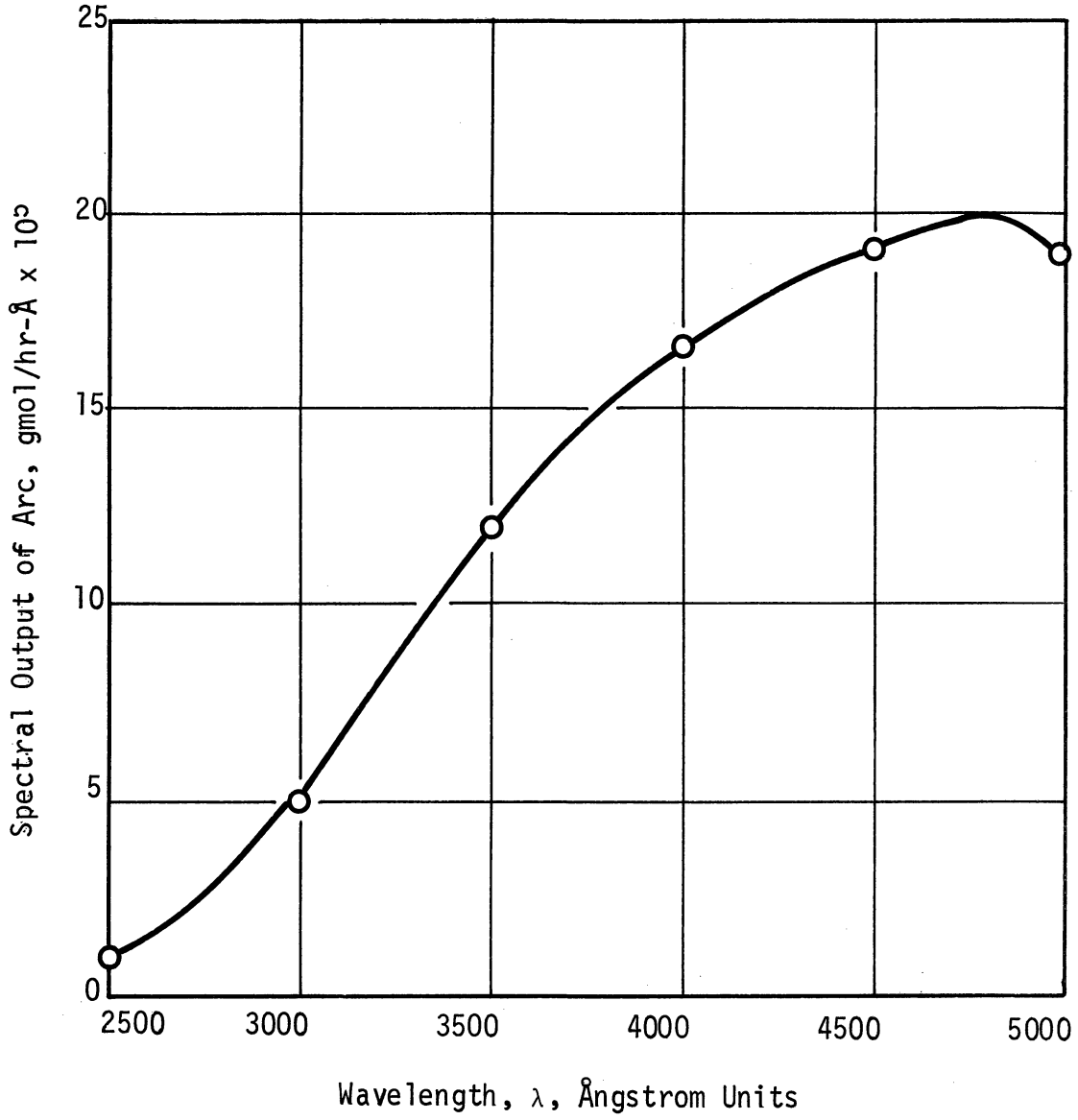

Fig. 14. Spectral output of the arc vs. wavelength for operation at a power input of 3.84 kw.

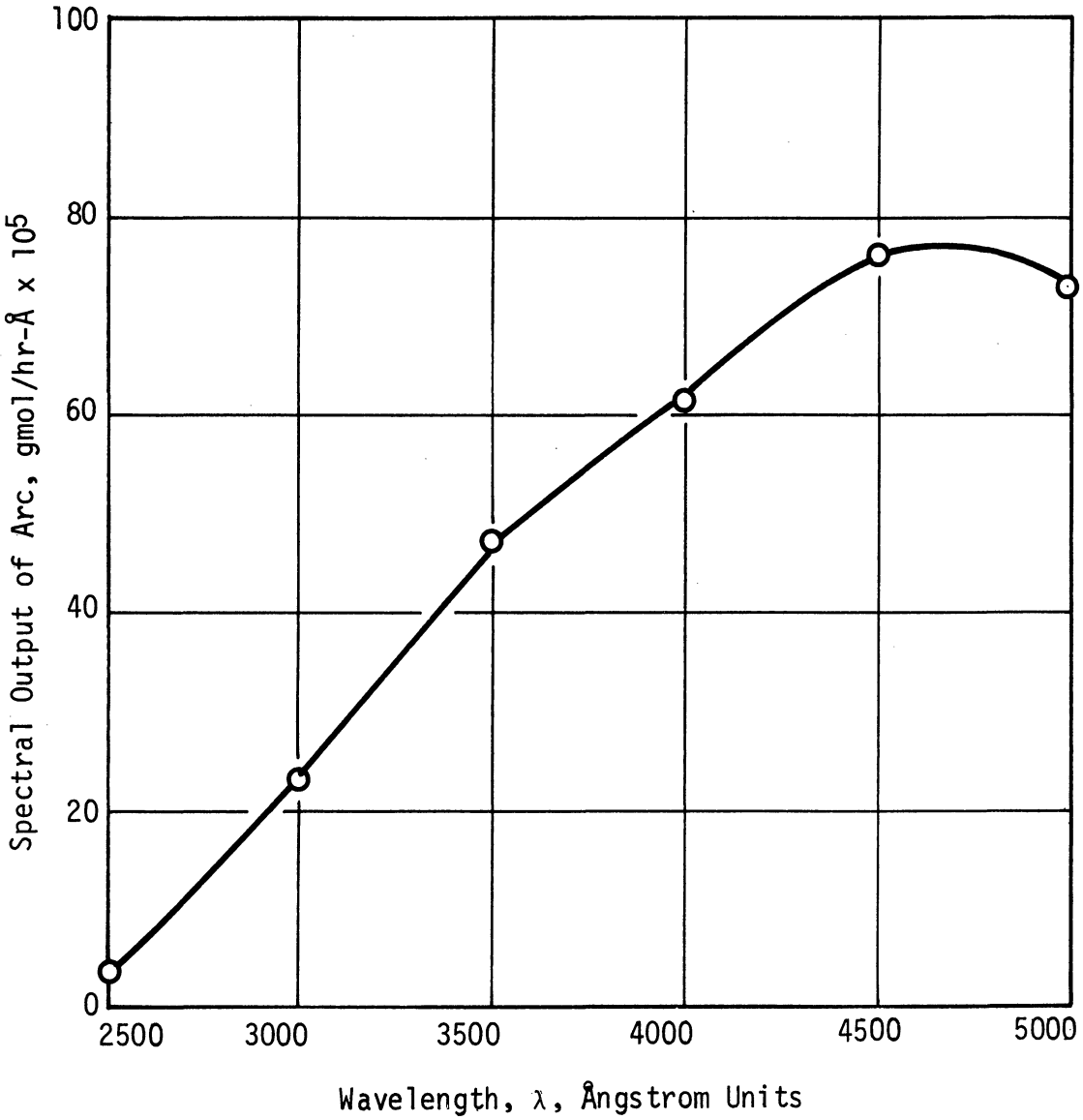

Fig. 15. Spectral output of the arc vs. wavelength for operation at a power input of 8.45 kw.

a function of wavelength for operation of the light source at 3.84 and 8.45 kw, respectively. Integrating under the spectral output curves with respect to wavelength, between the limits of 2500 and 5000 Å, indicates that there was approximately 0.314 and 0.862 gmol/hr of ultraviolet light available from the light source when it was operating at 3.84 and 8.45 kw, respectively.

Figures 16 and 17 present the uncorrected spectral radiance of the light source vs. wavelength at two different locations along the arc for operation at a power input of 3.84 kw. Figure 16 shows the radiation of the arc at a point near the tungsten cathode (position 7), while Fig. 17 shows the radiation emitted by the central region of the arc (position 12). Figure 18 presents the spectral radiance of the continuum for these two runs. It was obtained by multiplying the photomultiplier output by the calibration factor $R(\lambda)$.

Similar information is presented in Figs. 19, 20, and 21 for operation of the light source at 8.45 kw. The uncorrected spectral radiance of the arc is shown in Figs. 19 and 20 corresponding to positions 7 and 12 along the arc while the corrected spectral radiance for these two runs is shown in Fig. 21.

It is readily apparent from an analysis of Figs. 16 and 19 that, for position 7 or more generally for the region of the arc near the cathode, the amount of ultraviolet light which was emitted as line radiation was a very significant fraction of the total radiation emitted. Conversely, by analyzing Figs. 17 and 20 it can be concluded that, for

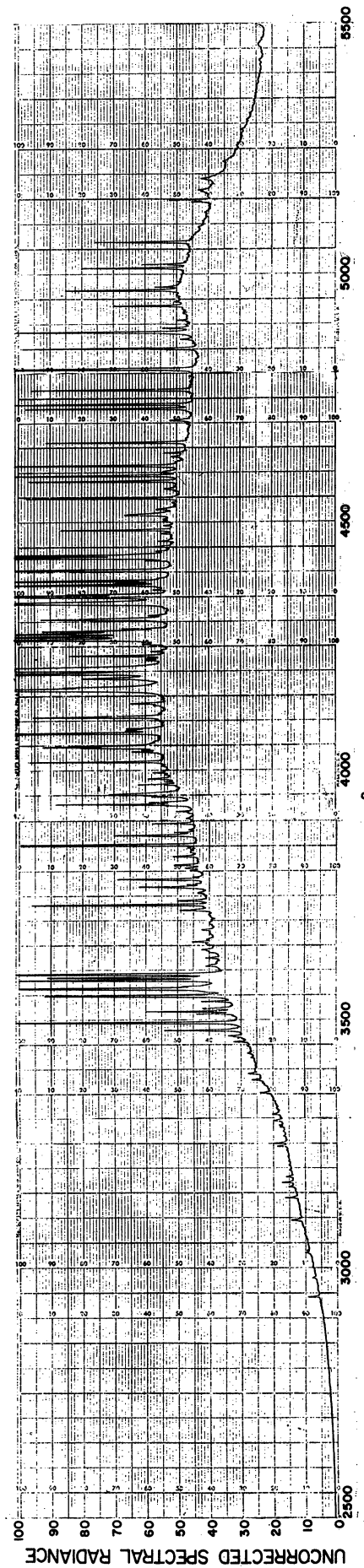

Fig. 16. Uncorrected spectral radiance at arc position no. 7 vs. wavelength for an arc power input of 3.84 kw.

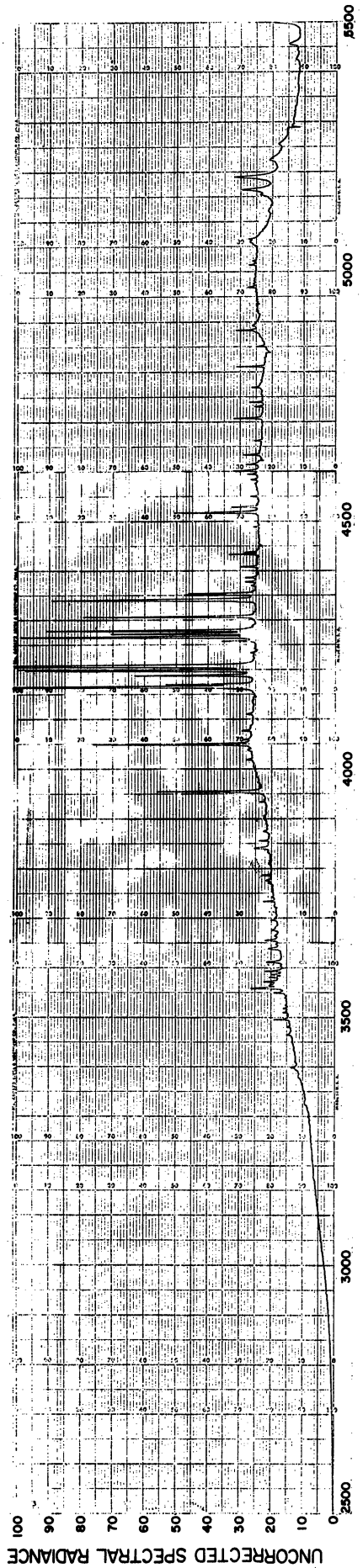

Fig. 17. Uncorrected spectral radiance at arc position no. 12 vs. wavelength for an arc power input of 3.84 kw.

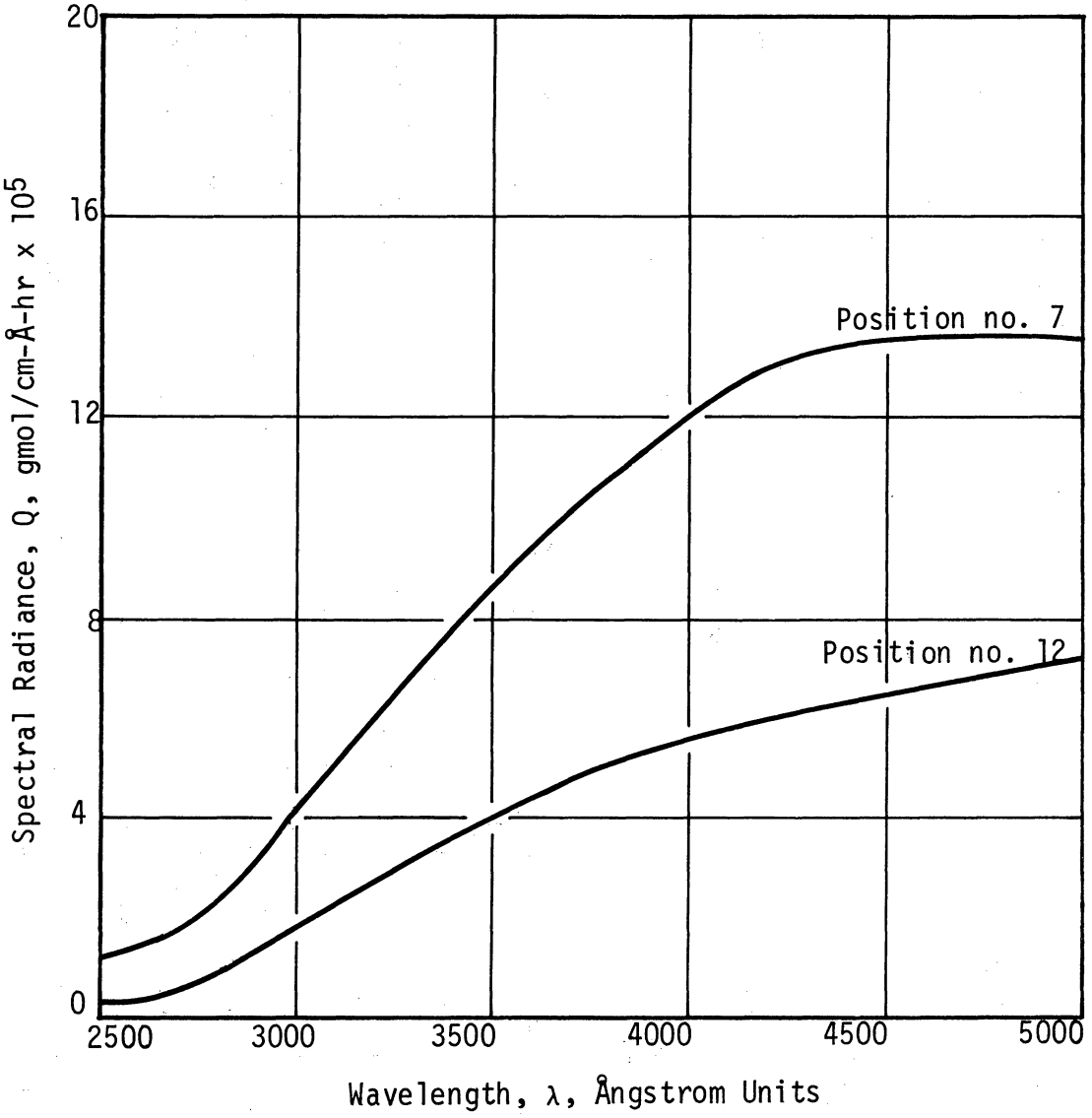

Fig. 18. Spectral radiance of continuum vs. wavelength at positions no. 7 and no. 12 along the arc for operation at 3.84 kw.

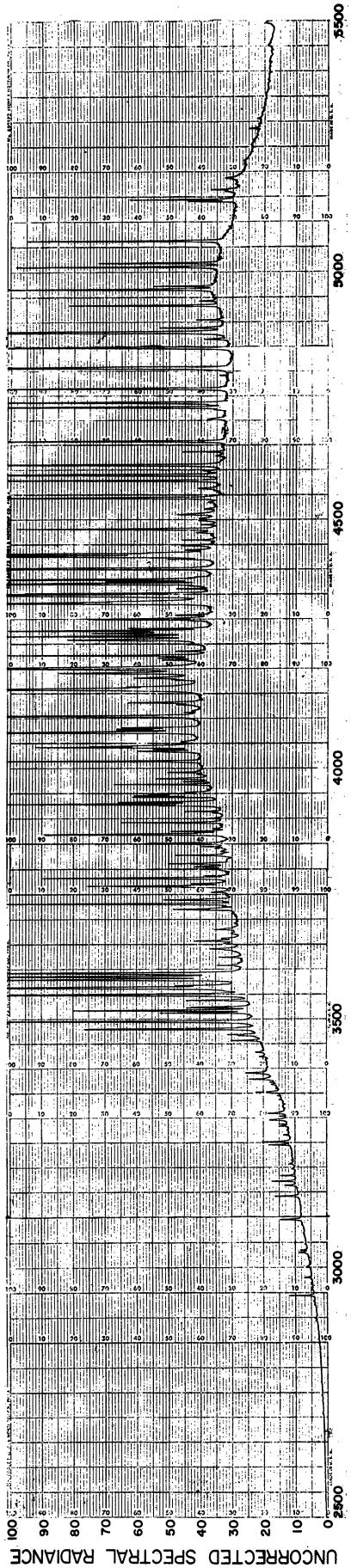

Fig. 19. Uncorrected spectral radiance at arc position no. 7 vs. wavelength for an arc power input of 8.45 kw.

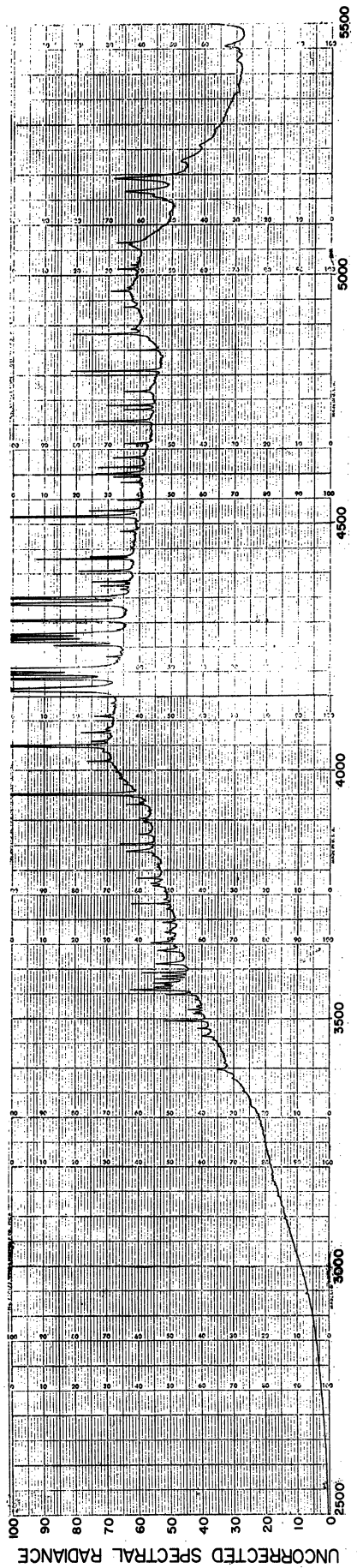

Fig. 20. Uncorrected spectral radiance at arc position no. 12 vs. wavelength for an arc power input of 8.45 kw.

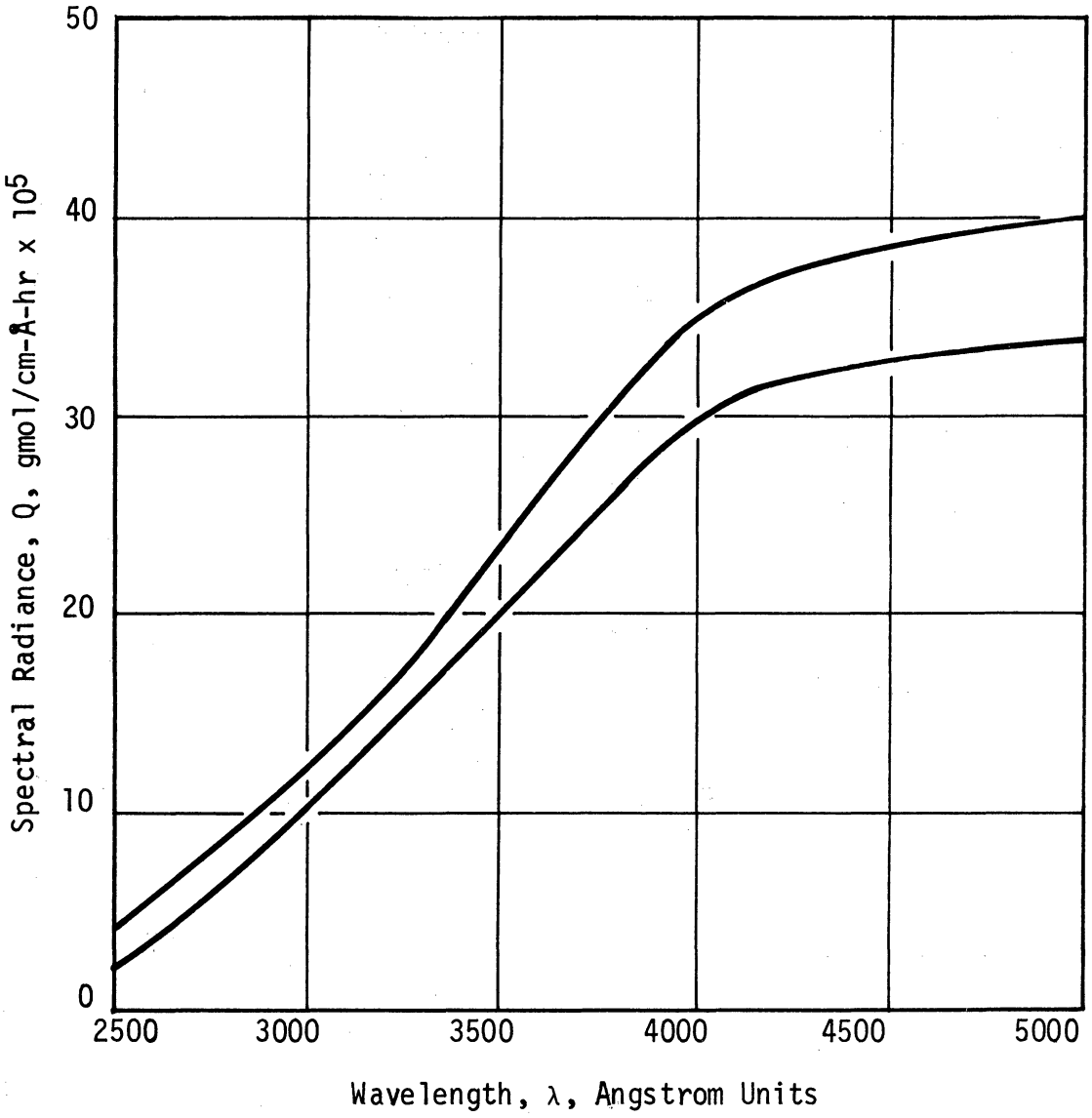

Fig. 21. Spectral radiance of continuum vs. wavelength at positions no. 7 and no. 12 along the arc for operation at 8.45 kw.

position 12 or more generally for regions of the arc not near the cathode, an insignificant fraction of the total radiation emitted was emitted as line radiation.

The variation in the spectral radiance of the arc with arc current (power input) to the light source is shown at several wavelengths in Figs. 22, 23, 24, and 25 corresponding to positions 5, 10, 15, and 20 along the arc.

It is noted that although the spectral radiance is greater in the region of the cathode, the rate of increase of the spectral radiance is greater in the vicinity of the anode. Over the range of power levels and wavelengths investigated, the data shown in Figs. 22, 23, 24, and 25 indicate that a 1% increase in arc current effects a 0.8% increase in spectral radiance near the cathode while the spectral radiance near the anode increases by 2.0%.

7.4 PREDICTION OF THE RATE OF LIGHT ABSORPTION BY REACTANTS

The 3.84 kw spectral output of the light source, shown in Fig. 14, and the light transmission properties of the 1.5 normal potassium nitrate and the 0.05 normal potassium iodide dye solutions, presented in Figs. 9 and 10, respectively, were used to calculate the spectral output of the light source as viewed through each of the dye solutions. The results of these calculations are shown in Fig. 26.

Using the molecular extinction curves for chlorine and sulfur dioxide presented in Figs. 3 and 4, respectively, it was possible to predict the

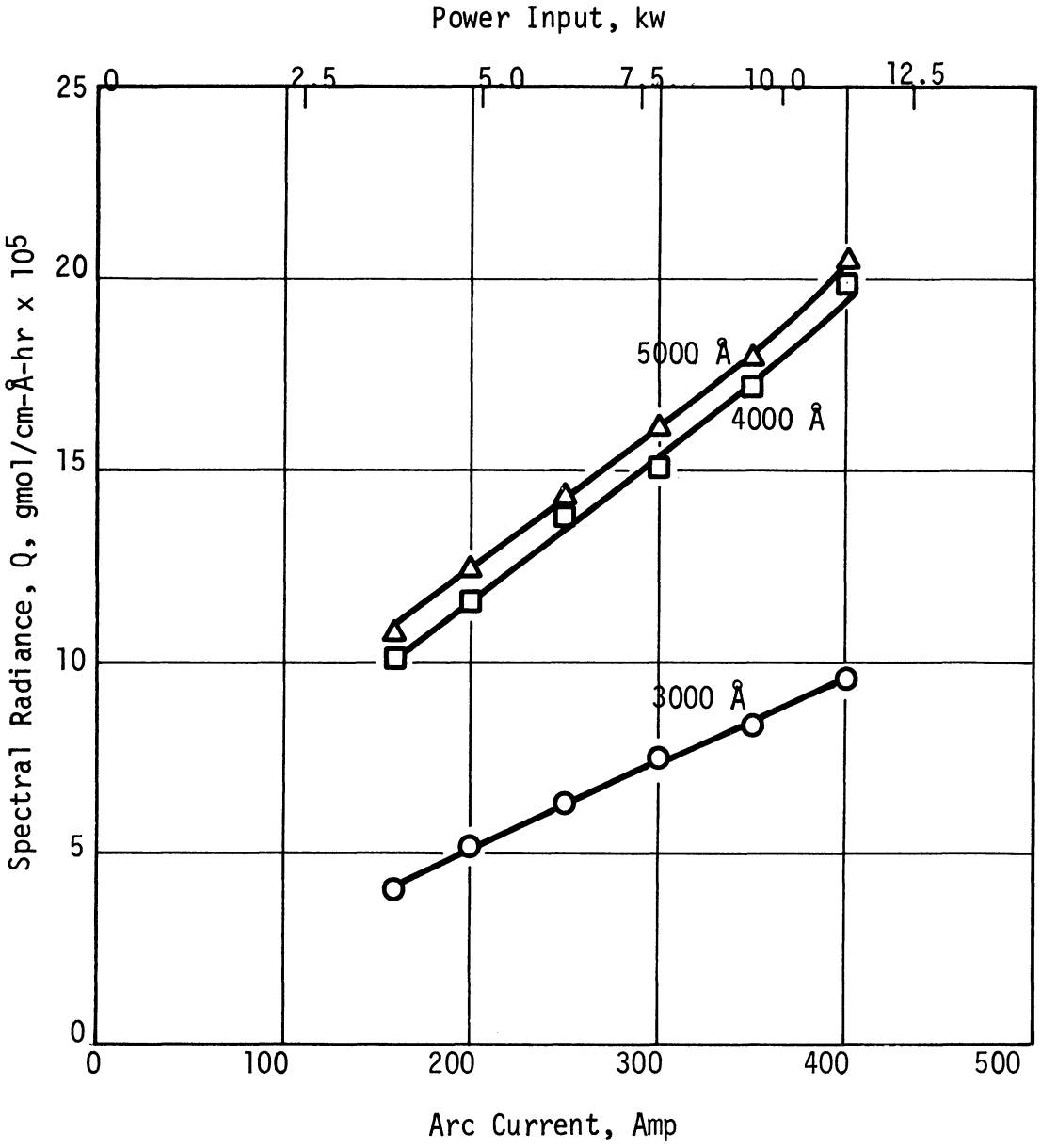

Fig. 22. Variation in spectral radiance with arc current at position no. 5 for several wavelength.

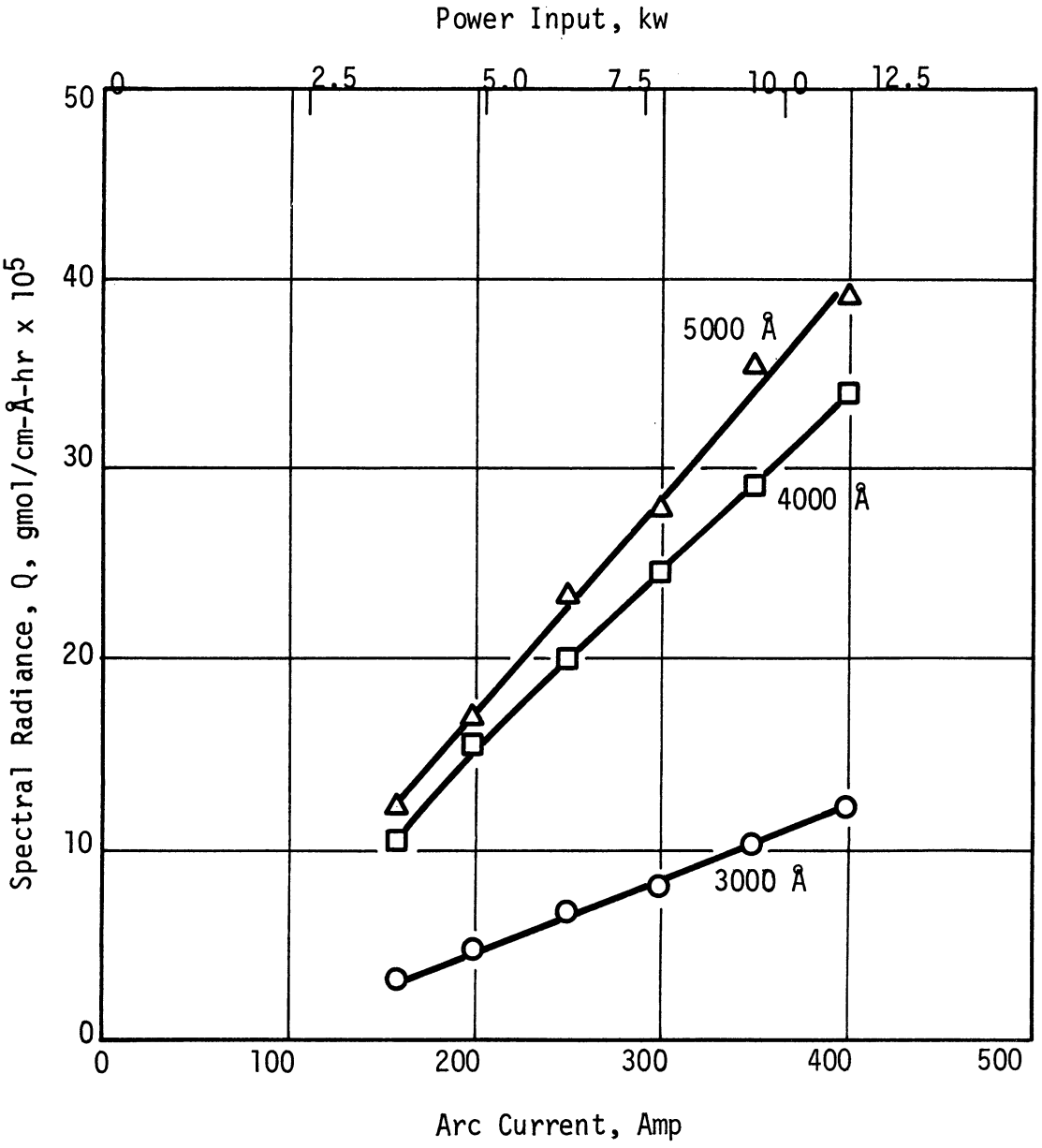

Fig. 23. Variation in spectral radiance with arc current at position no. 10 for several wavelengths.

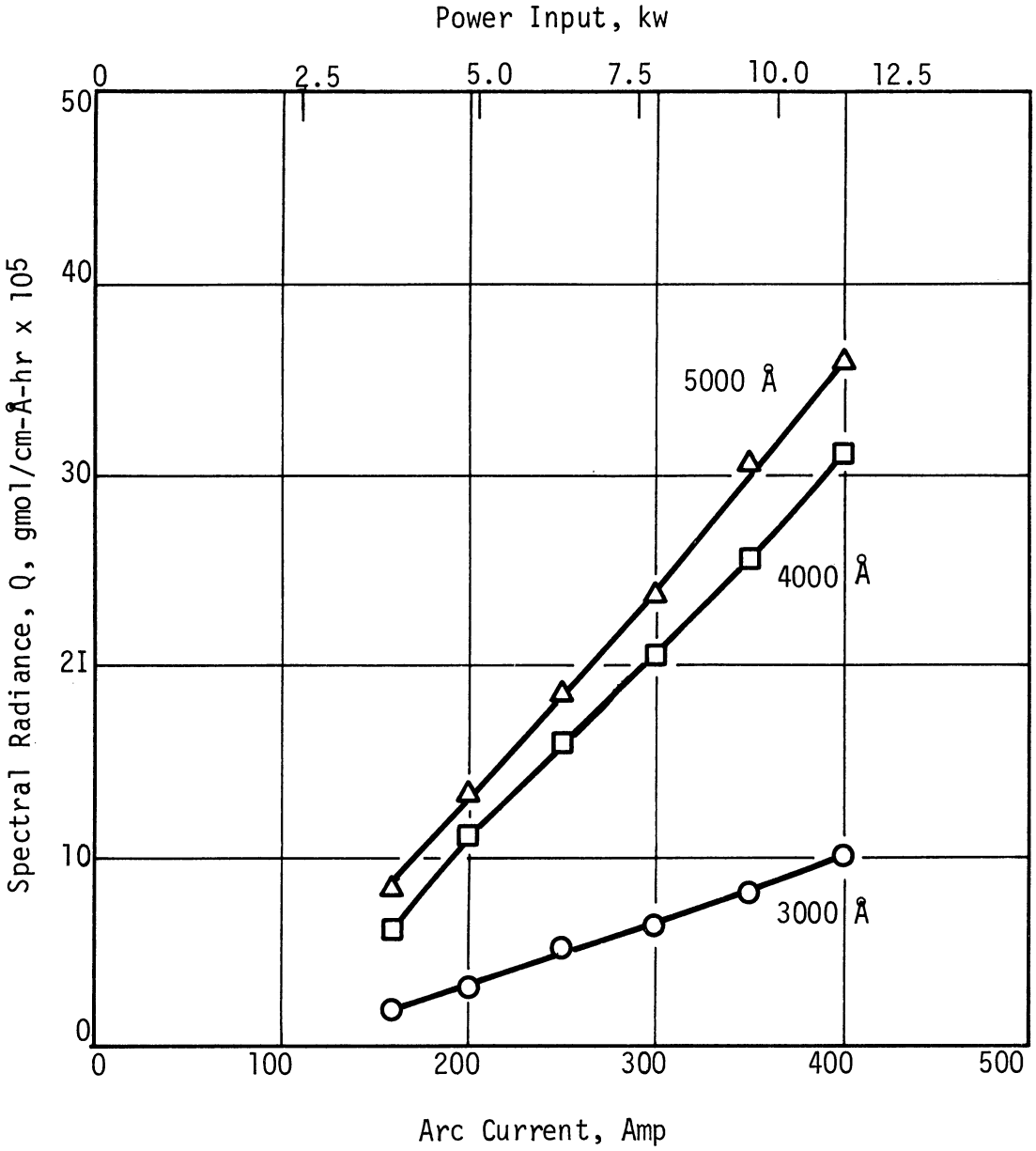

Fig. 24. Variation in spectral radiance with arc current at position no. 15 for several wavelengths.

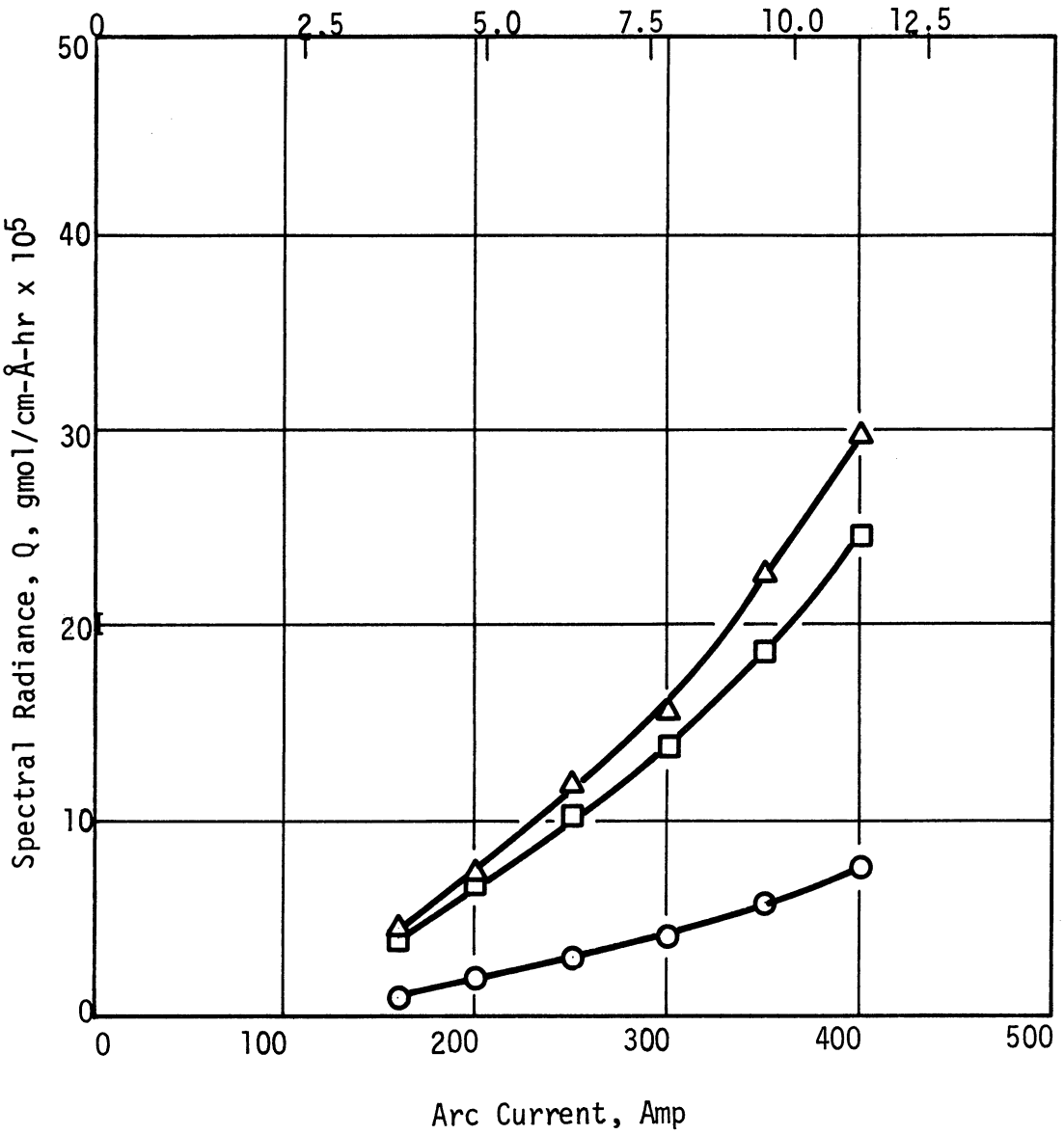

Fig. 25. Variation in spectral radiance with arc current at position no. 20 for several wavelengths.

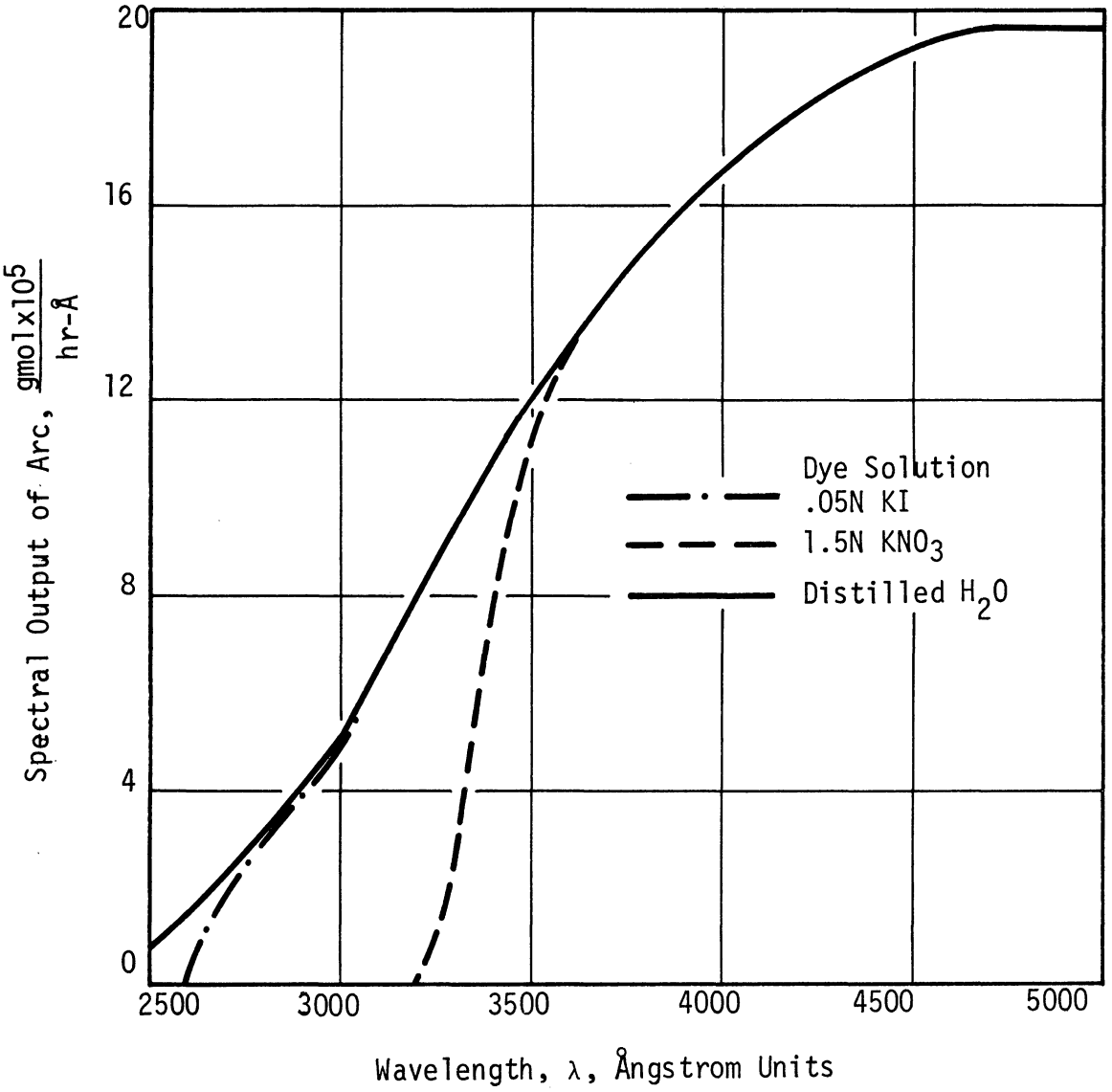

Fig. 26. The 3.84 kw spectral output of arc vs. wavelength.

fraction of the incident light which was absorbed in the reactor volume. The results of these calculations are shown in Fig. 27 for a reactant mixture of 2/3 sulfur dioxide and 1/3 chlorine, in Fig. 28 for an equimolar mixture of sulfur dioxide and chlorine and in Fig. 29 for a reactant mixture of 1/3 sulfur dioxide and 2/3 chlorine.

This information was then combined with the 3.84 kw spectral output of the light source as viewed through each of the dye solutions in order to predict the rate at which light was absorbed by the various reactant mixtures for operation with each of the dye solutions. The rates of light absorption, as a function of the wavelength, are shown in Figs. 29-35 for the various combinations of dye solution and reactant composition. Each figure presents the total predicted rate of light absorption as well as the predicted light absorption which is attributable to sulfur dioxide.

The gram-mole equivalents per hour of photons absorbed by the reactants for each combination of reactant composition and dye solution are obtained by integrating under the curves presented in Figs. 29-35 with respect to wavelength. The results of these calculations are presented in Table I.

TABLE I

PREDICTED GRAM-MOLE EQUIVALENTS OF LIGHT ABSORBED BY REACTANTS PER HOUR

(Ratios are Relative to 1/2 Cl_2, 1/2 SO_2)

Composition / Dye Solution	1/3 Cl_2 2/3 SO_2	1/2 Cl_2 1/2 SO_2	2/3 Cl_2 1/3 SO_2
1.5N KNO_3	.028	.038	.046
(Ratios)	.73	1.00	1.22
.05N KI—Cl_2 Absorption only	.039	.054	066
(Ratios)	.73	1.00	1.23
.05N KI--Total Absorption	.058	.070	.079
(Ratios)	.83	1.00	1.13

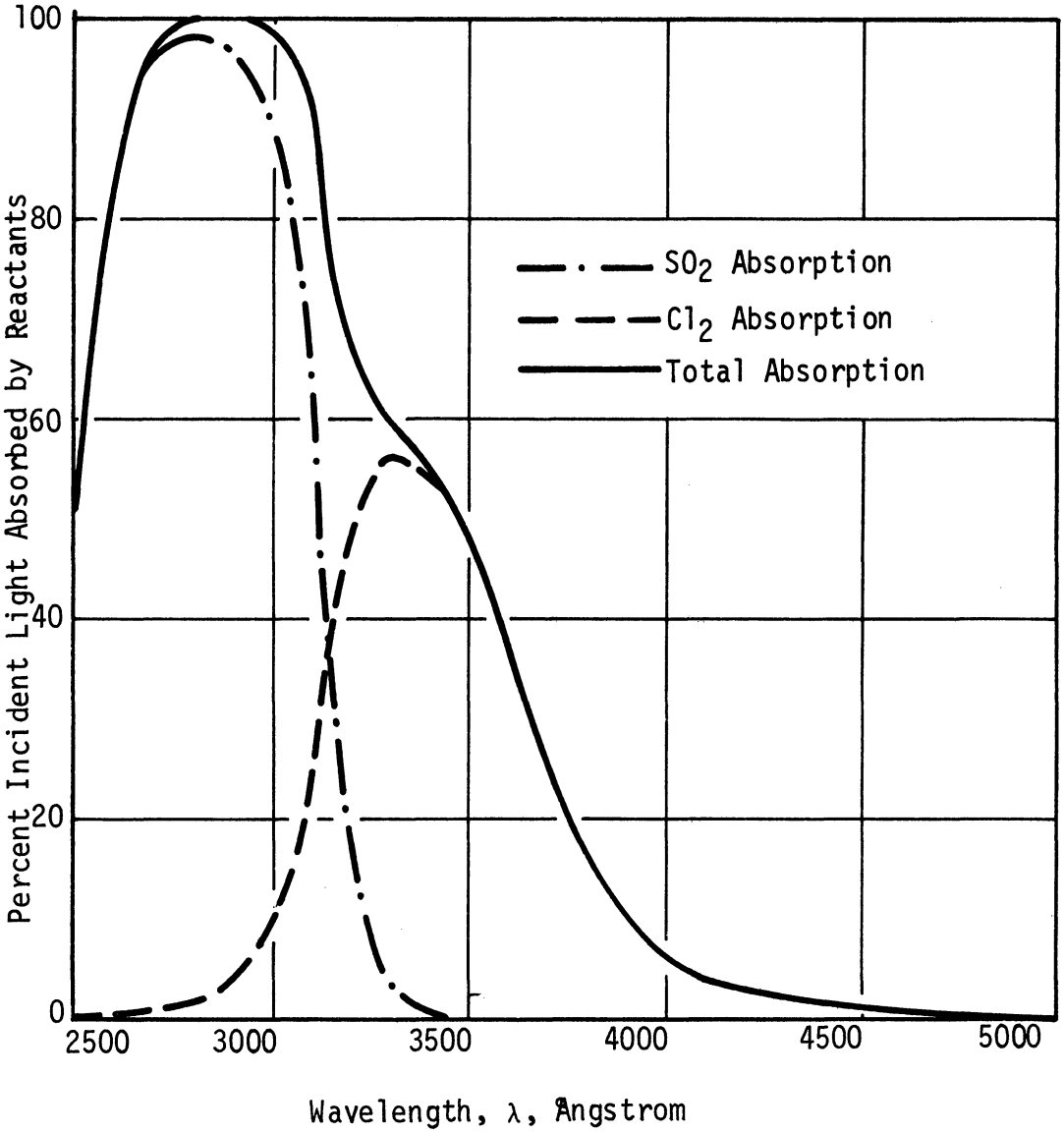

Fig. 27. Percent incident light absorbed vs. wavelength for reactants composition: 1/3 chlorine, 2/3 sulfur dioxide.

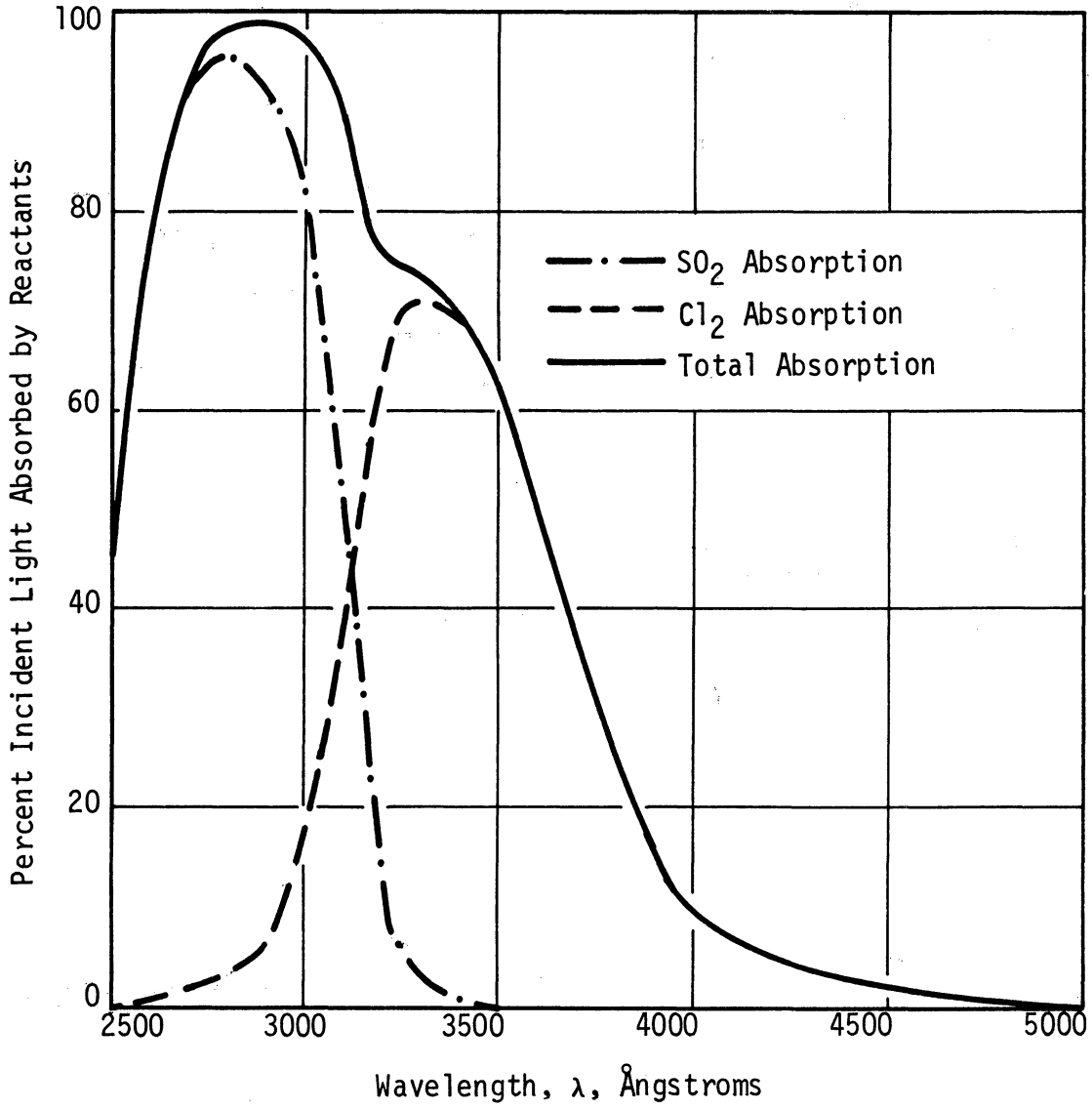

Fig. 28. Percent incident light absorbed vs. wavelength for reactants composition: 1/2 chlorine, 1/2 sulfur dioxide.

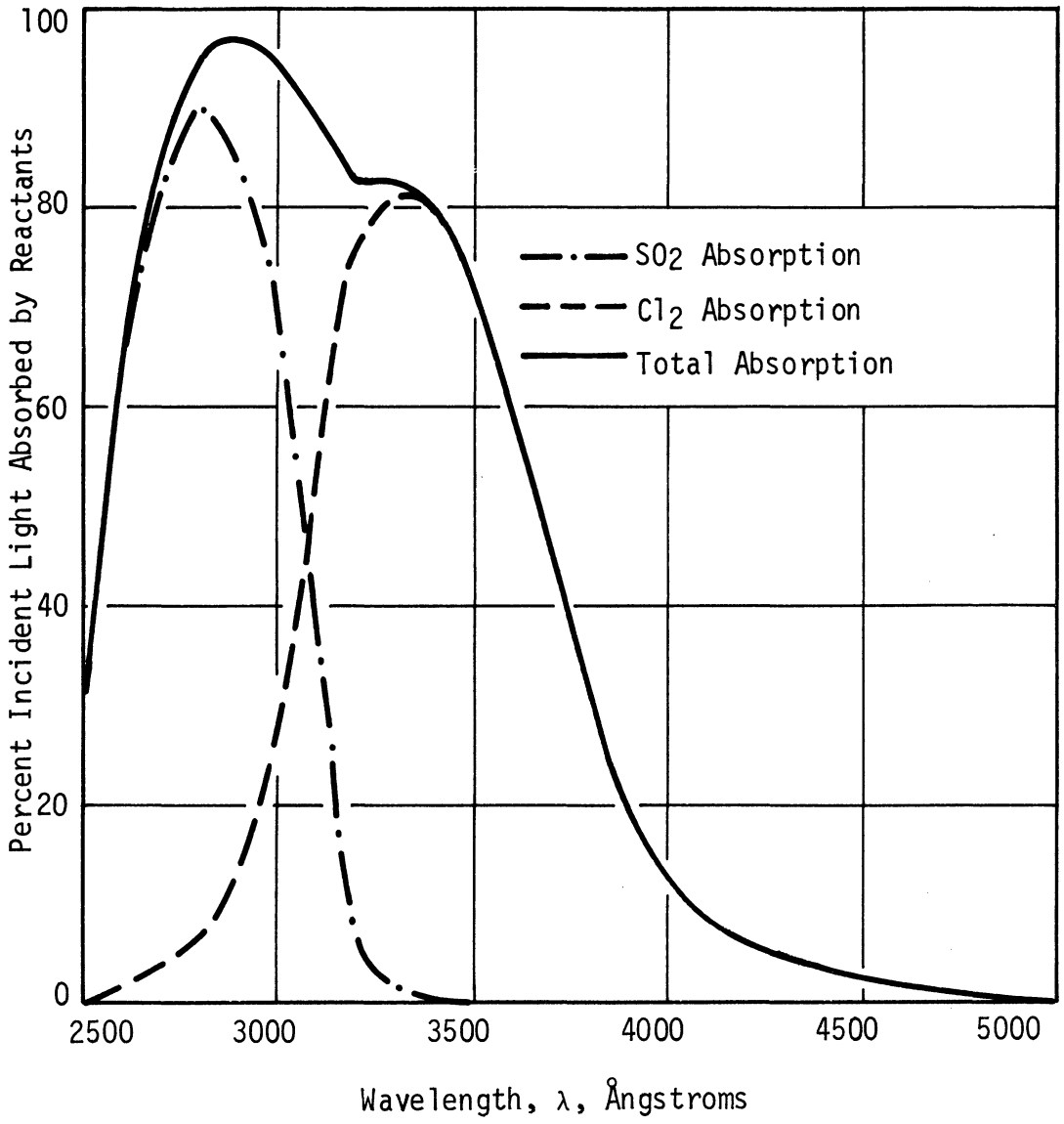

Fig. 29. Percent incident light absorbed vs. wavelength for reactants composition: 2/3 chlorine, 1/3 sulfur dioxide.

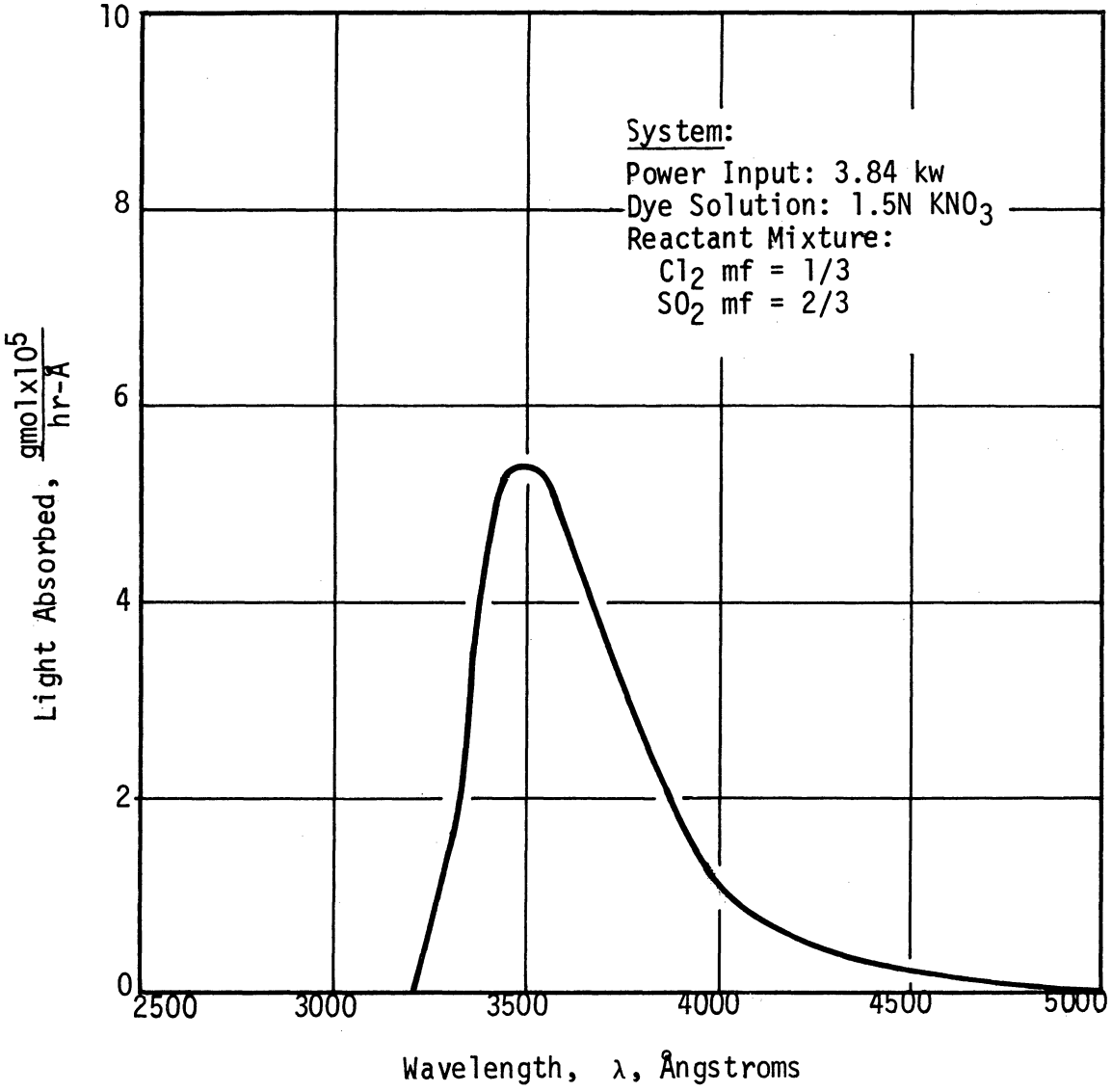

Fig. 30 Light absorbed by reactants vs. wavelength for reactants composition: 1/3 chlorine, 2/3 sulfur dioxide, while using KNO_3 dye solution.

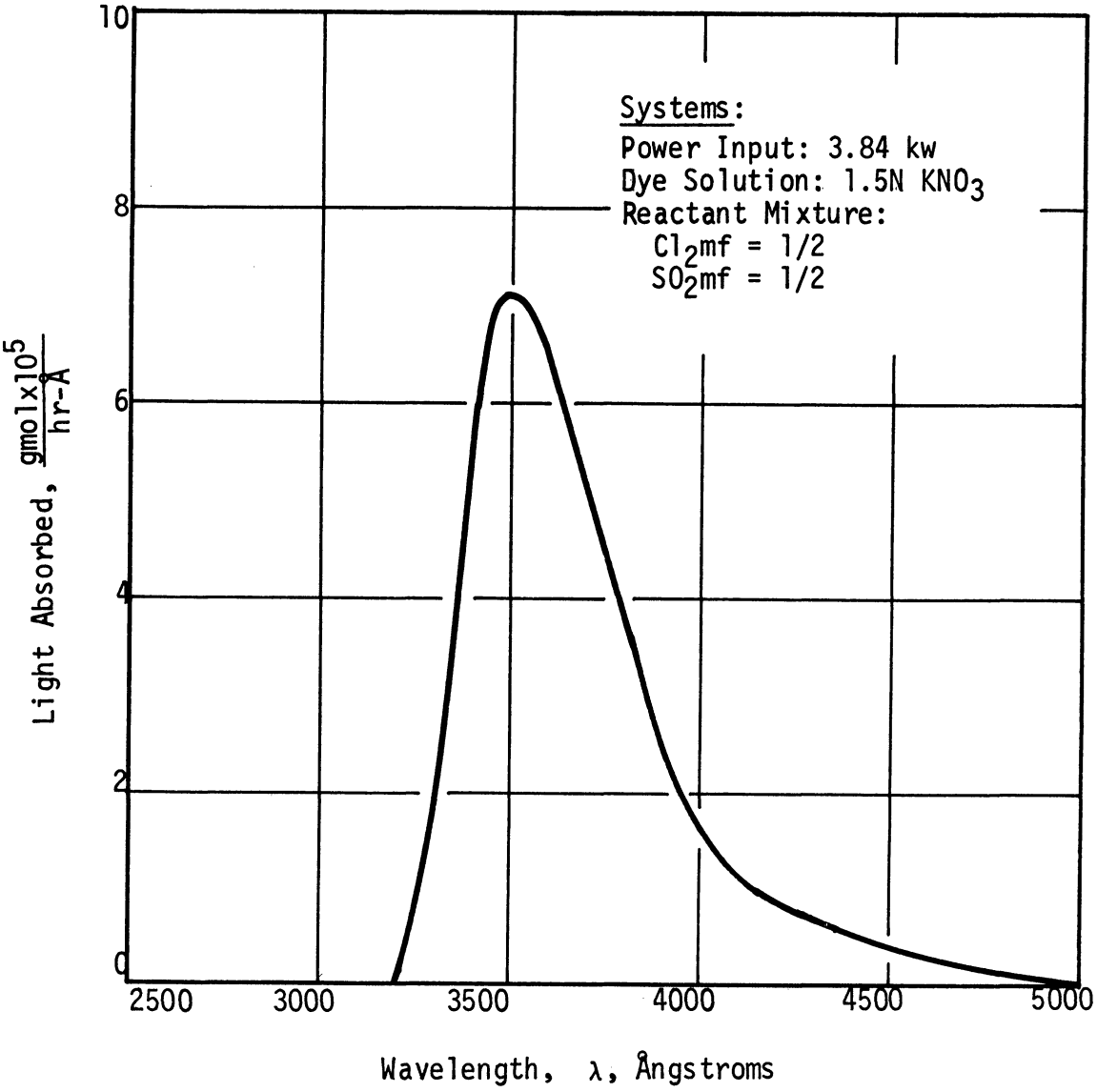

Fig. 31. Light absorbed by reactants vs. wavelength for reactants composition: 1/2 chlorine, 1/2 sulfur dioxide, while using KNO_3 dye solution.

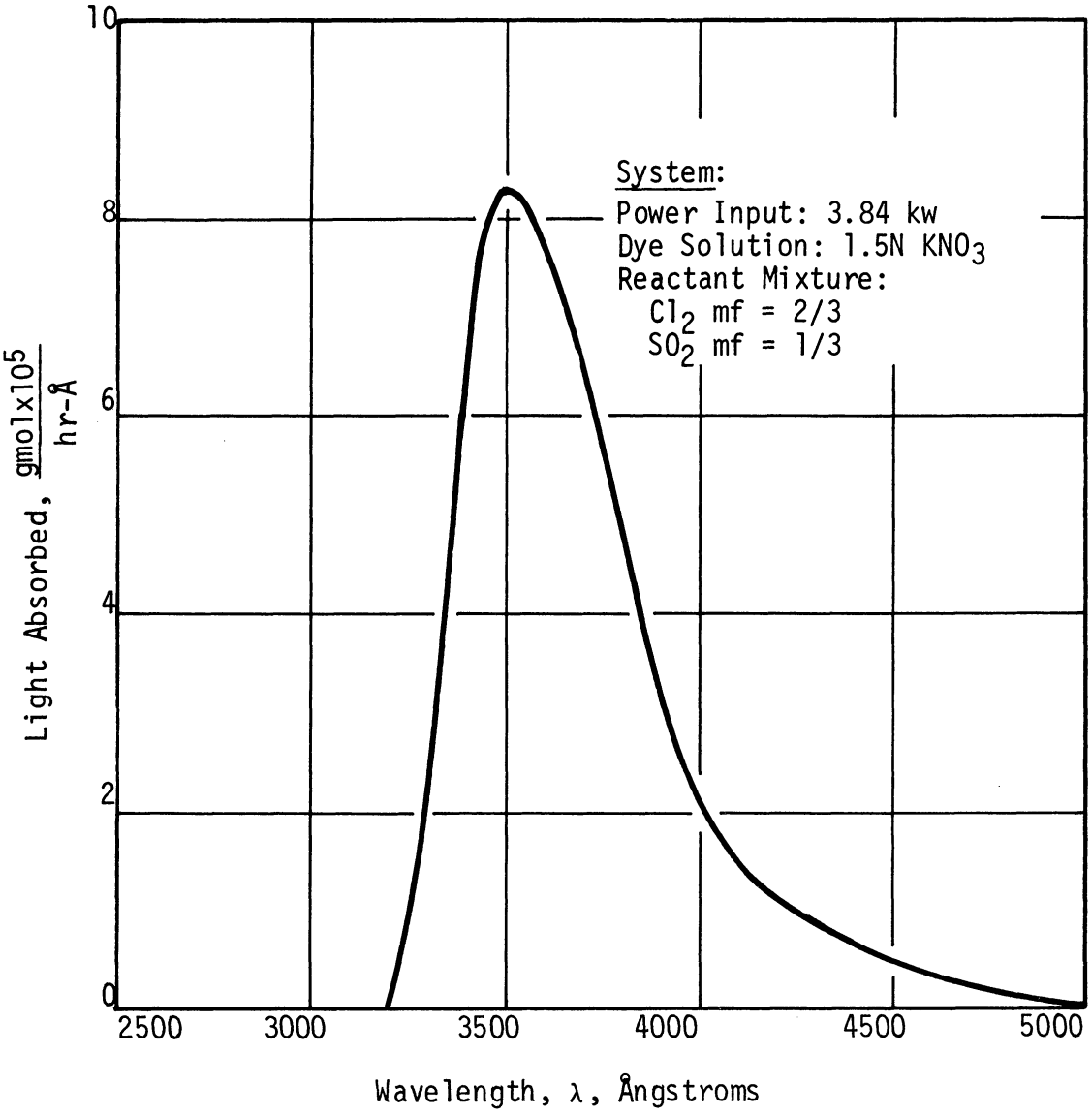

Fig. 32. Light absorbed by reactants vs. wavelength for reactants composition: 2/3 chlorine, 1/3 sulfur dioxide, while using KNO_3 dye solution.

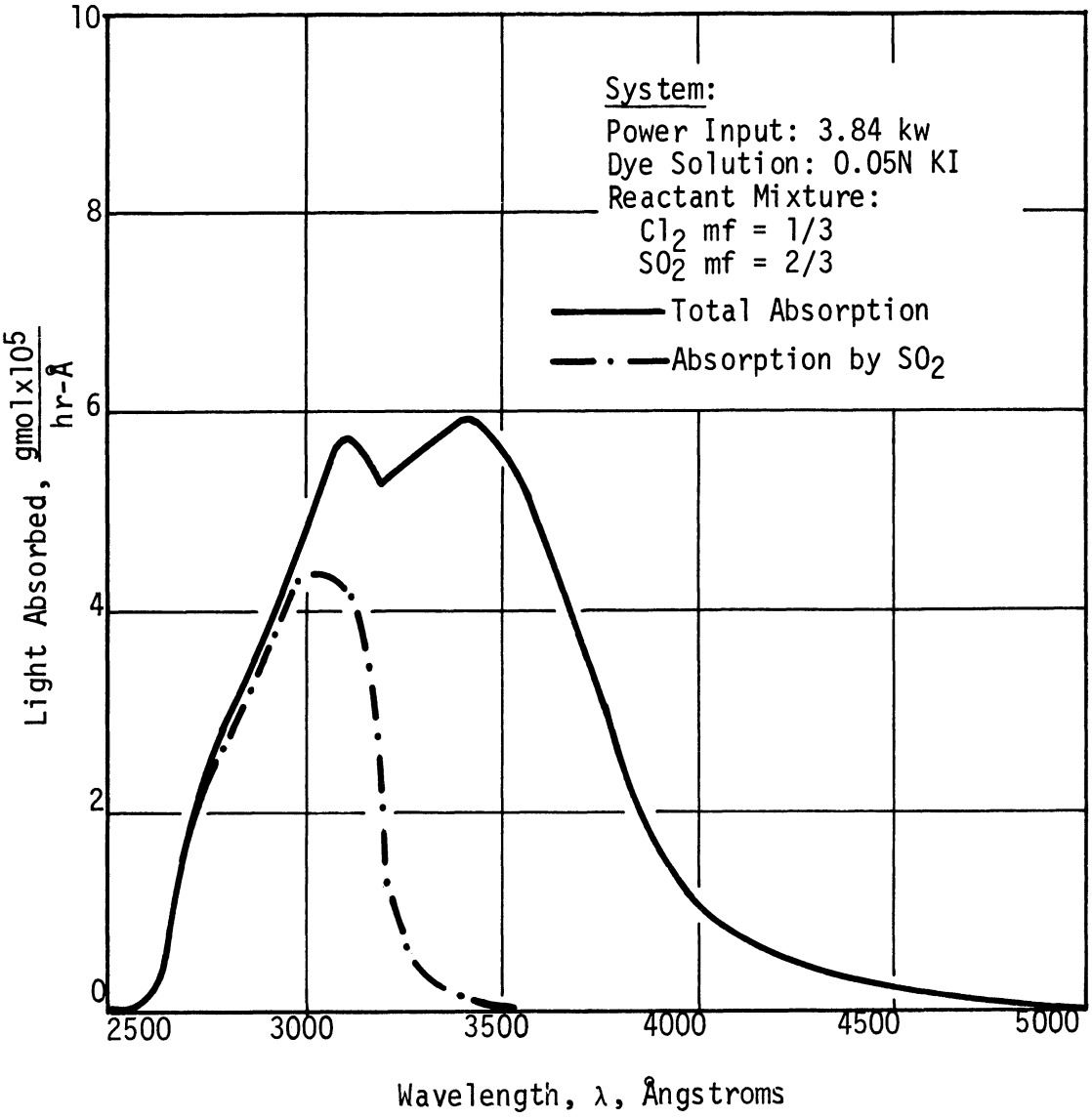

Fig. 33. Light absorbed by reactants vs. wavelength for reactants composition: 1/3 chlorine, 2/3 sulfur dioxide, while using KI dye solution.

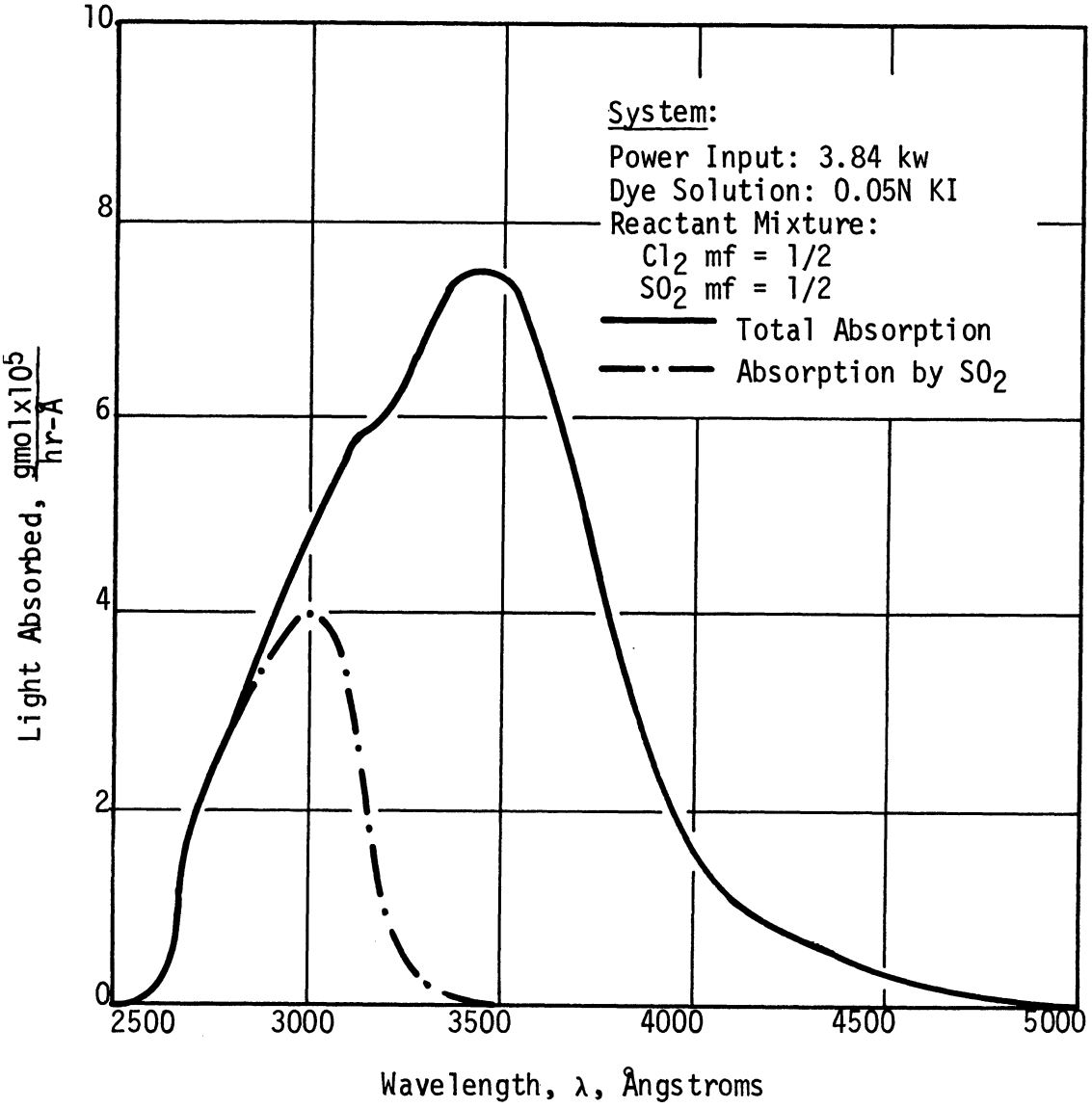

Fig. 34. Light absorbed by reactants vs. wavelength for reactants composition: 1/2 chlorine, 1/2 sulfur dioxide, while using KI dye solution.

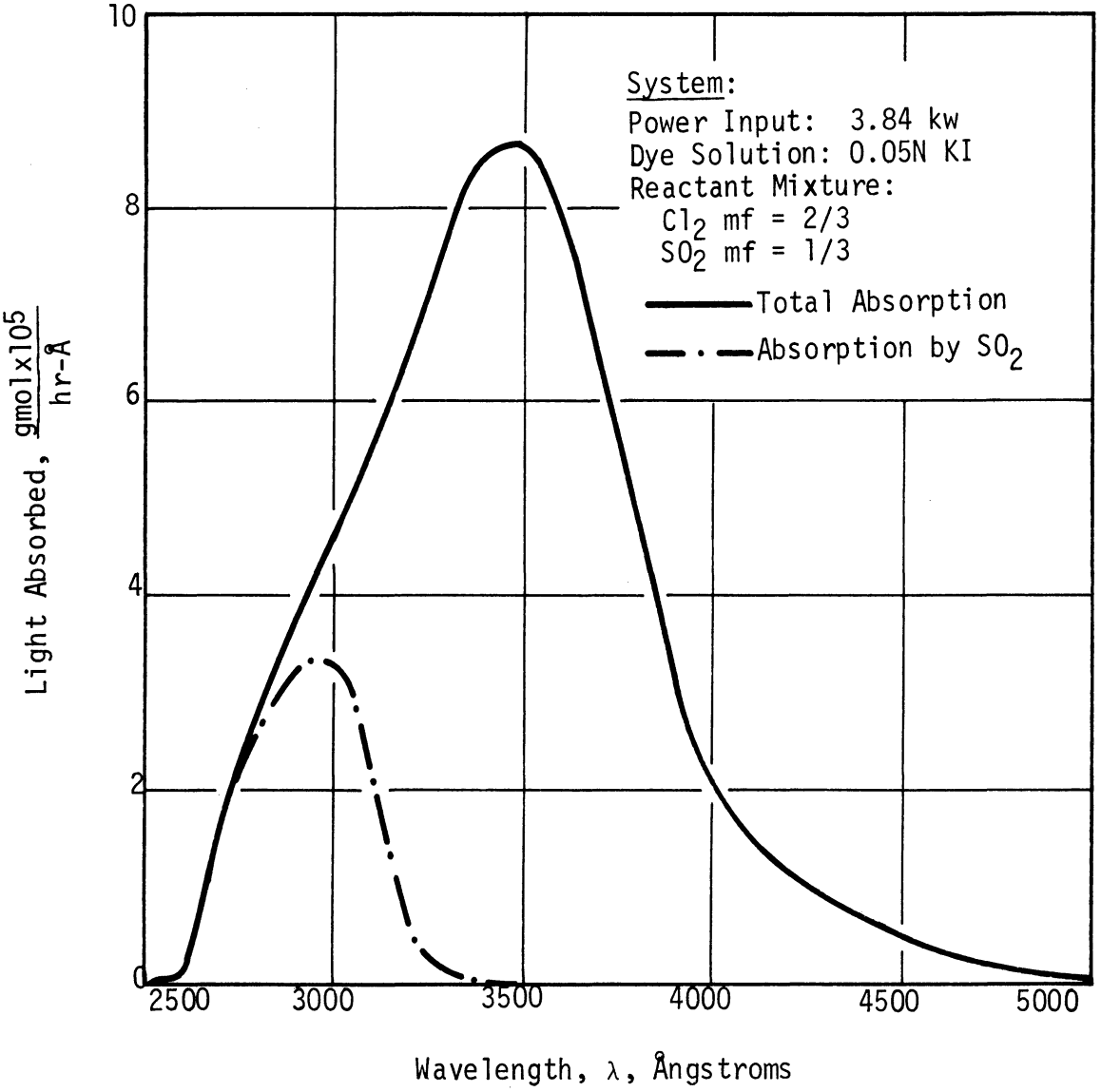

Fig. 35. Light absorbed by reactants vs. wavelength for reactants composition: 2/3 chlorine, 1/3 sulfur dioxide, while using KI dye solution.

8. ANALYSIS OF CHEMICAL REACTION DATA

8.1 GENERAL

The photochlorination of sulfur dioxide was investigated at a function of light intensity, reactant mixture composition, flowrate of reactants, temperature, pressure, and the wavelength of the light absorbed. Experimental data were analyzed using both a qualitative and a quantitative approach.

8.2 QUALITATIVE ANALYSIS

The reaction system used in this investigation was a nonisothermal, annular flow reactor with a nonconstant light flux along the reactor length. Such a system typically presents some difficulty in the presentation of experimental observations. For purposes of qualitative analysis it is of value to develop a logical method for the graphical presentation of experimental observations.

A computer oriented data analysis suggests the following rate expression for the photochemical reaction:

$$\frac{d[SO_2Cl_2]}{dt} = J - k[SO_2Cl_2]\sqrt{\frac{J}{[SO_2]}} \qquad (8.1)$$

where J is the volumetric rate of light absorption.

Letting (1+a) represent the ratio of the total concentration to the sulfur dioxide concentration in the feed stream, and letting G_o equal the molar feed rate, the above equation may be rewritten in terms of

the fractional conversion of sulfur dioxide, x, and the linear position along the reactor, z:

$$\frac{G_o}{A(1+a)}\left(\frac{dx}{dz}\right)_{G_o} = J - k\sqrt{\frac{J\cdot P}{RT(1+a-x)(1-x)}}\;x \qquad (8.2)$$

For qualitative purposes, at low fractional conversion, J and the term $k/\sqrt{RT}$ can be replaced by their mean values, J_m and k_m, respectively. The transformed rate equation is:

$$\frac{G_o}{A(1+a)}\left(\frac{dx}{dz}\right)_{G_o} = J_m - k_m\sqrt{\frac{PJ_m}{(1+a)}}\;x \qquad (8.3)$$

Integrating over the reactor length at constant feed rate yields:

$$\frac{A(1+a)L}{G_o} = \int_o^{x_o}\frac{dx}{J_m - k_m\sqrt{\frac{PJ_m}{(1+a)}}\;x} = \sqrt{\frac{(1+a)}{PJ_m}}\cdot\frac{1}{k_m}\,\ell n\left\{\frac{1}{1-k_m\sqrt{\frac{P}{J_m(1+a)}}\;x_o}\right\} \qquad (8.4)$$

Solving for x_o:

$$x_o = \sqrt{\frac{J_m(1+a)}{P\,k_m^2}}\left(1-e^{-\frac{k_m J_m^{1/2}P^{1/2}(1+a)^{1/2}AL}{G_o}}\right) \qquad (8.5)$$

Equation (8.4) can be used to define x_{eff}, the effective value of the fractional conversion:

$$\frac{A(1+a)L}{G_o} = \int_o^{x_o}\frac{dx}{J_m - k_m\sqrt{\frac{PJ_m}{(1+a)}}\;x} = \frac{x_o}{J_m - k_m\sqrt{\frac{PJ_m}{(1+a)}}\;x_{eff}} \qquad (8.6)$$

The variable x_o can be eliminated between Eqs. (8.4) and (8.6) to yield x_{eff} as a function of G_o:

$$x_{eff} = \sqrt{\frac{J_m(1+a)}{P\,k_m^2}} - \frac{G_o}{k_m^2 PAL}\left(1 - e^{-\frac{k_m J_m^{1/2} P^{1/2}(1+a)^{1/2} AL}{G_o}}\right) \qquad (8.7)$$

This expression can be rewritten in integral form as:

$$x_{eff} = \sqrt{\frac{(1+a)J_m}{P}}\,\frac{G_o}{k_m}\int_o^{1/G_o}\left(1-e^{-\frac{k_m J_m^{1/2} P^{1/2}(1+a)^{1/2} AL}{G_o}}\right) d(1/G_o) \qquad (8.8)$$

or alternatively, it can be written in the form:

$$x_{eff} = G_o \int_o^{1/G_o} x_o\, d(1/G_o) \qquad (8.9)$$

If no serious errors are involved in the above assumptions, a plot of the rate of production of sulfuryl chloride, $G_o x_o/(1+a)$, vs. x_{eff} should be a straight line. In such a case, the intercept at $x_{eff} = 0$ would be:

$$J_m V = \int_o^V J\,dV \qquad (8.10)$$

and the slope of the line would be:

$$\sqrt{\frac{PJ_m}{(1+a)}}\,k_m V = \sqrt{\frac{P}{R(1+a)}}\int_o^{V_k}\sqrt{\frac{J}{T}}\,dV \qquad (8.11)$$

Figure 36 shows the exit conversions for a typical set of experimental runs as a function of the inverse of the molar reactant feed rate. The data corresponds to operation of the light source at 3.84 kw while using 1.5 normal potassium nitrate dye solution. The feed stock consisted of an equimolar mixture of sulfur dioxide and chlorine.

The value of x_{eff} corresponding to each of the experimental points was obtained by graphically performing the integration indicated in

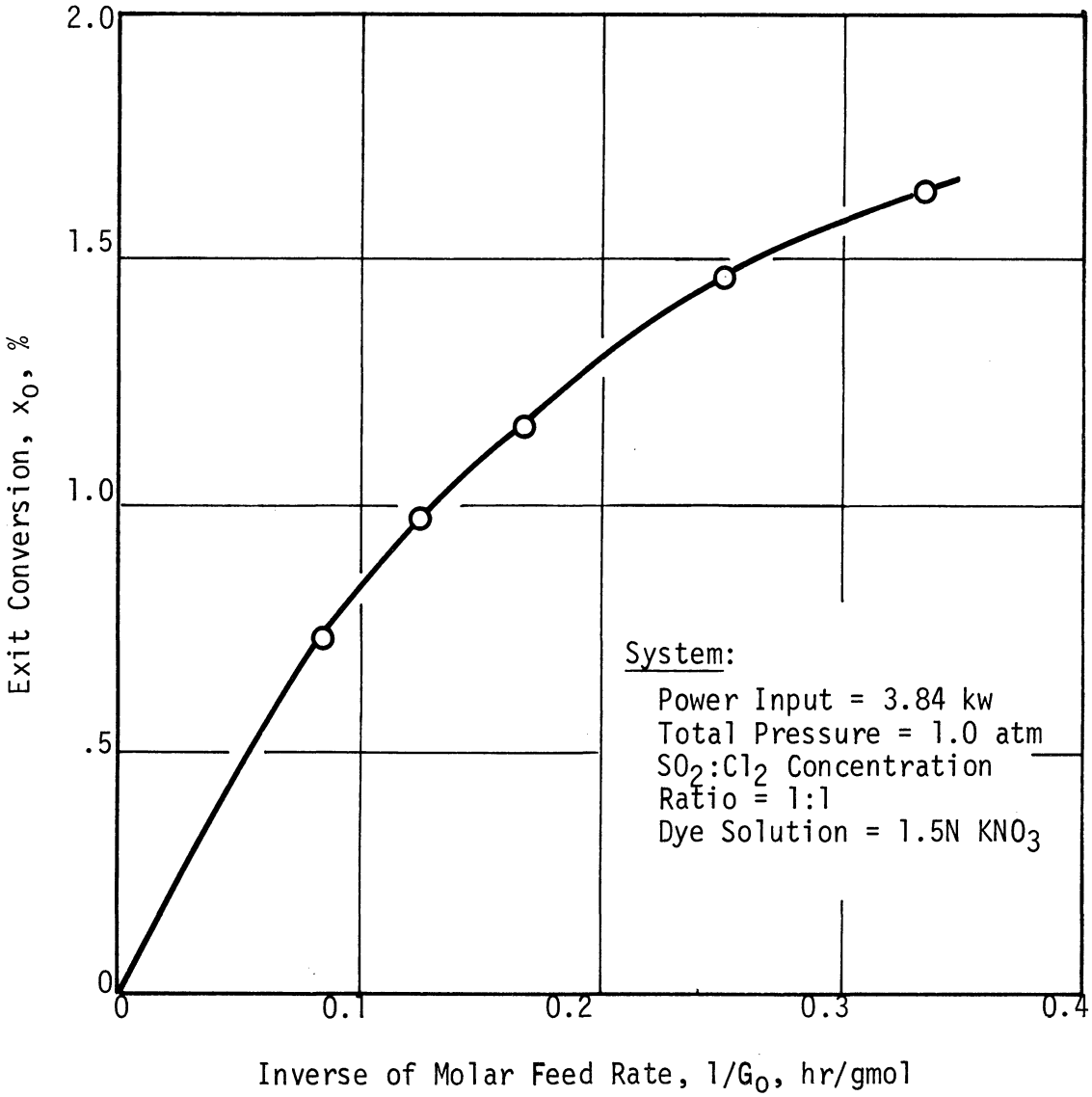

Fig. 36. Exit conversion of sulfur dioxide vs. the inverse of the molar feed rate.

Eq. (8.9). In Fig. 37, the experimental rates of production of sulfuryl chloride are shown as a function of the corresponding calculated values of x_{eff}. The extrapolated intercept of the plot of sulfuryl chloride production vs. x_{eff} is 0.053 gmol/hr.

The consistency of the experimental information shown in Figs. 36 and 37 indicates that no serious errors were involved in making the above assumptions relative to the rate equation.

8.3 EFFECT OF SULFUR DIOXIDE CONCENTRATION

In Eq. (8.1) it was stated that the rate of the forward reaction was dependent only upon the rate at which light was absorbed by the reactants while the rate of the reverse reaction was proportional to the inverse square root of the sulfur dioxide concentration.

To investigate these dependencies a series of experimental runs was made with a number of sulfur dioxide concentrations in the range 1/6 to 2/3 atm partial pressure. Throughout the series the light source was operated at a power input of 3.84 kw using 1.5 normal potassium nitrate as the dye solution. The chlorine concentration in the feed stream was maintained at a constant value of 1/3 atm during all runs. Through the addition of argon, the total pressure of the reactant mixture was maintained at 1 atm.

In order to develop a convenient method for the presentation of the experimental data consider again Eq. (8.1). If it is assumed that within an experimental run the concentration of sulfur dioxide remains rela-

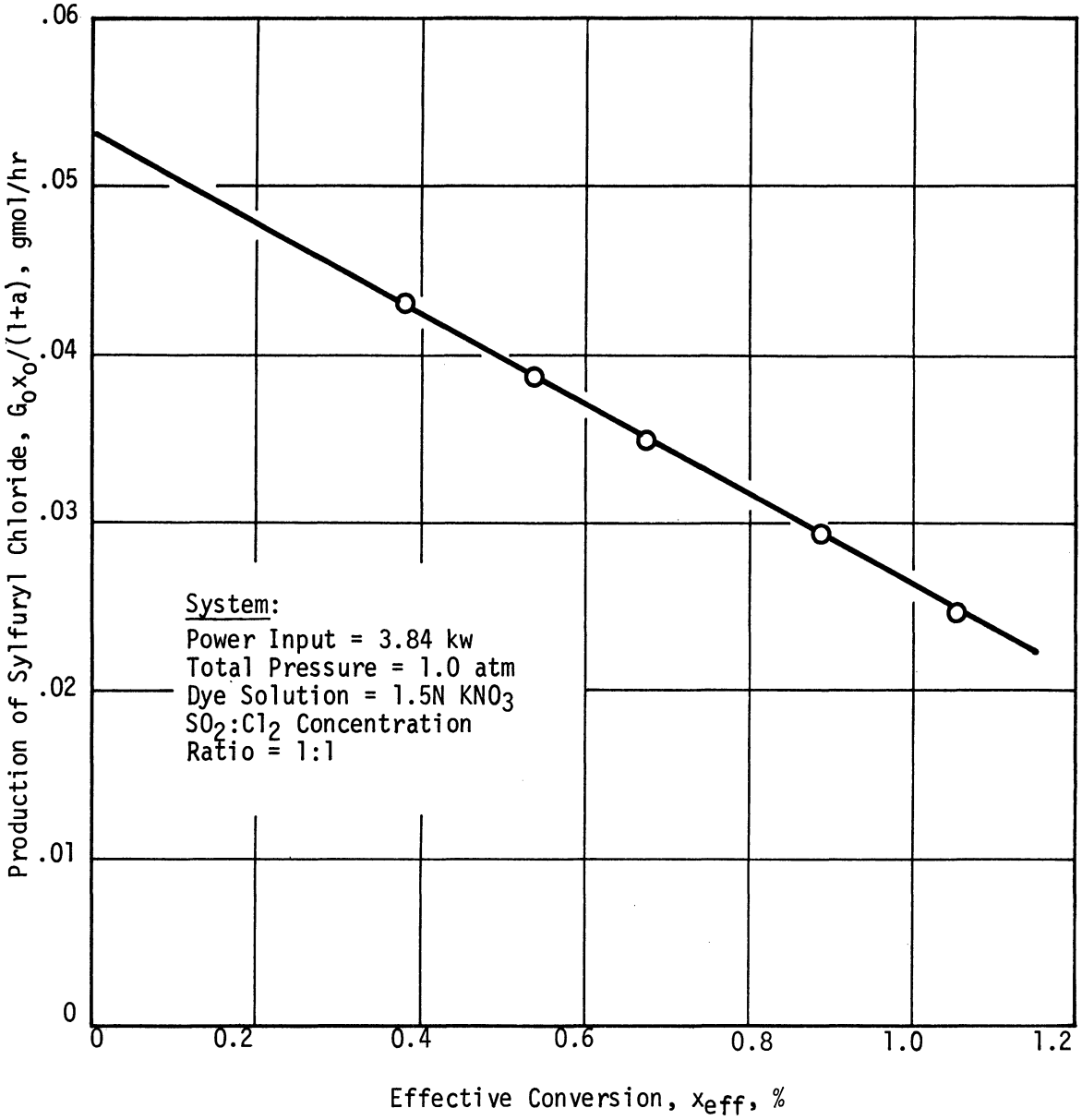

Fig. 37. Rate of production of sulfuryl chloride vs. effective conversion.

tively constant, the following new variables can be defined:

$$x' = \frac{x_o}{(1+a)^{1/2}} \tag{8.12}$$

$$G' = \frac{G_o}{(1+a)^{1/2}} \tag{8.13}$$

In terms of the new variables, Eq. (8.2) can be rewritten:

$$\frac{G'}{A}\left(\frac{dx'}{dz}\right)_{G'} = J - k\sqrt{\frac{J \cdot P}{RT}}\ x' \tag{8.14}$$

Making the same assumptions as in the earlier development, one obtains for the rate of production of sulfuryl chloride:

$$\frac{G_o x_o}{(1+a)} = G'x' = J_m - k_m\sqrt{J_m P}\ x'_{eff} \tag{8.15}$$

where x'_{eff} is defined according to:

$$x'_{eff} = G' \int_o^{1/G'} x' d\left(\frac{1}{G'}\right) \tag{8.16}$$

Figure 38 presents the experimentally determined exit conversion variables, x', for the series of runs, as a function of the corresponding value of the inverse feed rate variable, 1/G'. The data corresponds to operation of the light source at 3.84 kw while using 1.5 normal potassium nitrate dye solution. Data are presented for eight different sulfur dioxide partial pressures in the range 1/6 to 2/3 atm. Although there is a considerable amount of scatter in the data, there is no noticeable trend which can be correlated with the variation in sulfur dioxide partial pressure between the individual runs.

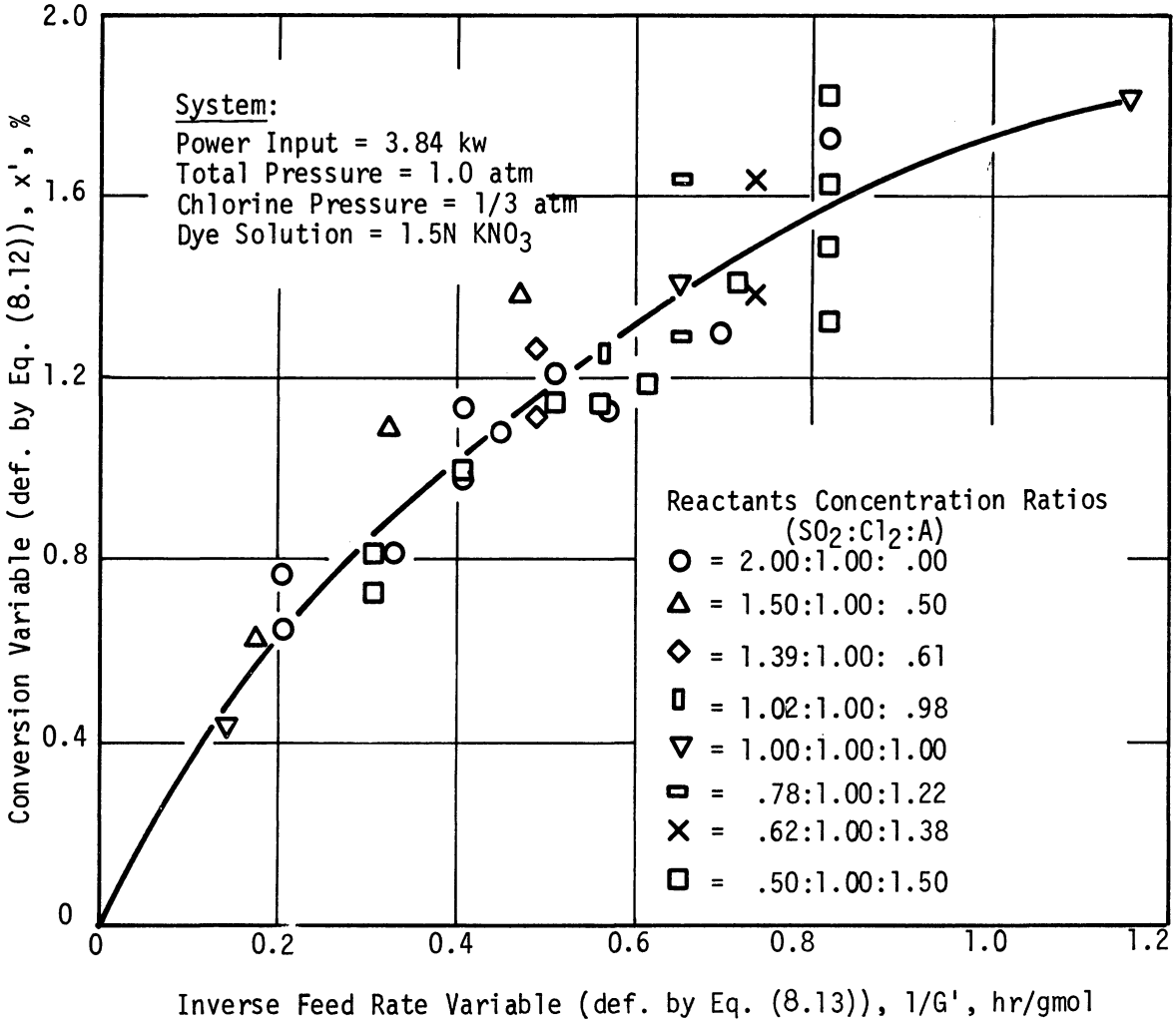

Fig. 38. Conversion variable vs. inverse feed rate variable for several partial pressures of sulfur dioxide while using KNO_3 dye solution.

According to the definition given in Eq. (8.16), the value of x'_{eff} corresponding to each of the experimental points was calculated. In Fig. 39, the rates of production of sulfuryl chloride are shown as a function of the corresponding calculated values of x'_{eff}. The extrapolated intercept of the plot corresponds to a production rate of 0.037 gmol/hr of sulfuryl chloride at zero conversion.

8.4 EFFECT OF TOTAL PRESSURE

Equation (8.1) suggests that the rates of the forward and reverse reactions are not dependent on the total pressure of the reactant mixture.

The validity of this statement was investigated in a series of experimental runs with varying total pressure. Runs were made at 1.0, 1.5, and 2.0 atm total pressure, while maintaining the partial pressures of chlorine and sulfur dioxide each constant at 0.5 atm. Through the addition of argon, the total pressure of the reactant mixture was increased to the desired value. Throughout the series of experiments the light source was operated at a power input of 3.84 kw using 1.5 normal potassium nitrate as the dye solution.

In order to develop a convenient method for the presentation of the experimental data consider again Eq. (8.1). It is convenient to define a new flowrate variable:

$$G'' = \frac{G_o}{P} \qquad (8.17)$$

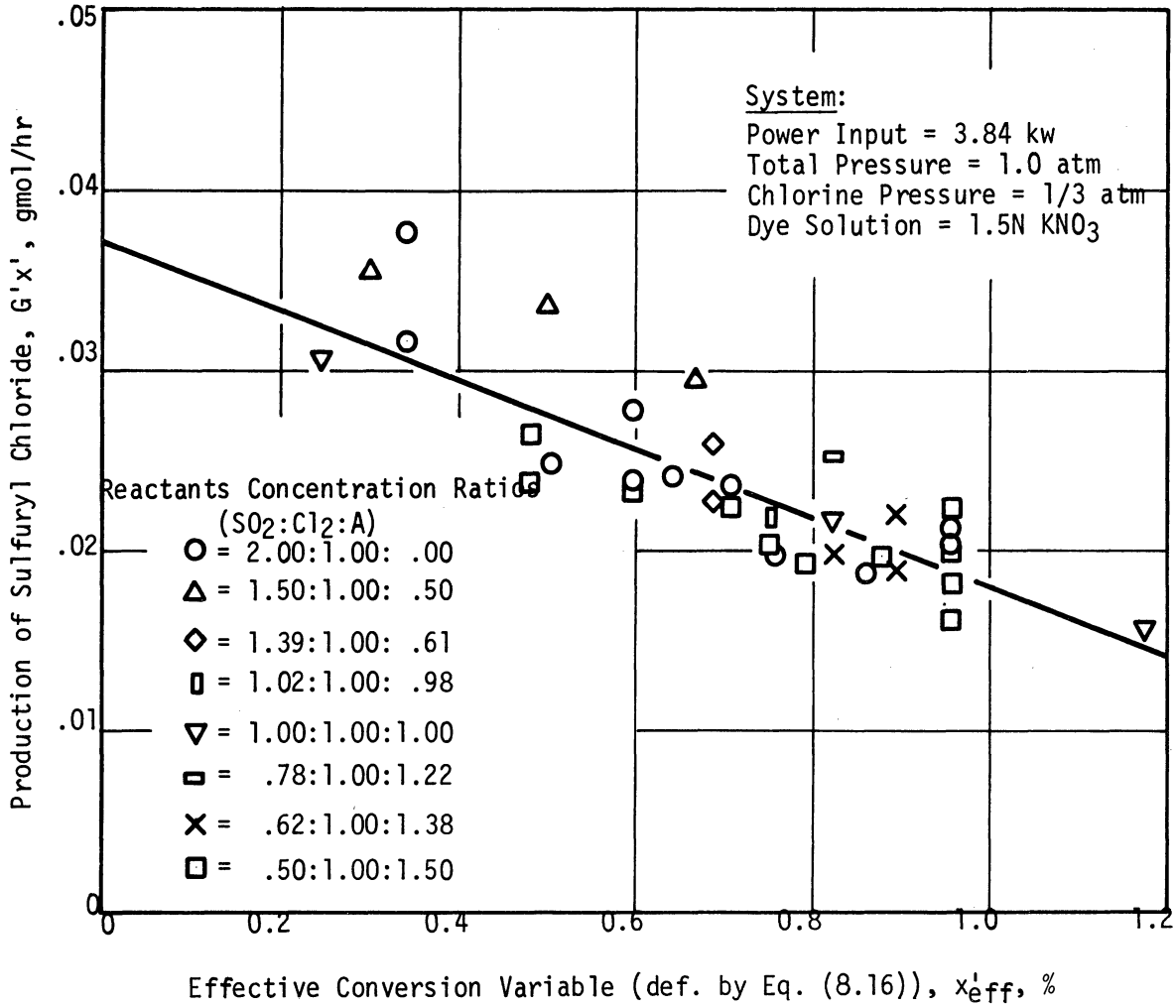

Fig. 39. Rate of production of sulfuryl chloride vs. effective conversion variable for several partial pressures of sulfur dioxide.

Making the standard assumptions discussed above, Eq. (8.2) can be re-written in terms of G":

$$\frac{G''P}{(1+a)}\left(\frac{dx}{dz}\right)_{G''} = J - k\sqrt{\frac{J\cdot P}{RT(1+a-x)(1-x)}}\,x \qquad (8.8)$$

where it is noted that:

$$P_{SO_2} = \left(\frac{P}{(1+a)}\right) \qquad (8.19)$$

Proceeding in a manner analagous to the above development, the rate of production of sulfuryl chloride is given by:

$$\frac{P}{(1+a)}\,G''x_o = J_m - k_m\sqrt{\frac{PJ_m}{(1+a)}}\,x''_{eff} \qquad (8.20)$$

where x''_{eff} is defined according to:

$$x''_{eff} = G''\int_0^{1/G''} x_o\,d\left(\frac{1}{G''}\right) \qquad (8.21)$$

Figure 40 presents the experimentally determined exit conversions, x_o, for the series of runs, as a function of the corresponding values of the inverse of the flowrate variable, G".

The data corresponding to the various values of the total pressure are adequately described by a single curve which confirms the fact that neither the forward nor the reverse rates are affected by the total pressure of the reactant mixture.

According to the definition given in Eq. (8.21), the value of x'_{eff} corresponding to each of the experimental points was calculated. In

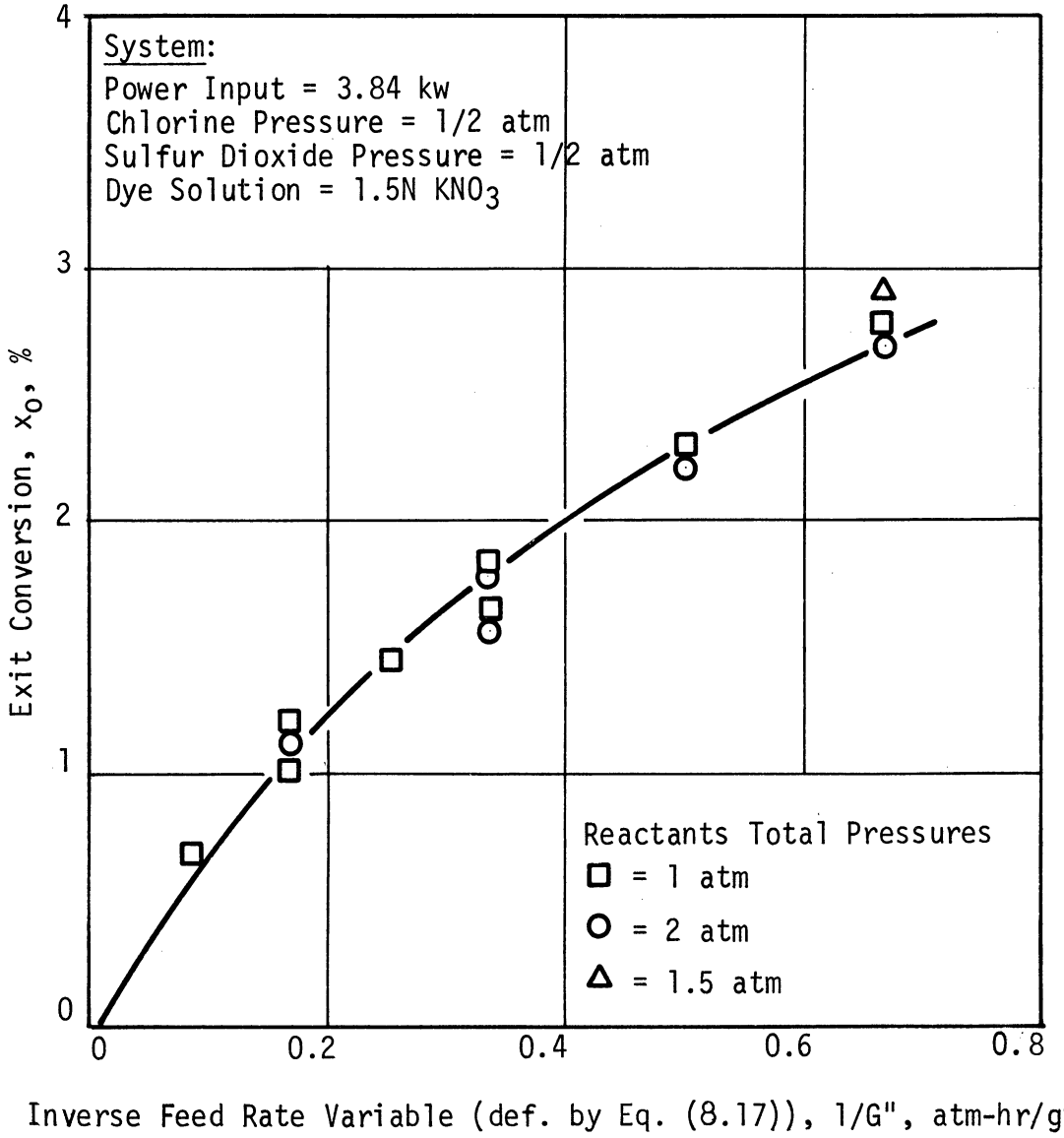

Fig. 40. Exit conversion of sulfur dioxide vs. inverse feed rate variable at several pressures.

Figure 41, the rates of production of sulfuryl chloride are shown as a function of the corresponding calculated values of x''_{eff}. The extrapolated intercept of the plot of sulfuryl chloride production vs. x''_{eff} is 0.048 gmol/hr.

8.5 EFFECT OF INLET TEMPERATURE ON THE FORWARD REACTION

According to the rate expression suggested in Eq. (8.1), the rate of the forward reaction should be dependent only upon the rate at which light is absorbed by the reacting gases. Two separate approaches were used in order to experimentally investigate the effect of temperature on the forward reaction.

A series of experimental runs was made in the temperature range 25 to 45°C using an equimolar feed mixture of sulfur dioxide and chlorine. Throughout the series of experiments the light source was operated at 3.84 kw using 1.5 normal potassium nitrate as the dye solution.

In order to study only the forward reaction a relatively high reactant feed rate of 8.0 gmol/hr was maintained for all runs in the series. For such a feed rate the reverse reaction rate is a small fraction of the forward rate and as a first approximation the reverse reaction can be ignored and the rate of production of sulfuryl chloride can be attributed to the forward rate.

The experimental observations are presented graphicaly in Fig. 42. As shown, the reaction rate decreased approximately 0.9%/°C of temperature increase.

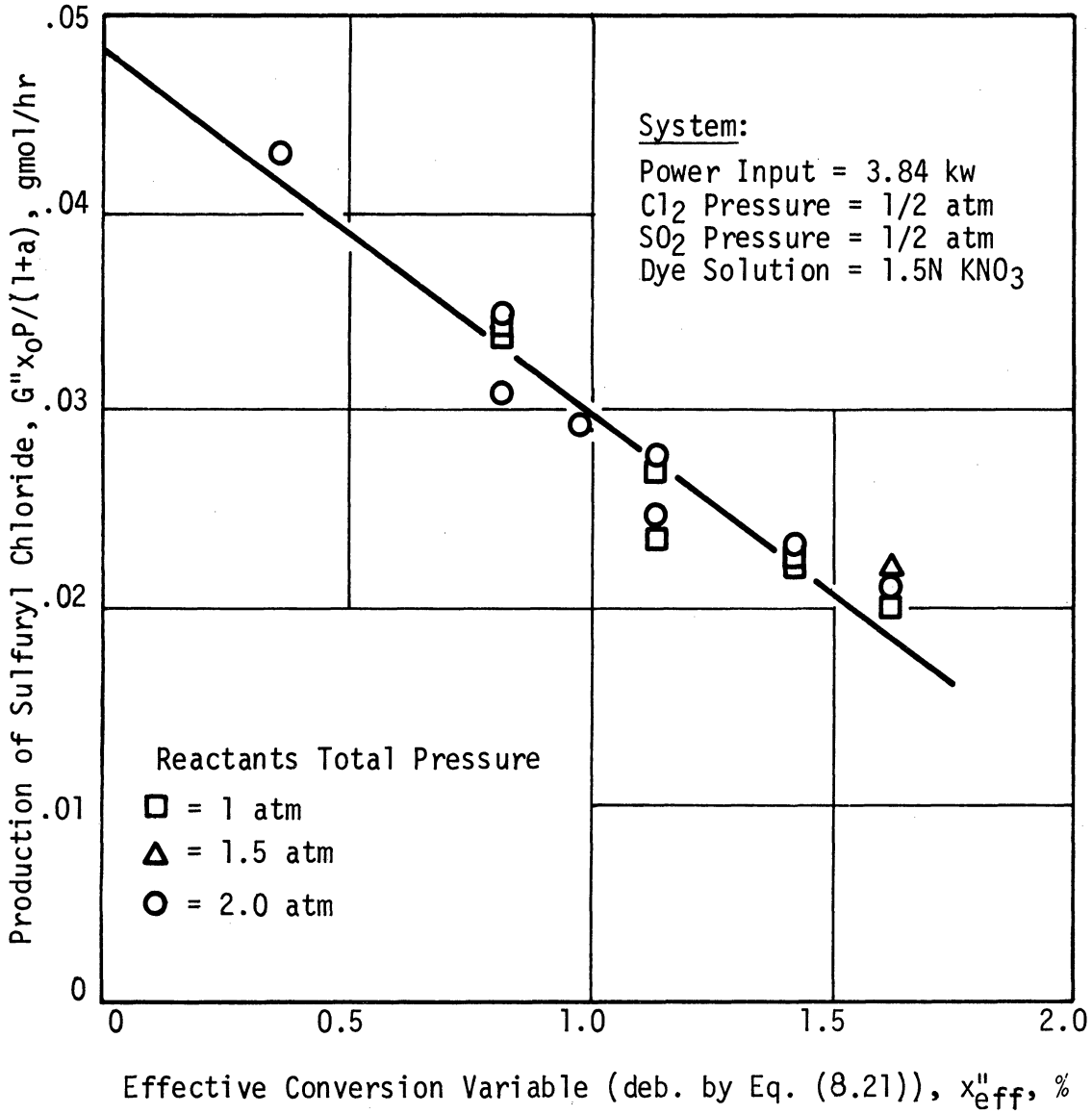

Fig. 41. Rate of production of sulfuryl chloride vs. effective conversion variable for several values of the total pressure.

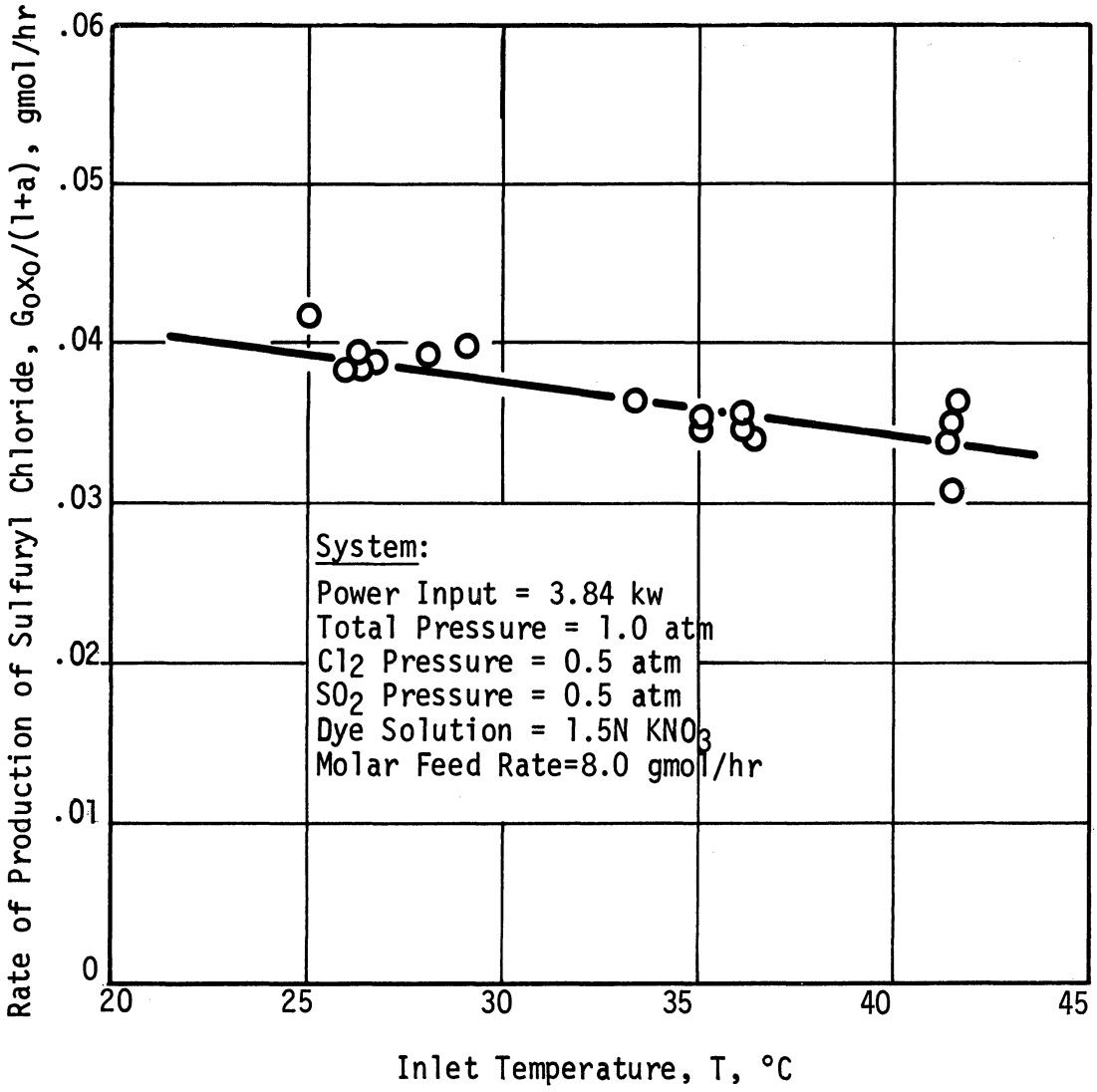

Fig. 42. Rate of production of sulfuryl chloride vs. temperature for a molar feed rate of 8.0 gmol/hr.

An alternative experimental approach to the problem was suggested by Eq. (8.5):

$$x_o = \sqrt{\frac{J_m(1+a)}{P\,k_m^2}} \left(1 - e^{-\frac{k_m J_m^{1/2} P^{1/2} (1+a)^{1/2} AL}{G_o}}\right) \tag{8.5}$$

Within a series of experiments, $\sqrt{J_m(1+a)/P\,k_m^2}$ and $(k_m J_m^{1/2} P^{1/2} (1+a)^{1/2} AL)$ are assumed to be functions only of temperature. The rate of production of sulfuryl chloride can be expressed as:

$$\frac{G_o x_o}{(1+a)} = \left(\frac{G_o}{(1+a)}\right) \sqrt{\frac{(1+a)J_m}{P\,k_m^2}} \left(1 - e^{-\frac{k_m J_m^{1/2} P^{1/2} (1+a)^{1/2} AL}{G_o}}\right) \tag{8.22}$$

In the limit as the molar feed rate, G_o, becomes large, this reduces to the rate of the forward reaction:

$$\frac{G_o x_o}{(1+a)} = \left(\frac{1}{(1+a)}\right) \left(\sqrt{\frac{J_m(1+a)}{P\,k_m^2}}\right) (k_m J_m^{1/2} P^{1/2} (1+a)^{1/2} AL) \tag{8.23}$$

If two experimental values of x_o vs. G_o are obtained at a given temperature, it is possible to evaluate corresponding values for the two parameter groupings in Eq. (8.5). The values of $\sqrt{(1+a)J_m/P\,k_m^2}$ and $(k_m J_m^{1/2} P^{1/2} (1+a)^{1/2} AL)$ can be calculated by standard curve fitting procedures. The third grouping in Eq. (8.23), $(1/(1+a))$, is known from the feed stream composition. In this way the initial rate at a specific temperature may be estimated.

A carefully done series of experiments was carried out at temperatures of 15.4, 26.2, and 32.9°C. At each temperature, experimental values of exit conversion were determined for total molar feed rates of

1.0 and 8.0 gmol/hr. Throughout the series the light source was operated at 3.84 kw using 1.5 normal potassium nitrate dye solution.

The experimental observations are tabulated in Table II. It is felt that these values represent the highest level of reproducibility attainable with the experimental apparatus used in this investigation.

TABLE II

DATA FOR DETERMINATION OF THE EFFECT OF TEMPERATURE ON THE REACTION

Temperature (°C)	Flowrate (gmol/hr)	Conversion (%)	Replicates	Scatter (±%)
15.4	8.0	1.126	3	5.0
15.4	1.0	3.521	1	5.0
26.2	8.0	1.085	3	4.0
26.2	1.0	3.816	2	1.0
32.9	8.0	1.039	3	2.5
32.9	1.0	3.919	2	0.4

The values of $\sqrt{J_m(1+a/Pk_m^2}$ and $k_m J_m^{1/2} P^{1/2} (1+a)^{1/2} AL$ which were calculated from this information are presented in Table III. The temperature

TABLE III

CALCULATED VALUES OF REACTION PARAMETERS AT SEVERAL TEMPERATURE

Temperature (°C)	$\sqrt{(1+a)J_m/P\ k_m^2}$ (%)	$k_m J_m^{1/2} P^{1/2} (1+a)^{1/2} AL$ (gmol/hr)
15.4	3.73	2.87
26.2	4.20	2.39
32.9	4.45	2.13

dependence of the forward rate as calculated from the above information is shown graphically in Fig. 43. As shown, the forward rate decreases 0.7%/°C of temperature increase.

There are three factors to which the observed decrease in forward rate with increasing temperature can be attributed. According to the ideal gas law, the molar concentration of chlorine in the reactant mixture decreases approximately .35%/°C of temperature increase.

The extinction coefficients for both chlorine and potassium nitrate are functions of temperature. Figure 44 depicts the effect of temperature on the molecular extinction coefficient of potassium nitrate. In qualitative terms, increasing the temperature of the potassium nitrate dye solution by 20°C shifts the "cut-off" region toward longer wavelengths by 20 Å. Consideration of the spectral output of the light source indicates that this effect should decrease the rate at which light is absorbed by the reactants by approximately 0.25%/°C of temperature increase.

The effect of temperature on the molecular extinction coefficient of chlorine is shown in Fig. 45. Decreasing absorption by chlorine may be estimated to cause the forward reaction to decrease by 0.1%/°C of temperature increase.

The total predicted effect is a decrease of 0.7%/°C of temperature increase. This value agrees well with the experimentally observed values of 0.7 and 0.9%/°C of temperature increase.

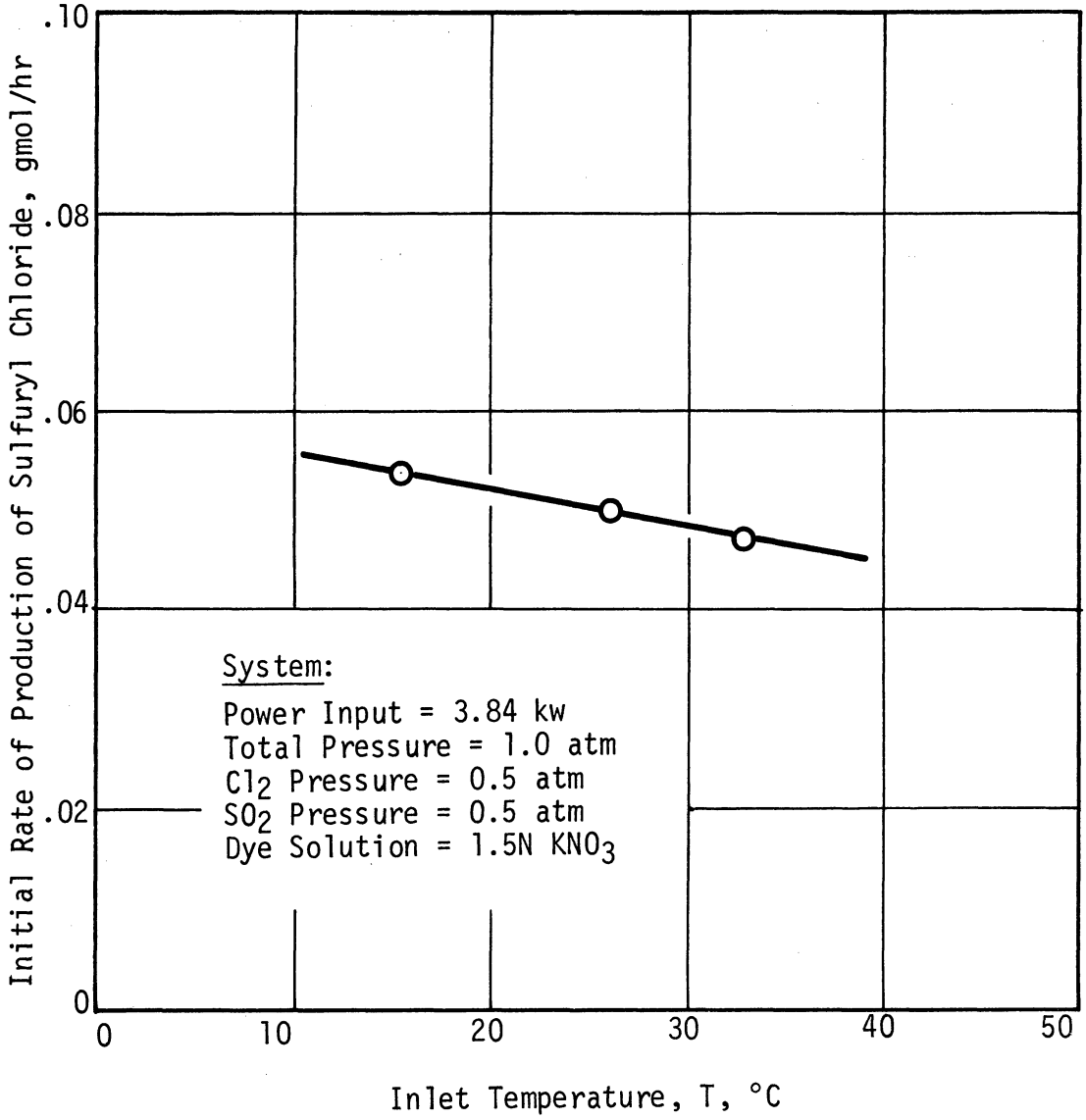

Fig. 43. Rate of the forward reaction as a function of inlet gas temperature.

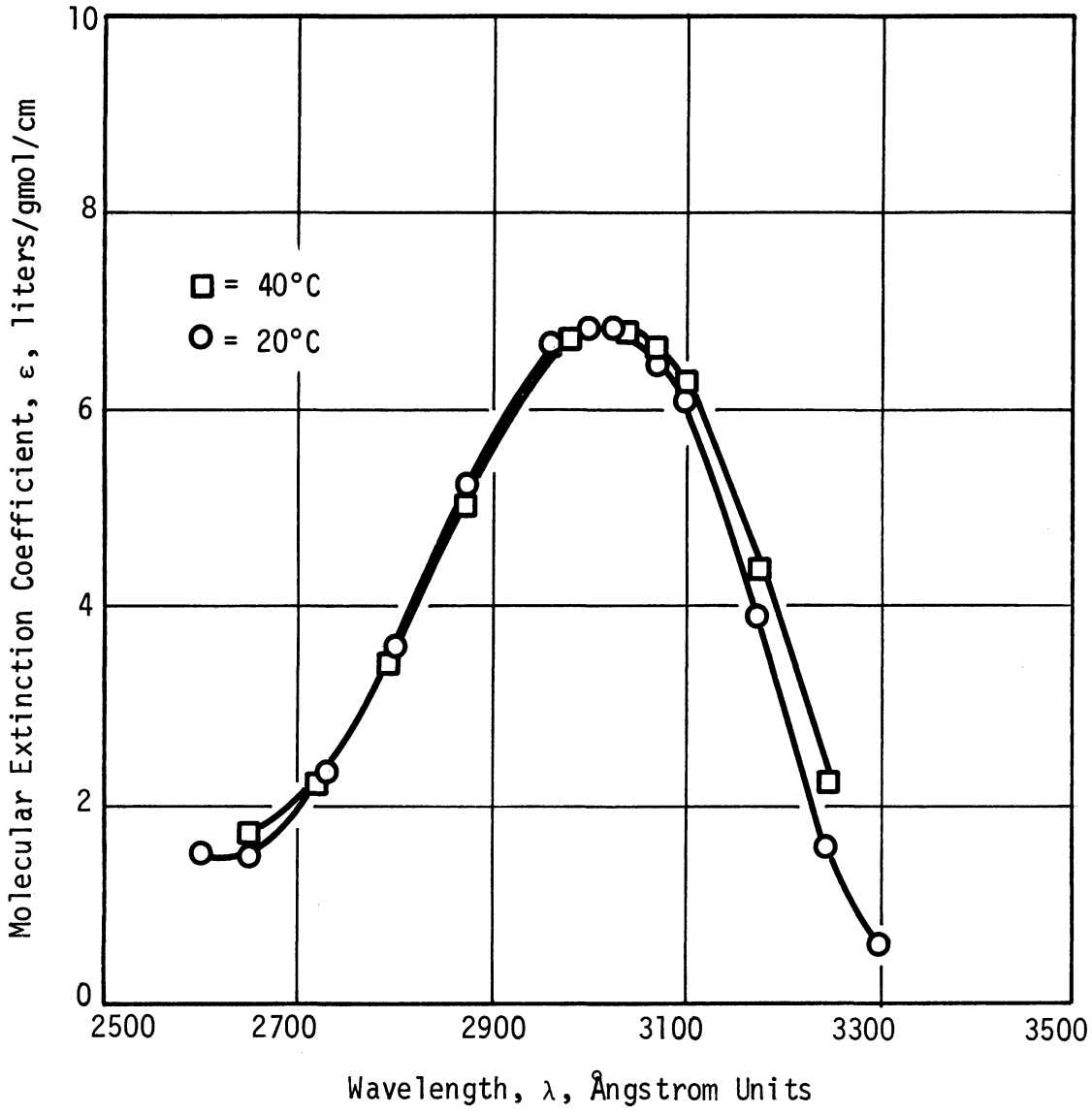

Fig. 44. Molecular extinction coefficient for potassium nitrate vs. wavelength at two temperatures.[28]

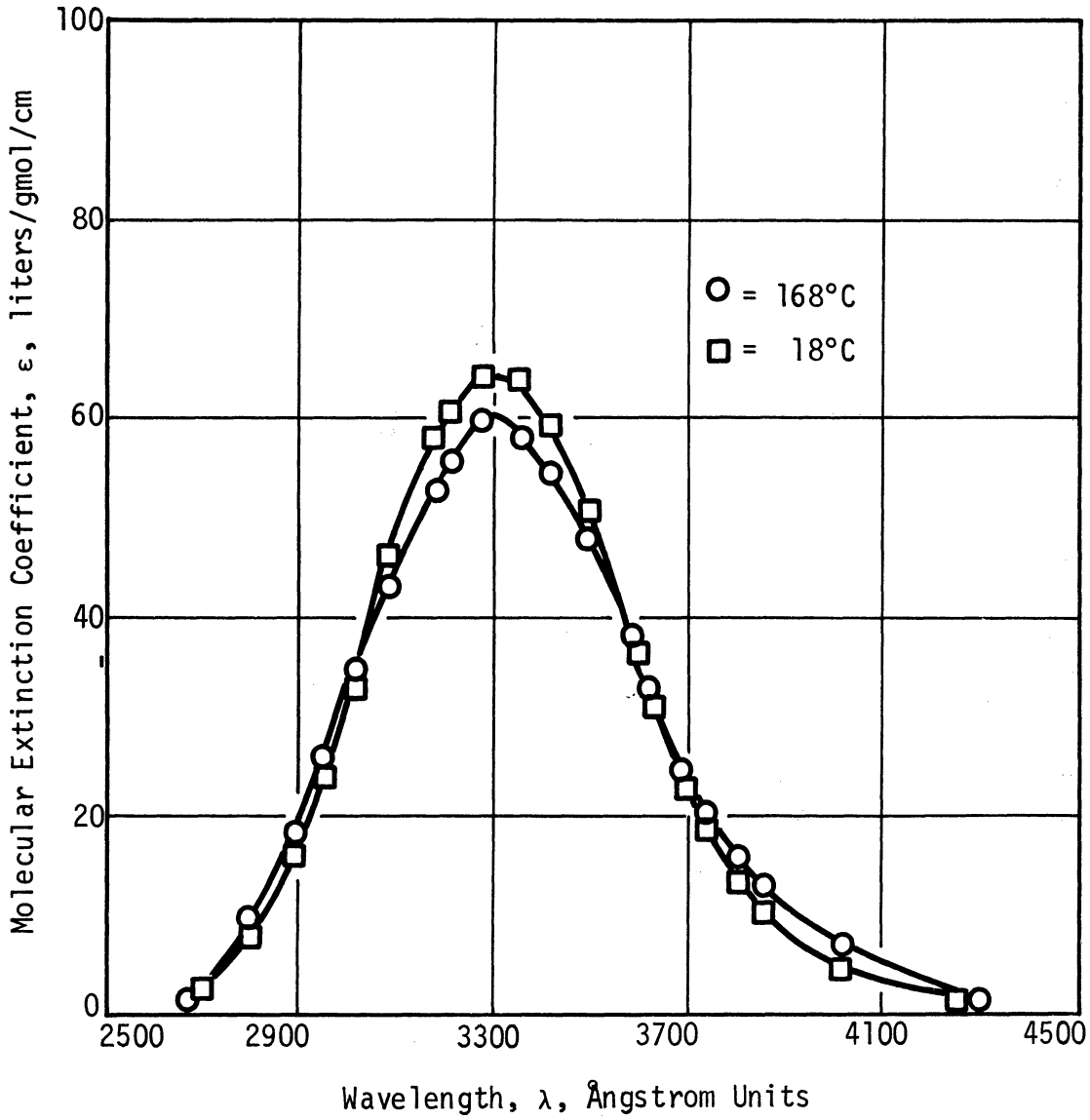

Fig. 45. Molecular extinction coefficient for chlorine vs. wavelength at two temperatures.[22]

8.6 EFFECT OF INLET TEMPERATURE ON THE RATE OF THE REVERSE REACTION

According to the mathematical formulation presented in Eq. (8.1), the rate of the reverse reaction is given by:

$$\frac{d[SO_2Cl_2]}{dt} = -k[SO_2Cl_2]\sqrt{J/[SO_2]} \qquad (8.24)$$

where k is a kinetic rate constant.

It is noted that the ratio of the two parameter groupings, $(k_m J_m^{1/2}(1+a)^{1/2}P^{1/2}AL)$ and $\sqrt{(1+a)J_m/P\ k_m^2}$, which were considered in the previous section is equal to k_m^2PAL. Assuming that k_m is an Arrhenius-type rate constant:

$$k_m = k_o e^{-\frac{E}{RT}} \qquad (8.25)$$

where k_o is the effective pre-exponential factor and E is the effective activation energy for the reverse reaction.

Equation (8.25) suggests that a plot of $\log_e(k_m^2PAL)$ vs. the inverse of the absolute temperature should be a straight line with slope equal to -2E/R.

Values of k_m^2PAL corresponding to 15.4, 26.2, and 32.9°C were calculated from the information presented in Table II. These values are listed in Table IV.

The values listed in Table IV are shown graphically in Fig. 46. The information plotted forms a straight line whose slope corresponds to an effective activation energy for the reverse reaction of -2.4 kcal.

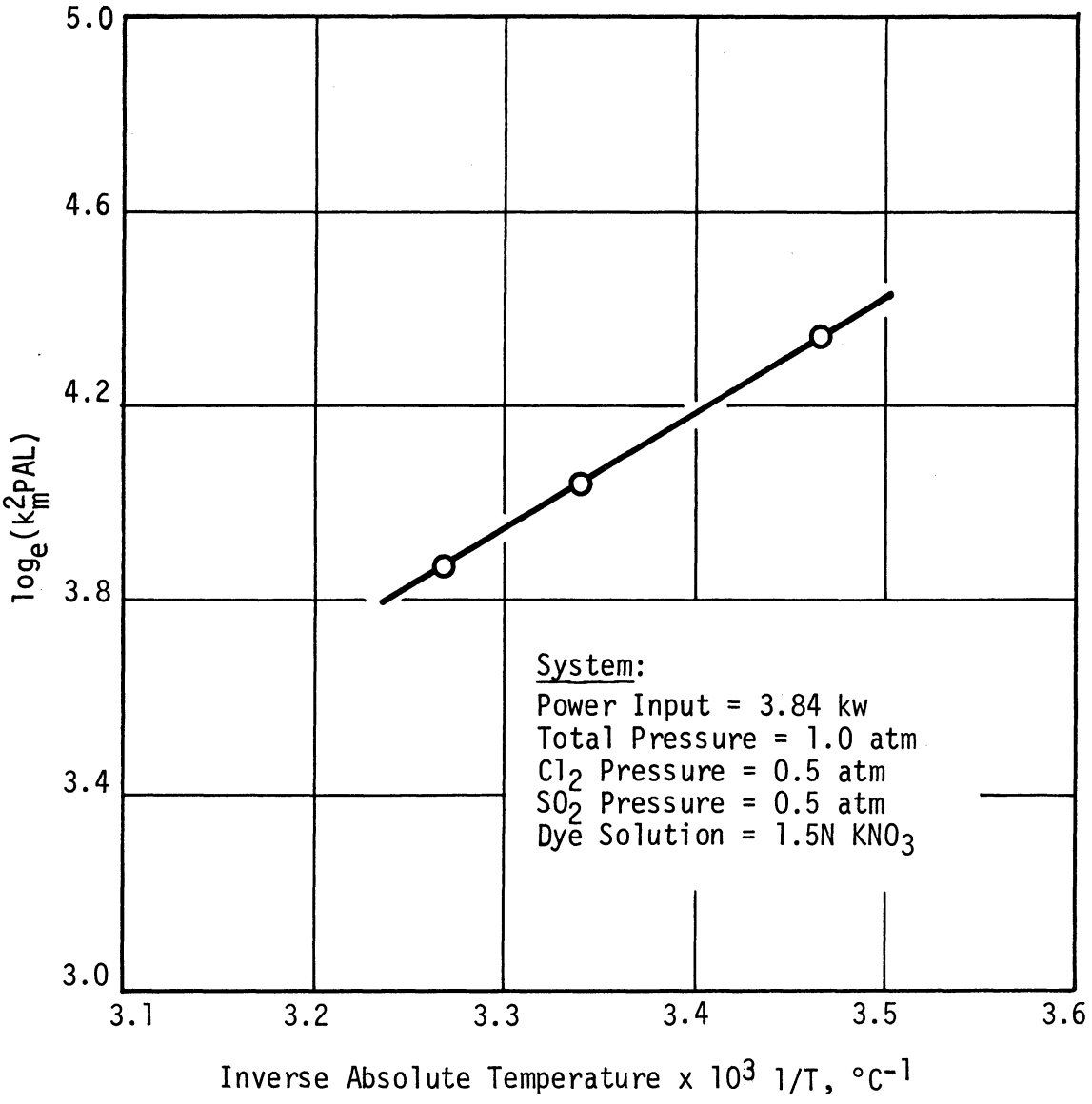

Fig. 46. Natural logarithm of $k_m^2 PAL$ vs. the inverse of the absolute temperature.

TABLE IV

DATA USED TO DETERMINE THE ACTIVATION ENERGY OF THE REVERSE REACTION

Temperature (°C)	k_m^2PAL (gmol/hr)	$\log_e(k_m^2 PAL)$	Inverse Temperature ($°K^{-1}$)
15.4	77.0	4.34	.003465
26.2	56.9	4.04	.003340
32.9	47.8	3.87	.003268

8.7 EFFECT OF WAVELENGTH ON THE REACTION

The experimental runs discussed in the earlier sections were made using 1.5 normal potassium nitrate as the dye solution. Because of this, the only light absorption which occurred was attributable to the chlorine absorption spectra. Of interest in this investigation was the experimental determination of the effect which the absorption of ultraviolet light by sulfur dioxide has on the total reaction.

In order to study the effect of sulfur dioxide absorption, the potassium nitrate solution was replaced by a 0.05 normal potassium iodide dye solution. Three series of runs were made with varying reactant mixture compositions while using potassium iodide dye solution. The sulfur dioxide to chlorine ratios used were 2:1, 1:1, and 1:2. Within each series, runs were made at total flowrates of 12.0, 6.0, 4.0, 3.0, 2.4, and 2.0 gmol/hr. As in earlier work the light source was operated with 3.84 kw of power input.

In Figs. 47, 48, and 49, the observed conversions of sulfur dioxide for the three series of runs is presented as a function of the inverse of the molar feed rate.

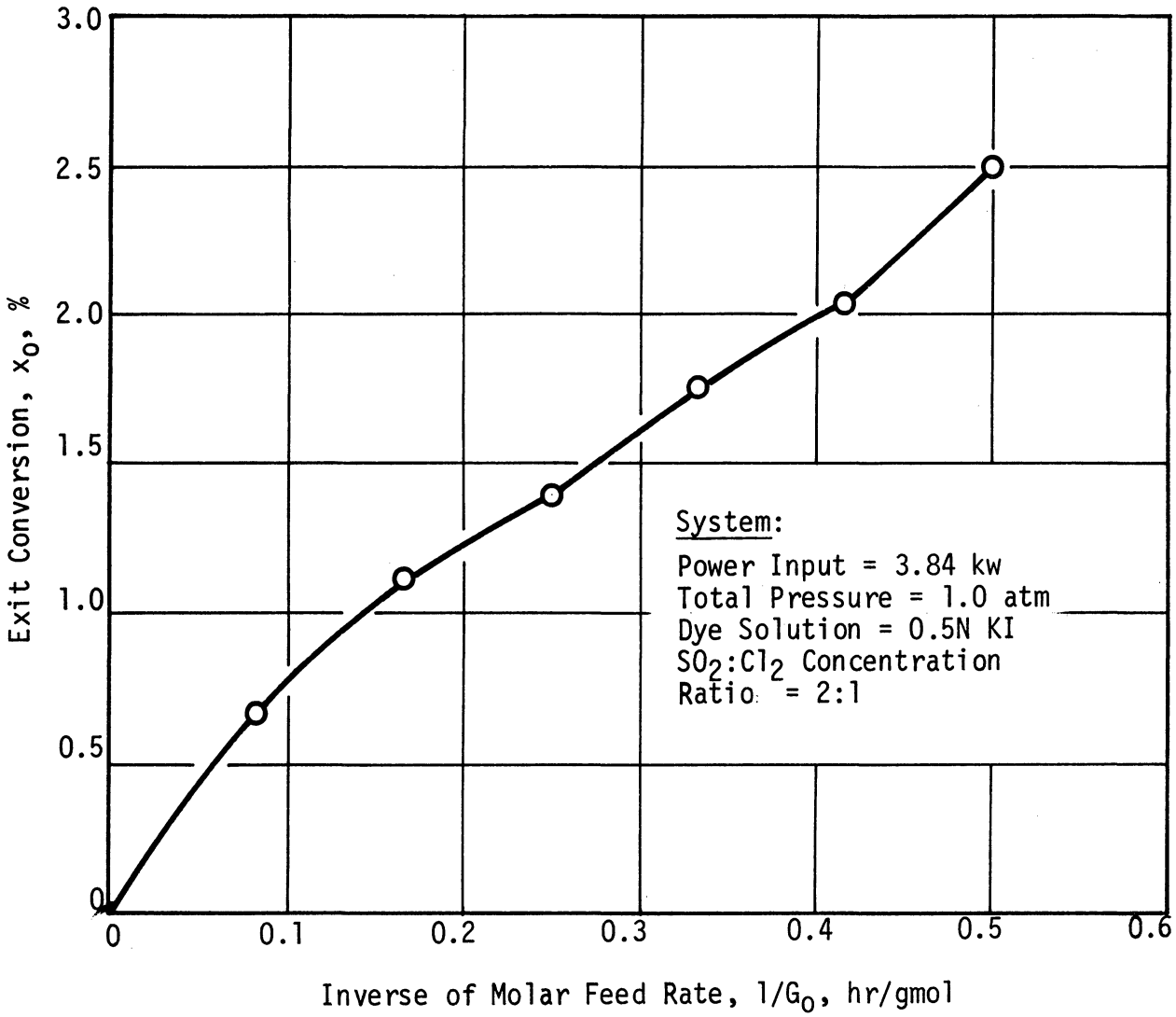

Fig. 47. Exit conversion of sulfur dioxide vs. inverse molar feed rate for reactants composition: 1/3 chlorine, 2/3 sulfur dioxide while using KI dye solution.

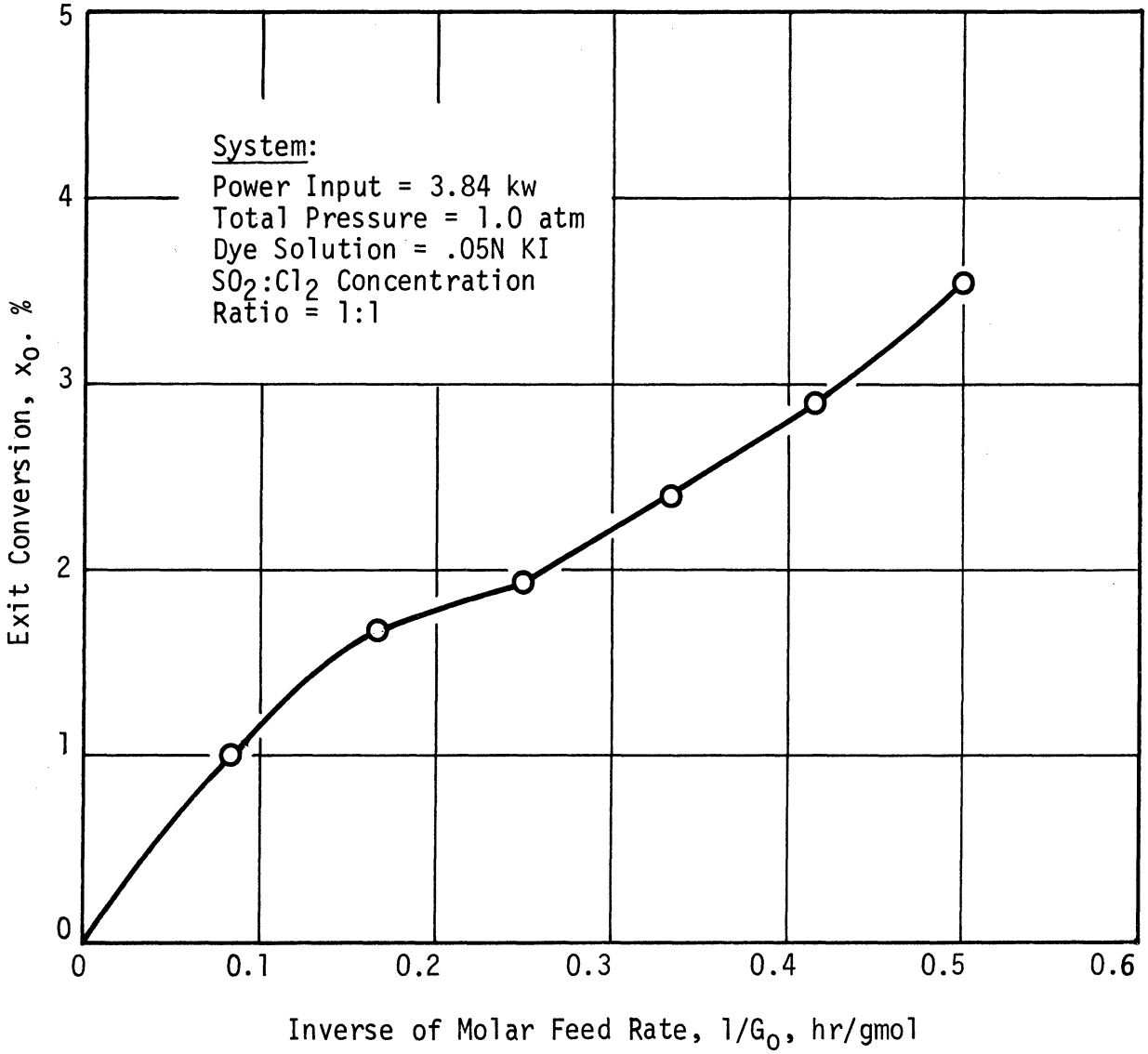

Fig. 48. Exit conversion of sulfur dioxide vs. inverse molar feed rate for reactants composition: 1/2 chlorine, 1/2 sulfur dioxide while using KI dye solution.

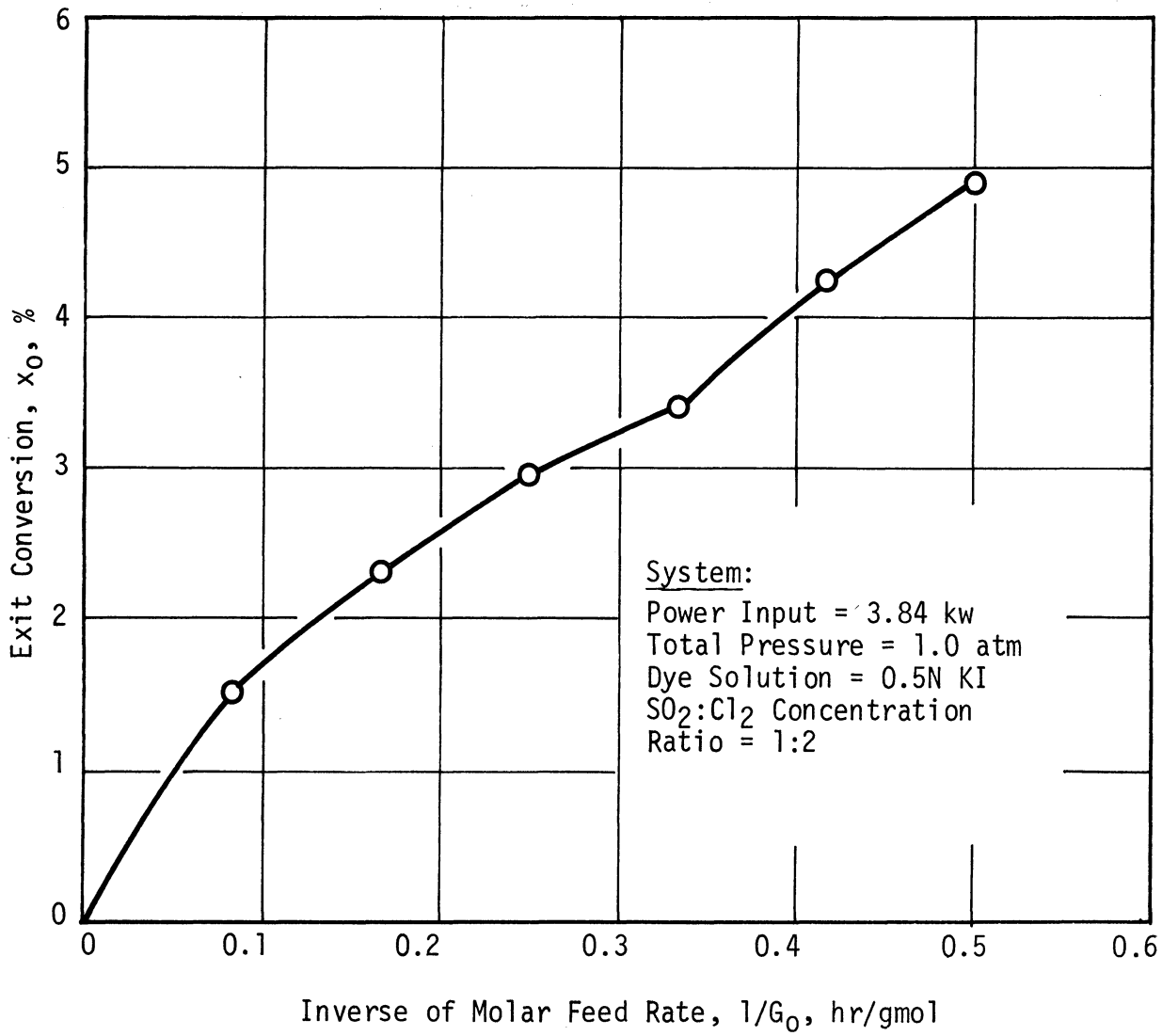

Fig. 49. Exit conversion of sulfur dioxide vs. inverse molar feed rate for reactants composition: 2/3 chlorine, 1/3 sulfur dioxide while using KI dye solution.

The values of x_{eff} corresponding to each of the experimental points was calculated according to the definition given in Eq. (8.9). The rates of production of sulfuryl chloride for each of the three series of runs are presented as a function of the corresponding calculated values of x_{eff} in Figs. 50, 51, and 52. The extrapolated rates of production at zero conversion corresponding to the three concentration ratios were, respectively, 0.064, 0.076, and 0.084 gmol of sulfuryl chloride per hour.

At low values of x_{eff}, the plots of sulfuryl chloride production rate vs. x_{eff} exhibit the expected linear relationship. However, for higher values of x_{eff}, the rate of production no longer decreased linearly with increasing x_{eff}. Instead, in all three cases, the rate of production leveled off at a value of approximately 0.034 gmol/hr.

8.8 QUANTITATIVE ANALYSIS

The experimentally determined values of exit conversion versus the inverse of the molar flowrate, as a function of the controllable parameters, were analyzed using an integral method of analysis.

Considering the flow of sulfuryl chloride into and out of an incremental length of the photochemical reactor yields the following:

$$\left.\frac{G_o x}{(1+a)}\right|_{z+\Delta z} - \left.\frac{G_o x}{(1+a)}\right|_{z} = rA\Delta z \qquad (8.26)$$

In the limit as the increment becomes arbitrarily small this reduces to:

$$\frac{dx}{dz} = \frac{(1+a)A}{G_o} r \qquad (8.27)$$

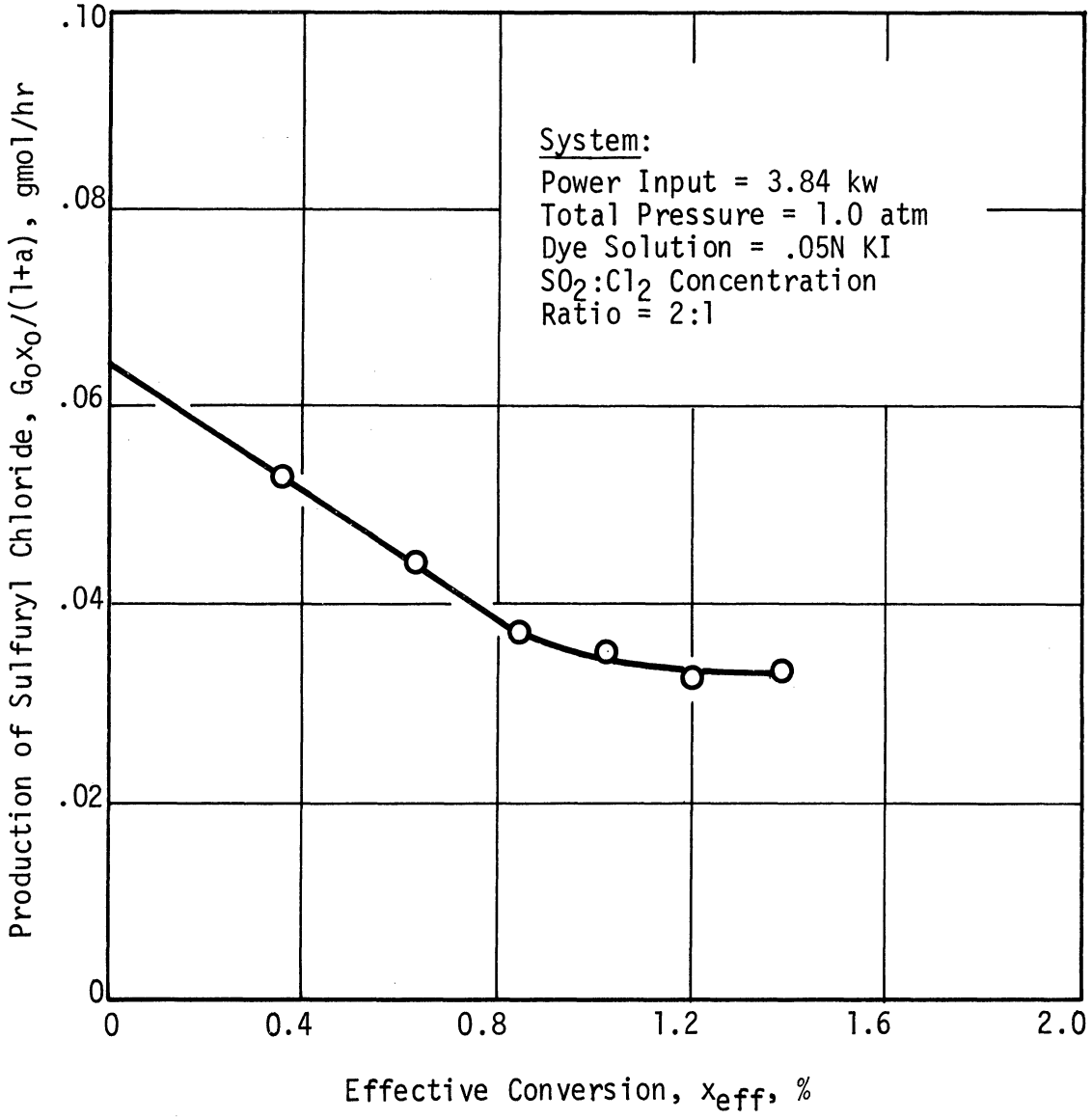

Fig. 50. Rate of production of sulfuryl chloride vs. effective conversion for reactants composition: 1/3 chlorine, 2/3 sulfur dioxide while using KI dye solution.

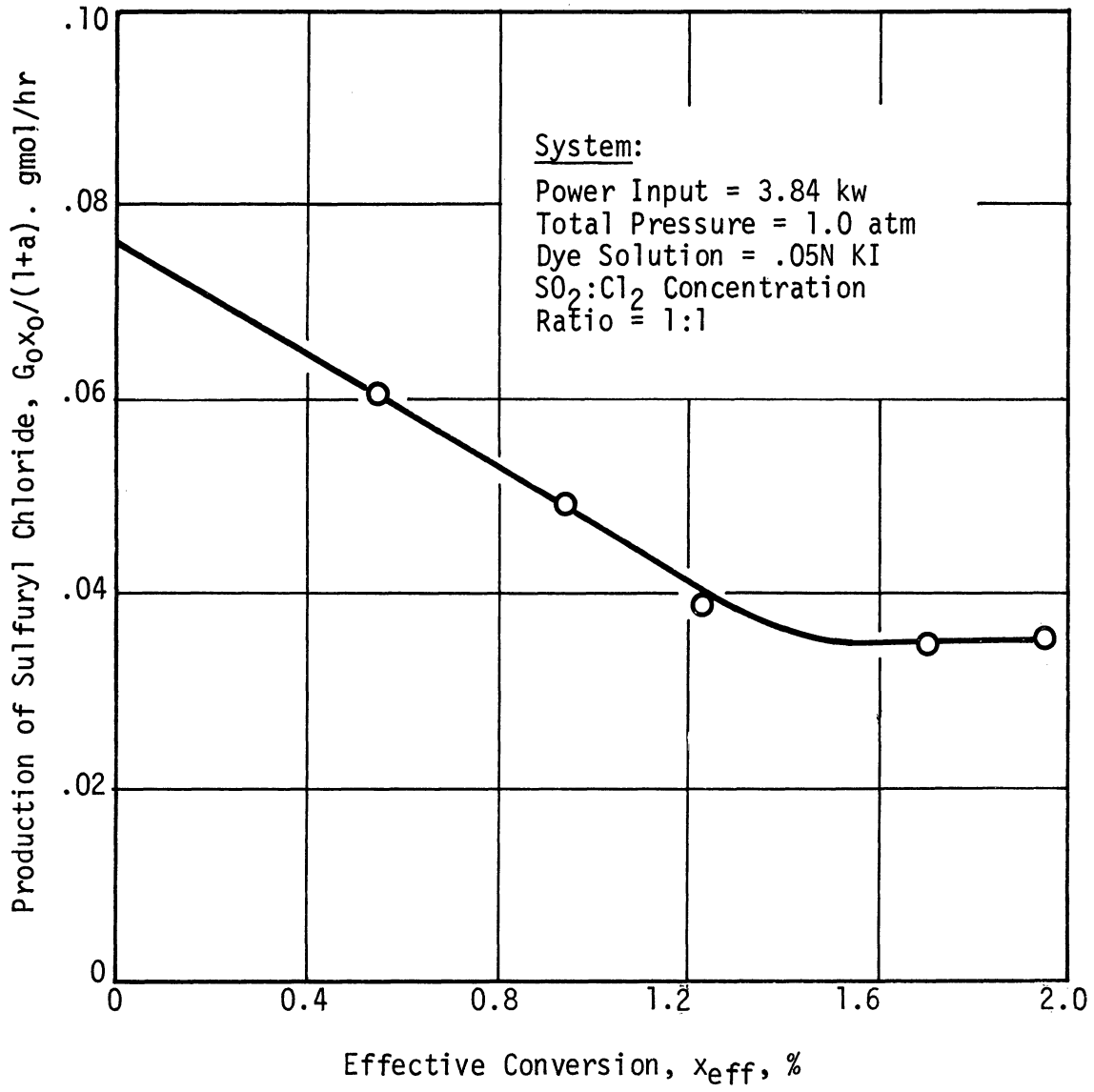

Fig. 51. Rate of production of sulfuryl chloride vs. effective conversion for reactants composition: 1/2 chlorine, 1/2 sulfur dioxide while using KI dye solution.

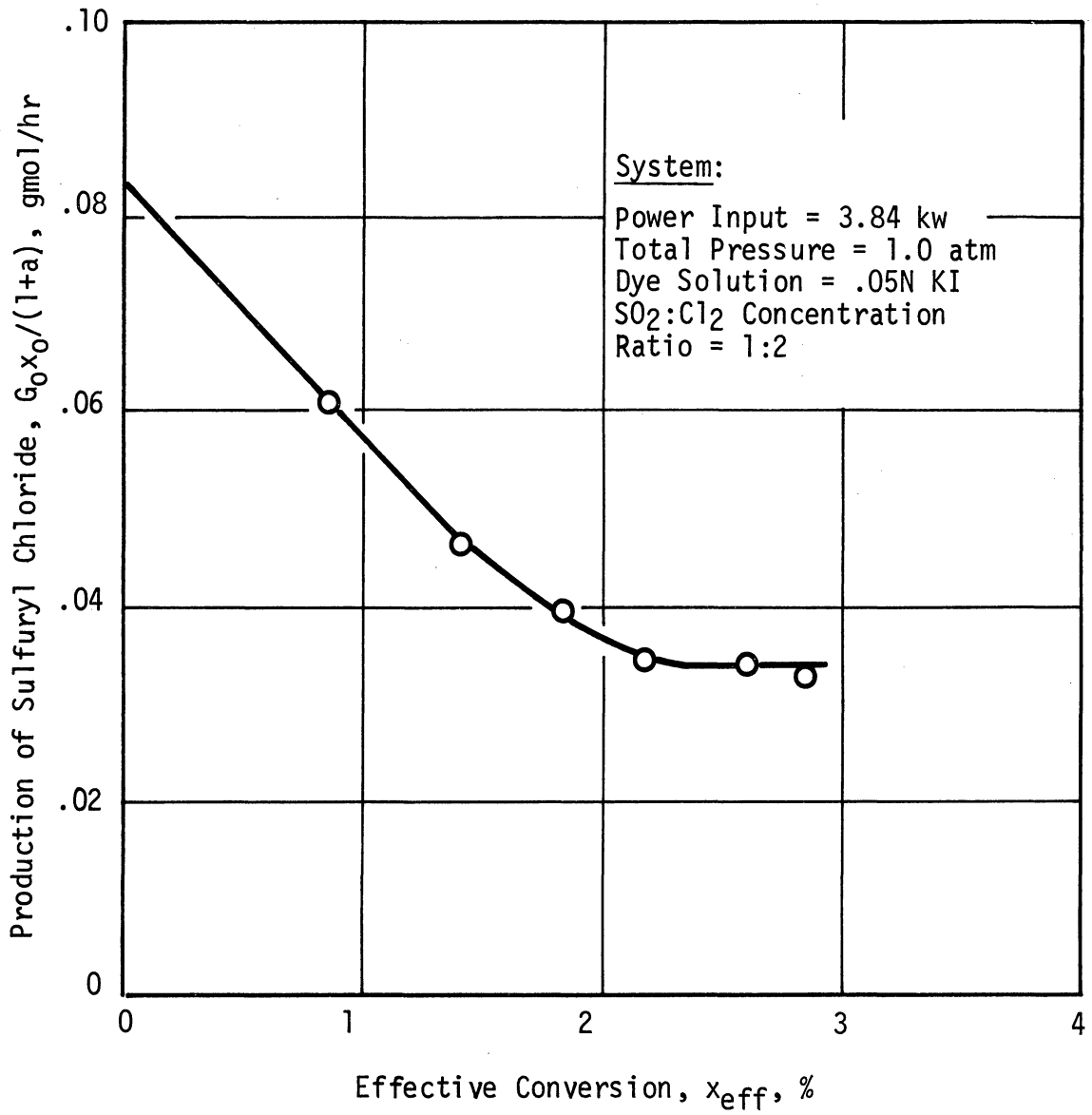

Fig. 52. Rate of production of sulfuryl chloride vs. effective conversion for reactants composition: 2/3 chlorine, 1/3 sulfur dioxide while using KI dye solution.

Similarly, considering the flow of energy into and out of an incremental length of the reactor yields the following relationship:

$$\frac{G_oT}{(1+a)}\{(1-x)c_{p_{SO_2}}+(a-x)c_{p_{Cl_2}}+xc_{p_{SO_2Cl_2}}\}\Big|_{z+\Delta z} - \frac{G_oT}{(1+a)}\{(1-x)c_{p_{SO_2}} + (a-x)c_{p_{Cl_2}}+xc_{p_{SO_2Cl_2}}\}\Big|_z = r\Delta H_r A\Delta z+WA\Delta z-U\bar{A}(T-T_o)\Delta z \qquad (8.28)$$

where W represents the volumetric rate of internal heat generation due to the absorption of light, $\bar{A}$ is the heat transfer area per unit of reactor length, U is the overall heat transfer coefficient for transfer of energy to the surroundings, and T_o is the temperature of the surroundings.

In the limit as the increment becomes arbitrarily small, this expression reduces to:

$$\frac{G_o}{(1+a)}\{c_{p_{SO_2}}(1-x)+c_{p_{Cl_2}}(a-x)+c_{p_{SO_2Cl_2}}x\}\frac{dT}{dz} + \frac{G_oT}{(1+a)}\{-c_{p_{SO_2}}-c_{p_{Cl_2}} +c_{p_{SO_2Cl_2}}\}\frac{dx}{dz} = r\Delta H_r A+WA-U\bar{A}(T-T_o) \qquad (8.29)$$

The expression for dx/dz obtained above can be substituted into the second term of this equation. When this is done the term can be rewritten as:

$$\frac{G_oT}{(1+a)}\{-c_{p_{SO_2}}-c_{p_{Cl_2}}+c_{p_{SO_2Cl_2}}\}\frac{dx}{dz} = T\{-c_{p_{SO_2}}-c_{p_{Cl_2}}+c_{p_{SO_2Cl_2}}\}Ar \qquad (8.30)$$

Since ΔH_r is equal to 13.68 kcal/gmol:

$$\Delta H_r \gg \{-c_{p_{SO_2}}-c_{p_{Cl_2}}+c_{p_{SO_2Cl_2}}\}T \qquad (8.31)$$

this term can be eliminated from consideration and the heat equation can be written:

$$\frac{G_o}{(1+a)}\{(1-x)c_{p_{SO_2}}+(a-x)c_{p_{Cl_2}}+xc_{p_{SO_2Cl_2}}\}\frac{dT}{dz} = r\Delta H_r A+WA-U\bar{A}(T-T_o) \qquad (8.32)$$

Assuming a function form for the rate of reaction, r;

$$r = r(x,z,T,a,G_o,J,\lambda) \qquad (8.33)$$

for specific values of G_o, a, and U, and for predicted distributions of W and light intensity along the reactor length, it is possible to simultaneously integrate the design and energy equations over the length of the reactor. Such an integration yields values of exit conversion versus the inverse of the molar flowrate, which may be compared with the experimental data for all combinations of the controllable parameters.

The distribution of the rate of heat generation due to light absorption and the rate of light absorption along the length of the reactor were predicted numerically using a digital computer. Inherent in these calculations was the assumption that the plasma light source could be considered as a line radiation source. The ramifications of this assumption are discussed in Appendix II.

The distribution of light intensity along the reactor length was calculated from measured values of the spectral radiance of the arc column using a mathematical algorithm which considered the physical

geometry of the reaction vessel and of the two electrodes. The predicted normalized distribution is shown graphically in Fig. 53.

Using the predicted distribution for heat generation and light absorption, various functional forms were assumed for the rate of reaction and Eqs. (8.27) and (8.32) were integrated simultaneously. The resulting relationships between exit conversion and the inverse of the molar flowrate for all combinations of the controllable parameters were then compared with the experimental data.

The rate expression which gave the best agreement with the experimentally determined exit conversion versus the inverse of the molar flowrate for all combinations of controllable parameters was:

$$\frac{d[SO_2Cl_2]}{dt} = J - k_o e^{-\frac{E}{RT}} [SO_2Cl_2] \sqrt{J/[SO_2]} \qquad (8.34)$$

In order to determine the values of the parameters E and k_o found in the rate expression and the value of U found in the energy equation, a nonlinear regression analysis was performed on that part of the data which was presented in Table II.

The parameter E was calculated to be -2.6 kcal/gmol while k_o was found to be 0.0542 $(sec)^{-1/2}$. The value of the overall heat transfer coefficient U was observed to be small. The best agreement with the experimental data was obtained when U was assumed to be zero, i.e., when the reaction was assumed to occur adiabatically.

In Figs. 54-56, the above rate expression together with the design and energy equations was used to predict the experimental curves ob-

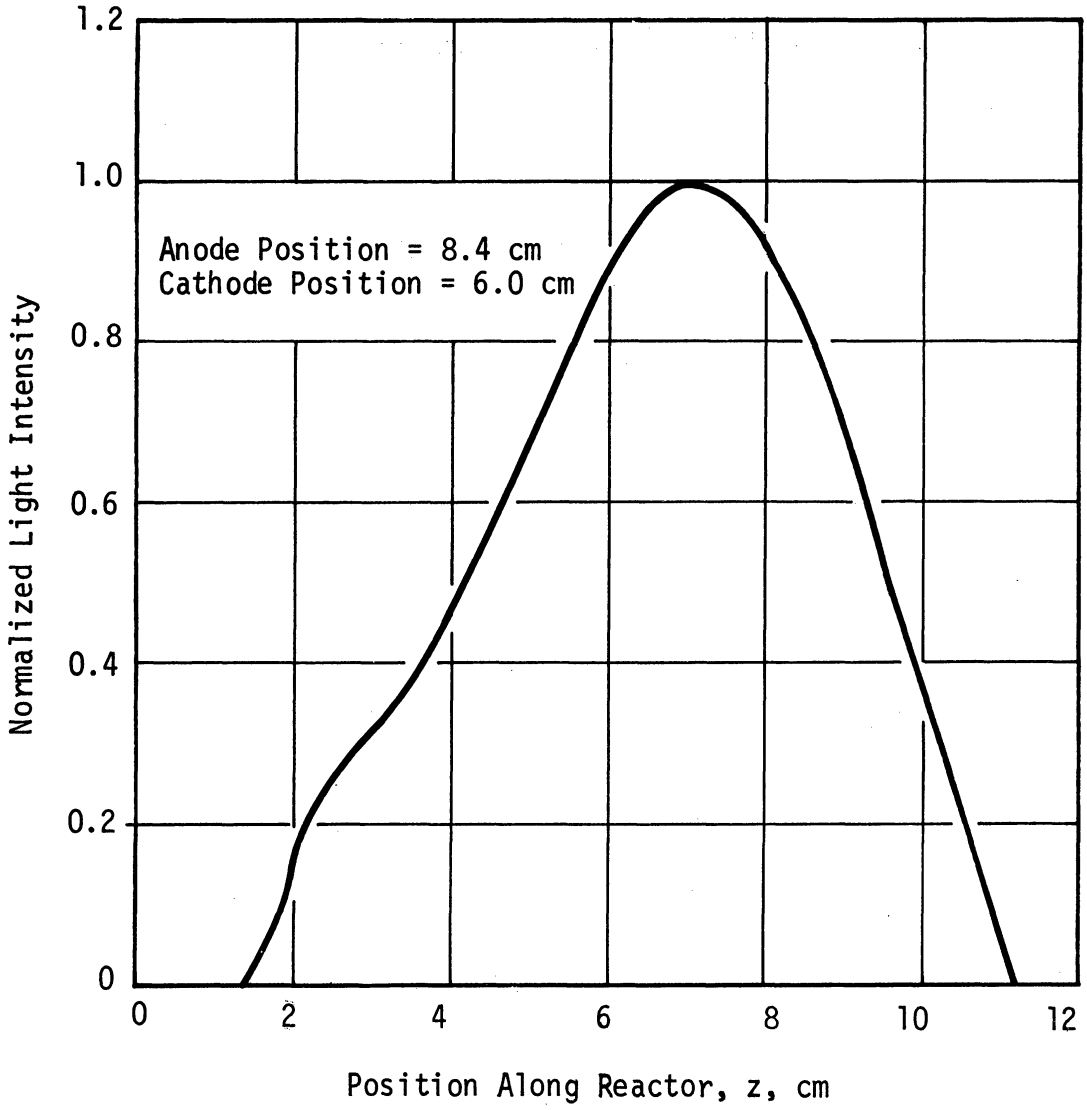

Fig. 53. Predicted variation of light intensity along the length of the reactor.

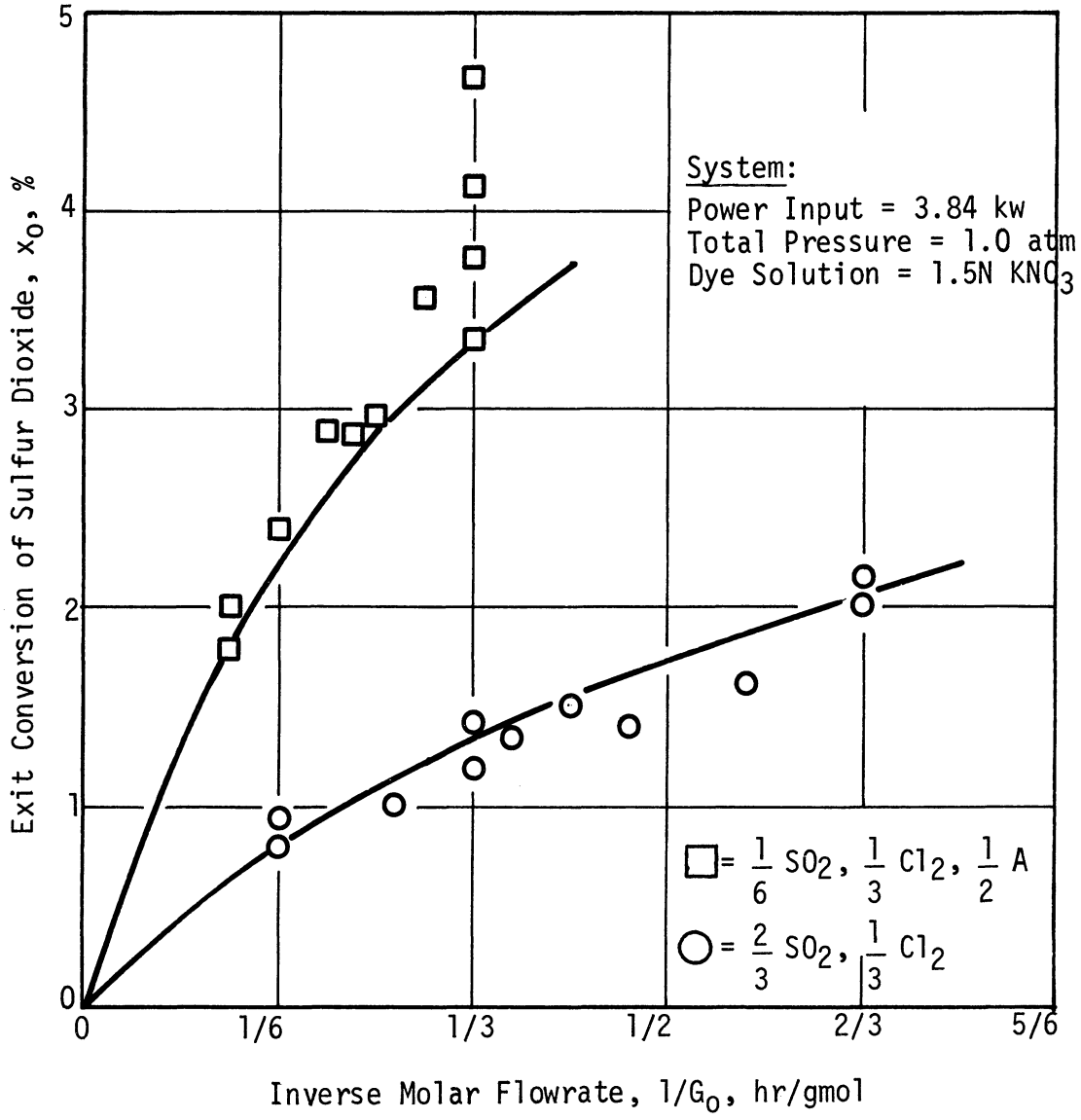

Fig. 54. Comparison of experimental data and predicted curves for several partial pressures of sulfur dioxide while using KNO_3 dye solution.

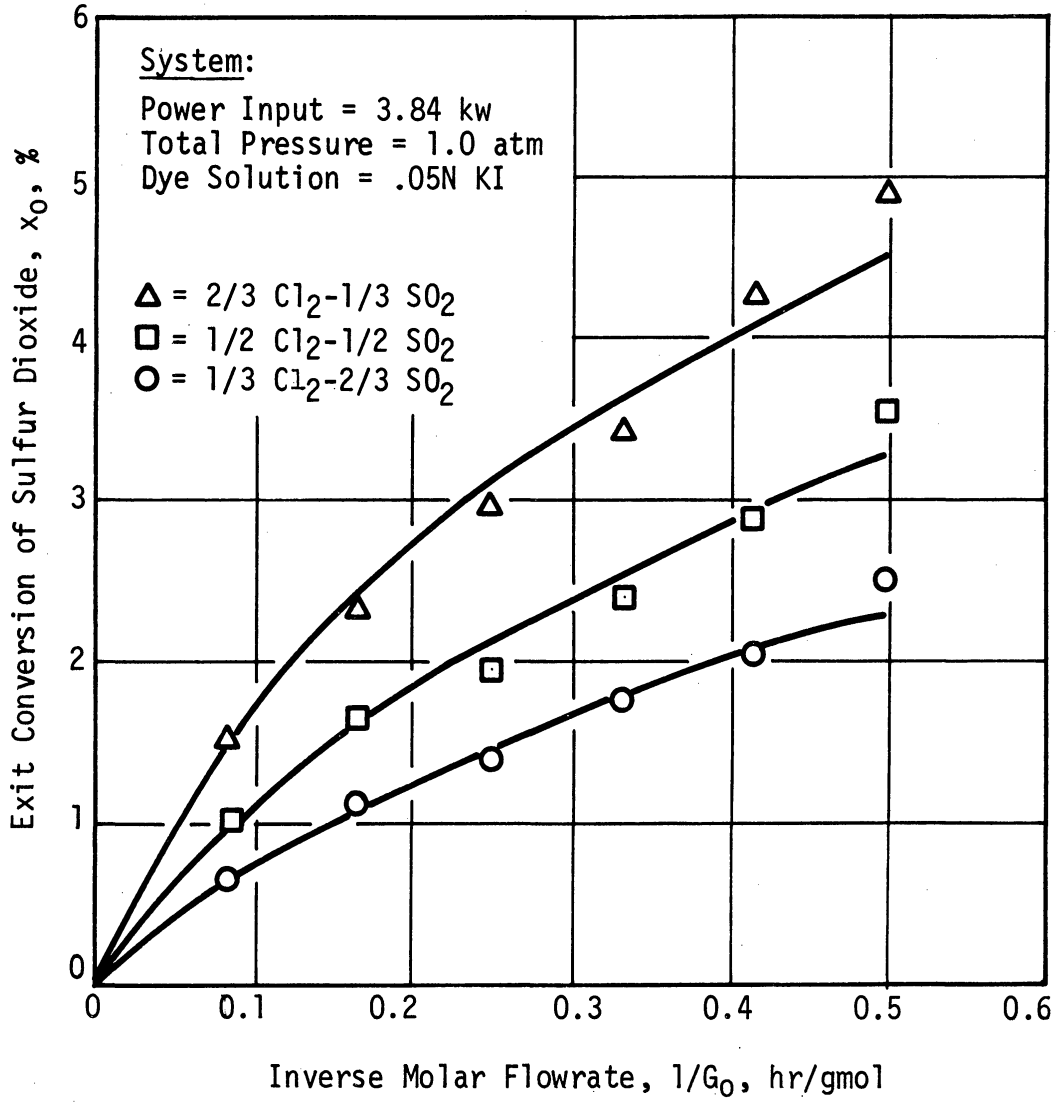

Fig. 55. Comparison of experimental data and predicted curves for several reactant mixtures while using KI dye solution.

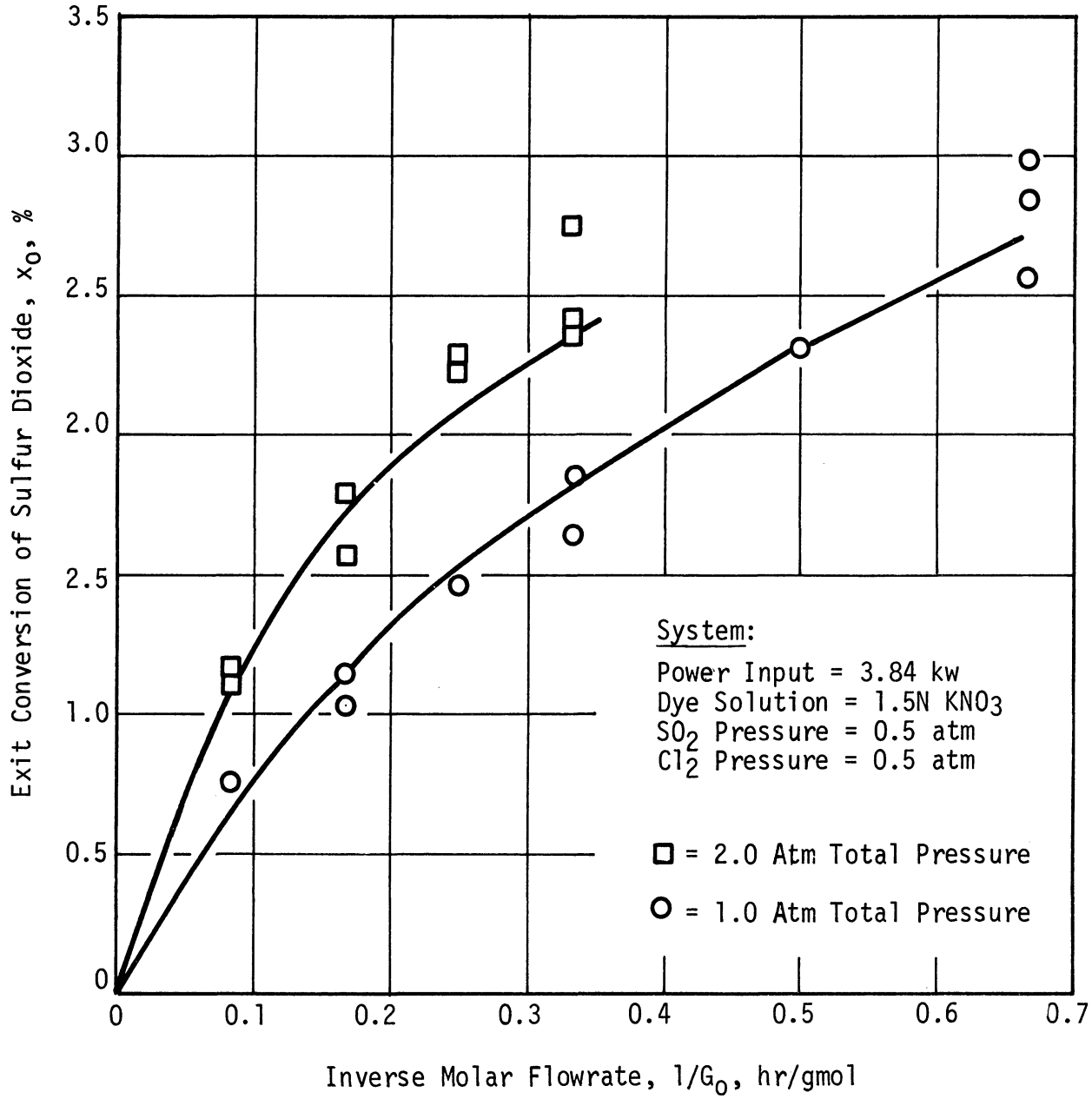

Fig. 56. Comparison of experimental data and predicted curves at two pressures while using KNO_3 dye solution.

tained for the various combinations of the controllable parameters. It is noted that the experimental data shown in Figs. 54-56 were not used in the nonlinear regression analysis.

9. DISCUSSION OF KINETIC RESULTS

The extrapolated initial rates of sulfuryl chloride production for the various combinations of reactants composition and dye solution are tabulated below:

TABLE V

OBSERVED INITIAL RATES EXPRESSED IN GRAM-MOLES PER HOUR

(Ratios are Relative to 1/2 Cl_2, 1/2 SO_2)

Composition / Dye Solution	1/3 Cl_2 2/3 SO_2	1/2 Cl_2 1/2 SO_2	2/3 Cl_2 1/3 SO_2
1.5N KNO_3	.037	.053,.048, .050	
(Ratios)	.74	Avg.=.050 1.00	
.05N KI	.064	.076	.084
(Ratios)	.84	1.00	1.11

If it can be said that the initial rate is equal to the rate of light absorption, then the forward rate is only dependent upon the rate at which light is absorbed by the reactants and the quantum yield for the forward reaction is 1.0 molecules of sulfuryl chloride formed per photon of light absorbed. Keeping in mind that the predicted rates of light absorption presented in Table I represent only continuum radiation, the information presented in Table V can be compared with the corresponding information presented in Table I.

For the case of the 1.5 normal potassium nitrate dye solution, the

predicted rates are 25% lower than the observed rates. The entries in Table I, corresponding to 1.5 normal potassium nitrate dye solution, represent light absorption by chlorine in the wavelength region 3200 to 5000 Å. From Figs. 16-20 it is observed that in this wavelength region approximately 25% of the total radiation emitted by the arc is in the form of line radiation which was not included in the predicted rates of light absorption.

Within the limits of experimental error, for the 1.5 normal potassium nitrate dye solution, it is concluded that the predicted rates of light absorption are equal to the corresponding extrapolated initial rates.

For the case of 0.05 normal potassium iodide dye solution, the agreement between the experimental extrapolated initial rates and the predicted total rates of light absorption, for the three different reactant compositions, is 0.064 vs. 0.058, 0.076 vs. 0.070, and 0.084 vs. 0.079, with all rates being expressed in gmol/hr.

From this observation it is concluded that the predicted rates of light absorption are equal to the corresponding extrapolated initial rates, and that deactivation of the excited sulfur dioxide molecules occurs via the following reaction:

$$SO_2^* + Cl_2 \rightarrow SO_2 + Cl\cdot + Cl\cdot$$

All of the parameter dependencies in the rate expression:

$$\frac{d[SO_2Cl_2]}{dt} = J - k_o e^{-\frac{E}{RT}} \sqrt{J/[SO_2]}\,[SO_2Cl_2] \qquad (9.1)$$

except for the J dependency of the reverse rate were observed experimentally. The reverse rate was observed to be a function of the rate of light absorption, however, scatter in the experimental data made it impossible to differentiate between a half-power J dependency and some other J dependency, e.g., a first power dependency.

There is both theoretical and experimental support for the half-power J dependence. In their investigation of the photochemical decomposition of sulfuryl chloride, Schumacher and Schott[7] definitely observed that the reaction rate was proportional to $\sqrt{J}$. Theoretically all postulated mechanisms which led to a $\sqrt{(SO_2)}$ term in the denominator of the reverse rate also led to a $\sqrt{J}$ term in the numerator of the reverse rate.

Earlier calculations suggest an effective activation energy of 13.6 kcal/gmol for the reverse rate while Schumacher and Schott[7] experimentally observed an effective activation energy for the decomposition reaction of 18 kcal, the effective activation energy observed during this investigation is, however, -2.6 kcal/gmol.

There are at least four possible explanations for this anomaly:

1. Serious errors in the thermodynamic values used to calculate the effective activation energy and correspondingly serious errors in the experimental observations made by Schumacher and Schott.

2. Serious errors in the experimental observations made during this investigation.

3. The actual reaction does not proceed according to the postulated reaction mechanism.

4. The Bodenstein stationary state hypothesis was not valid due to the short residence times and high light intensities encountered during this investigation.

Sufficient confidence is attached to the thermodynamic quantities and experimental data presented in this report and to the data reported by Schumacher and Schott to conclude that 1 and 2 do not explain the anomalous behavior which was observed.

Many possible reaction mechanisms were considered during this investigation. The only mechanism evaluated which was thermodynamically feasible and which led to the rate expression which was observed experimentally is the reaction scheme discussed in Section 4.4. It would be presumptious to say that all other mechanisms have been disproven, however, it is valid to state that of all the mechanisms considered the scheme suggested in Section 4.4 is the most plausible.

The most likely explanation for the anomaly is that in the present work the Bodenstein stationary state hypothesis was not valid due to short residence times and high light intensities whereas in the work by Schumacher and Schott longer reaction times and lower light intensities met the necessary conditions for the application of the stationary state hypothesis.

Szabó, Bérces, and Huhn[29,30] report that the thermal decomposition of sulfuryl chloride is described by a nonstationary state reaction

mechanism. They report that there was a 0.9- to 12-min induction period during which the Bodenstein assumption was not valid.

Thus, in qualitative terms, it is reasonable to assume that the anomalous behavior is attributable to 4. This statement is of a somewhat speculative nature. The type, quantity, and quality of experimental data necessary to either prove or disprove this statement is beyond the scope of this investigation.

10. SUMMARY AND CONCLUSIONS

The parameters affecting the photochemical chlorination of sulfur dioxide were studied experimentally in a flow system utilizing a plasma light source as a source of ultraviolet radiation.

The spectral radiance of the light source was characterized as a function of arc gas flowrate, power input to the arc, and position in the arc. The pressure in the arc of the light source was 1.0 atm. For power inputs of 3.84 and 8.45 kw there were, respectively, 0.314 and 0.862 gmol equivalents of photons emitted per hour in the 2500 to 5000 Å wavelength region.

The spectral radiance of the light source was not dependent upon the flowrate of the argon arc gas. It was, however, dependent upon position along the arc with the maximum spectral output occurring near the cathode. The position dependence was most pronounced at lower power inputs to the arc.

The photochemical reaction, for light in the wavelength region 2500 to 5000 Å, was observed to proceed according to the rate expression:

$$\frac{d[SO_2Cl_2]}{dt} = J - k_o e^{-\frac{E}{RT}\sqrt{J/[SO_2]}}[SO_2Cl_2] \qquad (10.1)$$

where J was the volumetric rate of light absorption.

The pre-exponential rate constant k_o and a value of 0.0542 $(sec)^{-1/2}$. The effective activation energy for the reverse reaction E was -2.6 kcal/gmol. This value differs drastically from the corresponding value of 18 kcal/gmol which was observed by previous investigators.

When sulfur dioxide absorbed light, the electronically excited molecule is deactivated by collision with chlorine molecules according to the reaction process:

$$SO_2 + h\nu \rightarrow SO_2^* \qquad (10.2)$$

$$SO_2^* + Cl_2 \rightarrow SO_2 + Cl\cdot + Cl\cdot \qquad (10.3)$$

The quantum yield for the forward reaction, within the limits of experimental error, was 1.0 molecules of sulfuryl chloride formed per photon of light absorbed.

Information reported in the literature, private communications with other workers in related research areas, and observations made during this investigation suggest definite possibilities for the plasma light source for both research and commercial applications.

Although, during this investigation only about 20% of the electrical energy was converted to light, it is felt that with more efficient second generation plasma light sources this figure might well exceed 90%, with 50% of the light in the 2000 to 5000 Å wavelength region.

The availability of large quantities of relatively inexpensive, high-intensity ultraviolet light is a significant advance in the technology of photochemistry. Photochemical processes which previously were not of commercial interest utilizing standard radiation sources may now merit further investigation.

Shortcomings which must be considered when applying the plasma light source to specific problems include the experimental difficulties and the presence of continuum radiation. Experience has shown that when high electrical power levels and light intensities are involved small variations in design can have a profound influence on the performance of equipment. Under the extreme conditions of current, voltage, light intensity, pressure and temperature which are inherent to the efficient operation of plasma light sources, there is no such thing as a minor equipment malfunction.

None of the experimental problems are of a nature that they may not be overcome by a combination of improved design and practical experience. Obtaining practical experience, however, can be an expensive undertaking.

The presence of continuum radiation can frequently mean that not only the reactants but also the products will absorb radiation. This can cause either secondary reactions involving the desired products or possibly decomposition of the products. During this investigation the undesirable portion of the continuous spectra was eliminated by using selective aqueous inorganic filter solutions. This technique may be of general applicability.

APPENDIX I

CALIBRATION OF SPECTROGRAPHIC EQUIPMENT

In order to calibrate the photomultiplier tube and the optical system standard sources whose spectral radiances were calculable were observed spectrographically. The current output of the photomultiplier tube as a function of wavelength was then compared with the spectral radiance of the standard source. This ratio $R(\lambda)$ represented the spectral-response characteristic function for the photomultiplier tube, electronic circuit and the optical system.

For wavelenths longer than 3000 Å, the calibration was made by using a ribbon filament tungsten lamp as the standard source. The lamp was positioned so that its rays followed the same optical path as those from the light source and so that the spectrograph slit subtended the same solid angle of radiation from either source.

A 6-volt, 108-watt filament lamp manufactured by the General Electric Company was used for the calibration. Power for the lamp was supplied by a 6-volt transformer connected in series with a Variac and a Sola 118-volt constant voltage transformer.

The apparent temperature of the tungsten ribbon was measured with a calibrated Leeds and Northrup disappearing filament optical pyrometer. The true temperature of the filament was calculated from the apparent temperature by using DeVos's values for the emissivity of tungsten,[33]

the transmittance of the pyrex glass lamp envelope,[34] and an estimate of reflection.

During calibration procedures the ribbon filament operated at a true temperature of 2636°K. With the temperature known, Planck's radiation law and values for the emissivity of tungsten were used to calculate the spectral radiance of the tungsten filament.

For wavelengths below 3000 Å, the photomultiplier tube circuit was calibrated by spectrographically observing the continuous spectrum of the hydrogen lamp from a Beckman DU spectrophotometer.

The spectral radiance of a hydrogen lamp is determined solely by the temperature of the emitting hydrogen plasma. The spectral radiance is given by[35]:

$$I_\lambda = K\lambda^{-1} \exp(-c_2/\lambda T) \qquad (I.1)$$

with K being a proportionally constant.

In order to determine the temperature of the hydrogen lamp, the above equation was rewritten:

$$\lambda I_\lambda = K \exp(-c_2/\lambda T) \qquad (I.2)$$

and logarithms were taken of both sides:

$$\log(\lambda I_\lambda) = \log K - c_2/\lambda T \qquad (I.3)$$

A semilog plot of λI_λ vs. $1/\lambda$ for the wavelength region calibrated with the tungsten filament had a slope of c_2/T from which the temperature

of the hydrogen plasma was calculated. The technique is demonstrated in Fig. 57.

With the temperature of the hydrogen known, the proportionality constant K was evaluated and the continuous spectrum of the hydrogen lamp used to calibrate the photomultiplier tube over the wavelength region 2000 to 3000 Å.

A plot of the normalized inverse of the spectral-response characteristic function, $R(\lambda)$, is presented in Fig. 58.

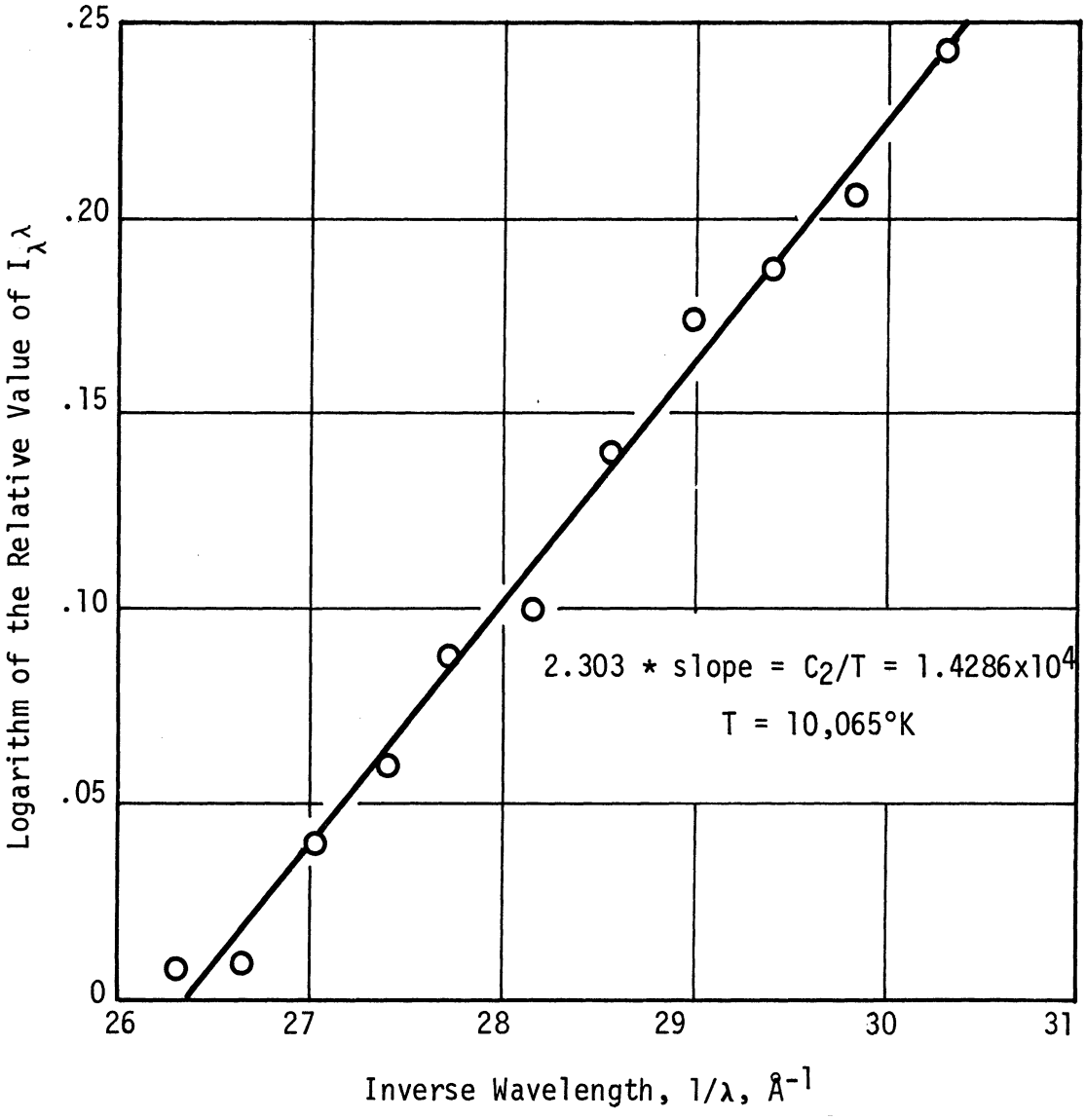

Fig. 57. Evaluation of hydrogen lamp gas temperature.

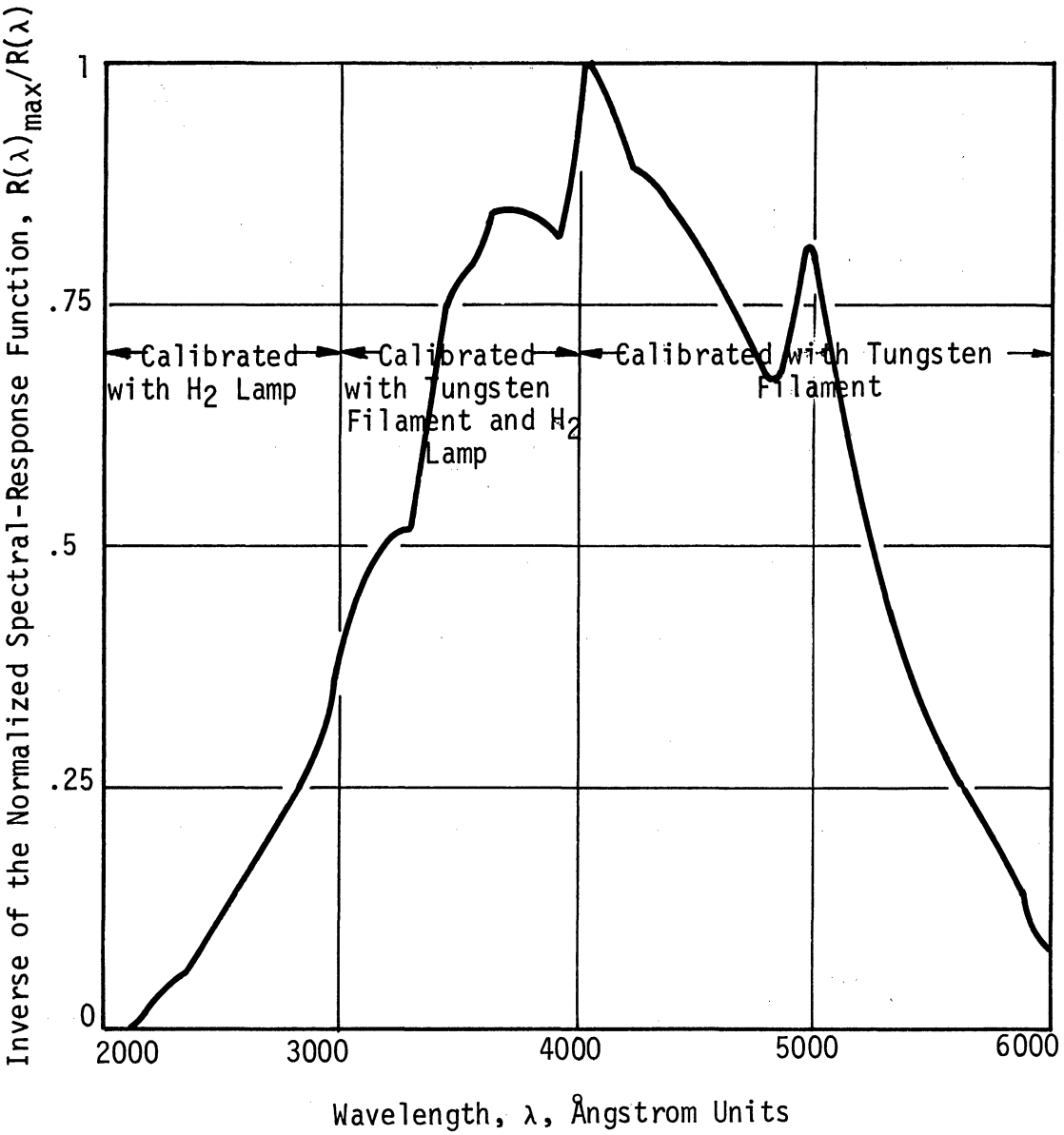

Fig. 58. Normalized sensitivity of the photomultiplier circuit as a function of wavelength.

APPENDIX II

LINE SOURCE APPROXIMATION

A considerable simplification in calculations was effected by assuming that the arc column could be represented as a linear radiation source rather than considering it as an extended source.

A partial justification for this assumption can be obtained by considering the scheme shown in Fig. 59. A transparent radiating cylinder of gas having a length, L, and a radius, R_o, is aligned on a common axis with an infinitely long second cylinder of radius R_1. The radiating cylinder is characterized by a constant value E representing the radiation-emission rate from the gas per unit of volume in all directions from a small volume element of the cylinder.

The amount of light emitted by a small volume element of the radiating gas which passes through a small area of the larger cylinder can be shown to be:

$$\frac{E \cdot R_1}{4\pi} \cdot \frac{(R_1 - r\cos(\theta-\phi)) \cdot r\,d\phi\,dr\,dx\,d\theta\,dy}{((x-y)^2+R_1^2+r^2-2rR_1\cos(\theta-\phi))^{3/2}} \qquad \text{(II.1)}$$

Integrating over the various dimensions yields the total radiation passing through the outer cylinder per unit of axial length:

$$\frac{E \cdot R_1}{4\pi} \int_{-L/2}^{L/2} dx \int_{o}^{R_o} r\,dr \int_{o}^{2\pi} d\theta \int_{o}^{2\pi} \frac{(R_1 - r\cos(\theta-\phi))\,d\phi}{((x-y)^2+R_1^2+r^2-2R_1\cos(\theta-\phi))^{3/2}} \qquad \text{(II.2)}$$

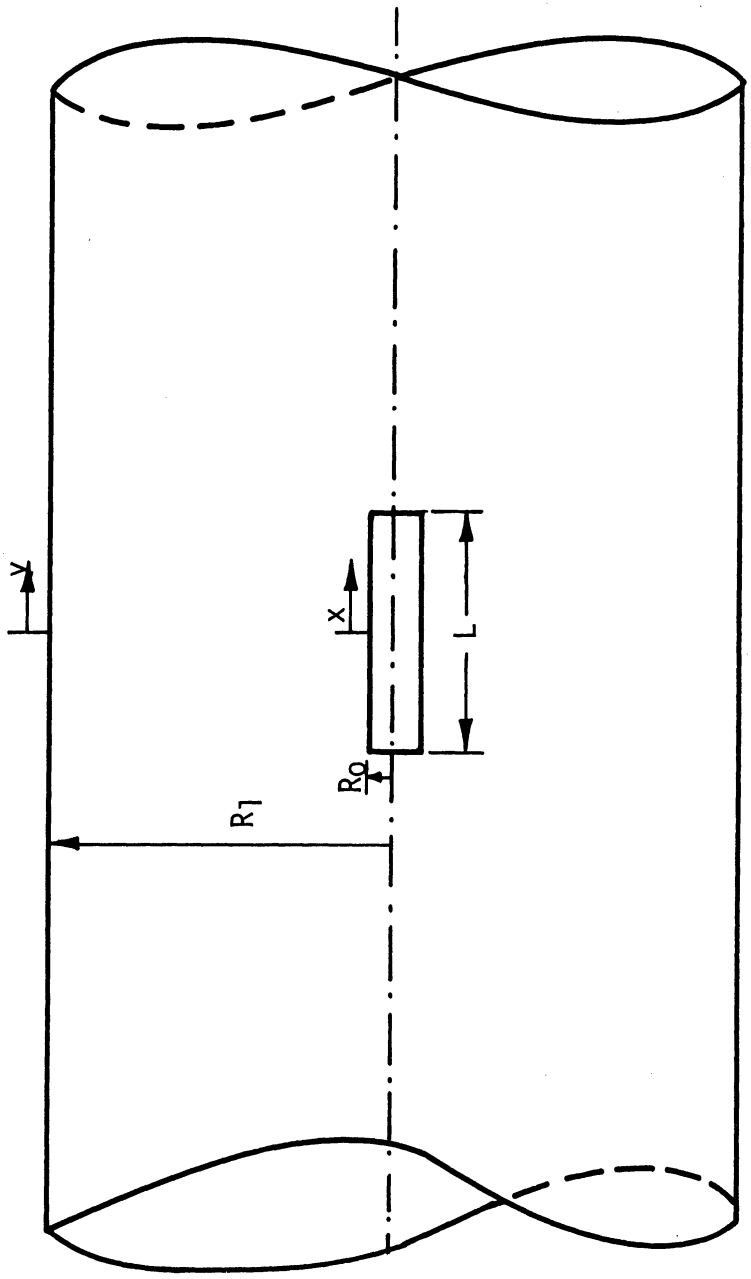

Fig. 59. Schematic diagram of an extended radiation source.

A standard table of integrals permits integration of quantity (II.2) over the range of the variable x; this yields:

$$\frac{E\cdot R}{4\pi}\int_0^{R_o}\int_0^{2\pi}\int_0^{2\pi}\frac{(R_1-r\cos(\theta-\phi))}{(R_1^2+r^2-2rR_1\cos(\theta-\phi))}\left\{\frac{(\frac{L}{2}-y)}{((\frac{L}{2}-y)^2+R_1^2+r^2-2rR_1\cos(\theta-\phi))^{1/2}}\right.$$

$$\left.(x)\frac{(\frac{L}{2}+y)}{((\frac{L}{2}+y)^2+R_1^2+r^2-2rR_1\cos(\theta-\phi))^{1/2}}\right\}rdrd\theta d\phi \qquad (II.3)$$

Now consider a similar situation with a radiating line of length L replacing the radiating cylinder. It is assumed that the total emissions by both sources are equal, that is, $\pi R_o^2 E$ is the radiation-emission rate from the source per unit of length in all directions from a small element of the line. The amount of light emitted by a linear increment of the line which passes through a small area of the outer cylinder is:

$$\pi R_o^2 E\cdot\frac{R_1^2 d\theta dydx}{4\pi((x-y)^2+R_1^2)^{3/2}} \qquad (II.4)$$

Integrating over the x and θ dependencies yields the total radiation passing through the outer cylinder per unit of axial length:

$$\frac{\pi R_o^2 E}{2}\left(\frac{(\frac{L}{2}-y)}{((\frac{L}{2}-y)^2+R_1^2)^{1/2}}+\frac{(\frac{L}{2}-y)}{((\frac{L}{2}+y)^2+R_1^2)^{1/2}}\right) \qquad (II.5)$$

The values of quantity (II.2) and quantity (II.5) can now be compared. If it can be shown that the integrand of (II.2) is only a weak function of r and $(\theta-\phi)$, i.e., is only a function of R_1, it can readily be seen that the light distribution resulting from the line source as-

sumption is exactly that resulting from the more rigorous assumption of an extended source.

In order to investigate these dependencies the following parameter values, characteristic of the light source used in this investigation, were assumed:

$$\begin{aligned} R_o &= 0.15 \text{ cm} \\ L &= 2.41 \text{ cm} \\ R_1 &= 3.63 \text{ cm} \end{aligned} \qquad \text{(II.6)}$$

Using these values in the calculations, the value of the integrand of (II.2) was computed at various points in the functional plane ($0 \leq (\theta-\phi) \leq 2\pi$, $0 \leq r \leq R_o$). The numerical investigation indicated that the integrand varied by less than ±3% from the line source approximation for arbitrary points in the plane. It is felt that for the values of the parameters indicated in (II.6), the error involved in equating quantity (II.2) with quantity (II.5) is less than 1%.

APPENDIX III

THERMODYNAMIC CONSIDERATIONS

In order to be able to discuss the various intermediate reactions which have been suggested for the photochemical formation and decomposition of sulfuryl chloride, it is of value to consider the energetics of the individual reactions involved.

Of primary interest is the heat of dissociation of the sulfur-chlorine bonds in sulfuryl chloride. No definitive determination of this value is at present available in the literature. It is possible, however, to estimate a reasonable value of the bond energy by using available information.

One method for deducing the sulfur-chlorine bond energy is to first calculate the total bond energy of sulfuryl chloride and subtract from this quantity the energy associated with the sulfur-oxygen bonds. The resulting quantity is twice the bond dissociation energy of the sulfur-chlorine bond.

The heat of reaction at 0°K for the chlorination of sulfur dioxide, as determined by Londergan,[8] is 12.795 kcal/gmol. Coupling this value with the heats of formation of sulfur dioxide and chlorine[36-38] at 0°K from the monatomic gaseous elements, the total bond energy of sulfuryl chloride is calculated to be 424.3±1 kcal/gmol.

The sulfur-oxygen bonds in sulfuryl chloride have been studied spectrographically by Samuel[39-41] who reports a bond dissociation en-

ergy of 108.6 kcal/mol. Since the two sulfur-oxygen bonds account for 217.2 kcal/mol, this indicates that the bond dissociation energy for the sulfur-chlorine bonds in sulfuryl chloride is 53.5 kcal/gmol.

Due to a lack of confidence in the sulfur-oxygen bond energy reported by Samuel, an uncertainty estimate of ±5 kcal/gmol is attributed to this value.

A second method for deducing the sulfur-chlorine bond energy is to consider the thermal decomposition of sulfuryl chloride. The primary step in the decomposition reaction is believed to involve unimolecular fission of the sulfur-chlorine bond in sulfuryl chloride. For such a case the activation energy of the primary step is a lower limit for the bond energy. (see Benson,[12] Chapter XI).

The thermal decomposition of sulfuryl chloride was studied first by Smith,[42] and somewhat later by Szabó and Bérces.[31,32] Although each suggests a completely different scheme for the reaction mechanism, there is reasonable agreement between the observed activation energies. Smith, studying the decomposition reaction in the temperature range 279 to 329°C, observed activation energies in the range 46.4 to 55.7 kcal/gmol, while Szabó and Bérces for experiments in the temperature range 275 to 350°C report an activation energy of 46.6 kcal/gmol.

A third means of estimating the sulfur-chlorine bond energy in sulfuryl chloride is to make the assumption that it is equal to the sulfur-chlorine bond energy as determined for other molecules. Samuel[39-41] has spectrographically determined the sulfur-chlorine bond dissociation

energy, D_o^o, for the compounds listed below:

TABLE VI

SULFUR-CHLORINE BOND ENERGIES FOR VARIOUS MOLECULES

Compound	Bond Energy (Kcal/gmol)
SCl	55.4
S_2Cl_2	52.0
SCl_2	52.0
$SOCl_2$	48.5

For purposes of this investigation the heat of reaction at 0°K, ΔH_o^o, for the reaction:

$$SO_2Cl_2 \rightarrow SO_2Cl\cdot + Cl\cdot \qquad \text{(III.1)}$$

will be assumed to be 52.0 kcal/gmol. The uncertainty in this value is estimated to be 3 kcal/gmol.

Assuming a pyramidal structure for the $SO_2Cl\cdot$ free radical,[16] statistical thermodynamics[42] permits the estimation of S_{298}^o and $(H_{298}^o - H_o^o)$. The calculated values are 66.56 entropy units and 3.71 kilocalories/gram-mole.

Using the above information, in conjunction with standard thermochemical tables,[36-38] it is possible to tabulate the thermodynamic quantities associated with each of the intermediate reactions which have been postulated.

TABLE VII

ENERGETICS OF THE INDIVIDUAL INTERMEDIATE REACTIONS

Reaction	ΔH°_{0}	ΔH°_{298}	ΔS°_{298}	ΔG°_{298}
(1) $Cl_2 = Cl\cdot + Cl\cdot$	57.04	57.84	25.63	50.20
(2) $SO_2 + Cl\cdot = SO_2Cl\cdot$	-17.8	-16.1	-32.2	- 6.5
(3) $SO_2Cl\cdot + Cl\cdot = SO_2Cl_2$	-52.0	-55.4	-31.6	-46.0
(4) $SO_2Cl_2+Cl\cdot = SO_2Cl\cdot+Cl_2$	- 5.0	- 2.5	5.9	- 4.2
(5) $SO_2 + Cl_2 = SO_2Cl_2$	-12.8	-13.67	-38.14	- 2.29

APPENDIX IV

PRODUCT ANALYSIS

The product mixture of sulfur dioxide, chlorine, and sulfuryl chloride was analyzed utilizing the infrared absorption properties of sulfur dioxide and sulfuryl chloride.

Sulfur dioxide has an infrared absorption peak at 4.00 μ while sulfuryl chloride absorbs strongly at 7.05 μ. Neither sulfuryl chloride nor chlorine absorbs appreciably at 4.00 μ, however, a strong sulfur dioxide absorption peak centered at 7.4 μ partially overlaps the sulfuryl chloride peak and its absorption at 7.05 μ had to be considered in the calculations.

The infrared spectrophotometer was calibrated at 4.00 μ by measuring the optical density of samples of sulfur dioxide as a function of the pressure of sulfur dioxide in the sample. The resulting information is plotted in Fig. 60. Similarly the optical density at 7.05 μ of various samples of sulfuryl chloride was measured as a function of the sulfuryl chloride sample pressure. Figure 61 shows the results of the sulfuryl chloride calibration.

The experimentally measured proportionality constant equating the optical density at 4.00 μ to the sulfur dioxide pressure was 8.39×10^{-3} $(\text{cm Hg})^{-1}$, while the equivalent factor for sulfuryl chloride at 7.05 μ was observed to be 0.489 $(\text{cm Hg})^{-1}$. The proportionality constant for sulfur dioxide absorption at 7.05 μ was 5.95×10^{-4} $(\text{cm Hg})^{-1}$.

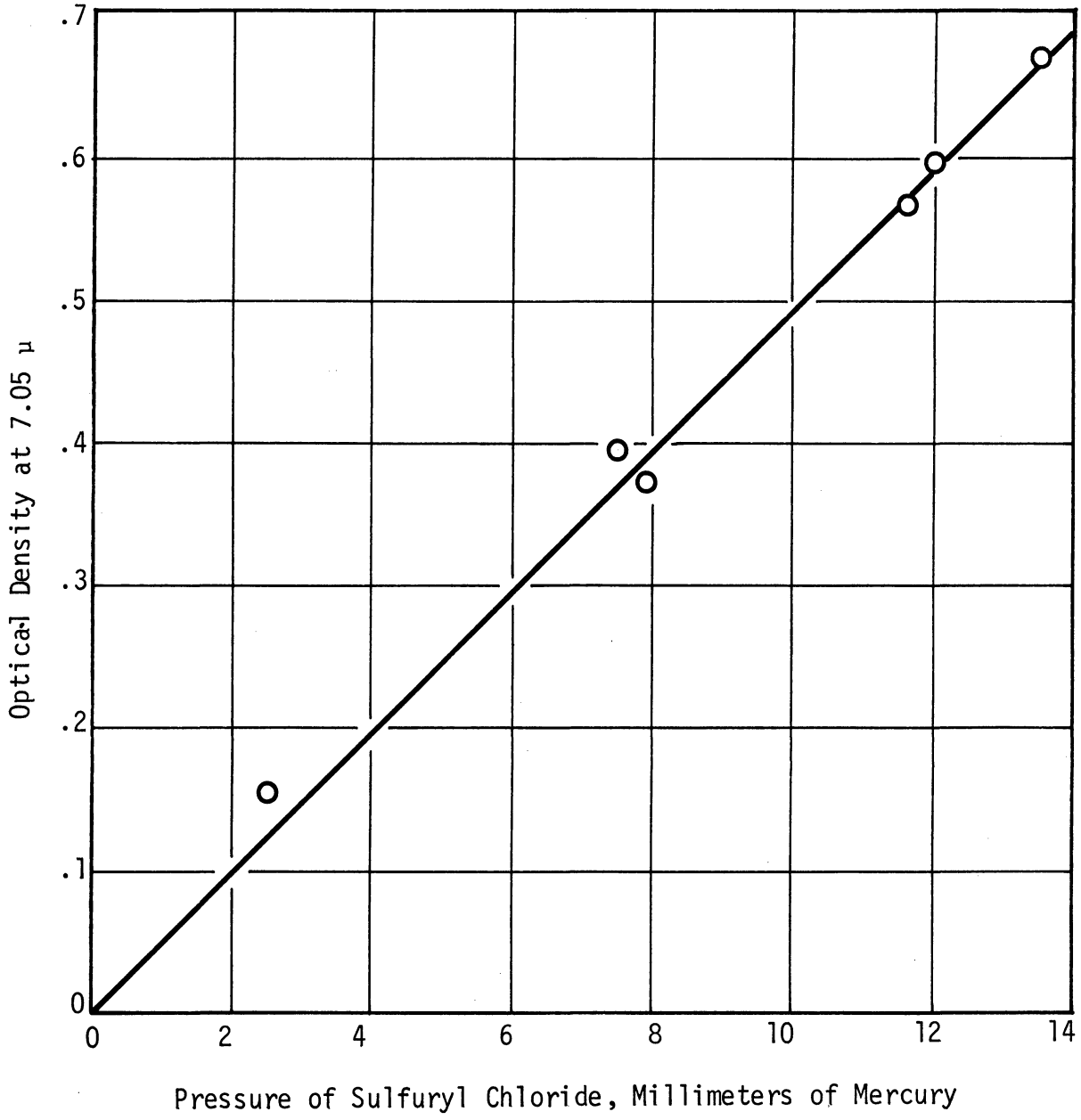

Fig. 60. Optical density at 7.05μ vs. the partial pressure of sulfuryl chloride in an infrared gas sample.

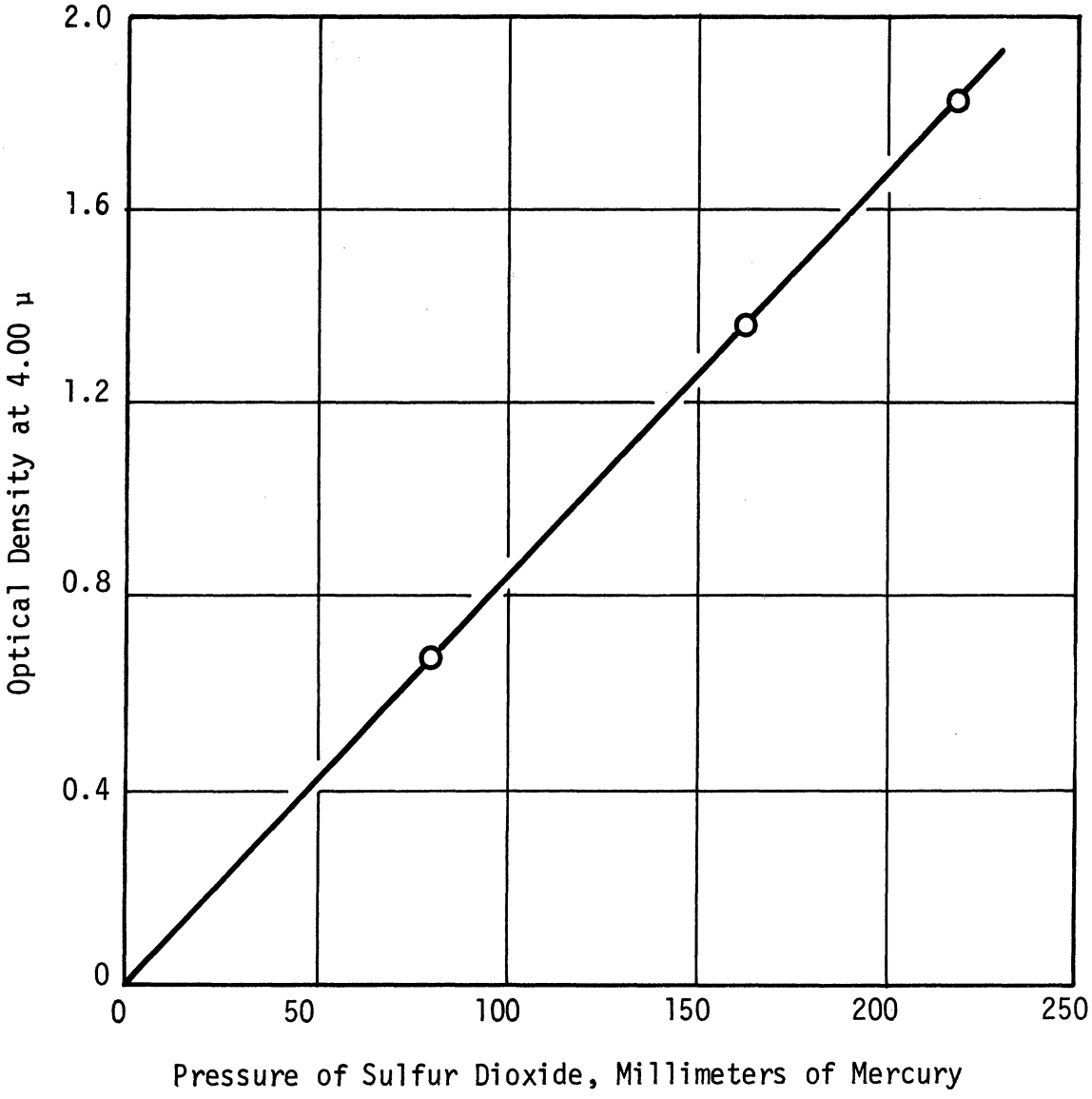

Fig. 61. Optical density at 4.00μ vs. the partial pressure of sulfur dioxide in an infrared gas sample.

The product gas stream was sampled periodically by flowing a portion of the stream through a pyrex glass vessel fitted with stopcocks. Using a vacuum manifold system, part of this gas sample was transferred from the glass vessel to an infrared gas analysis cell equipped with sodium chloride windows. An infrared spectrogram was then prepared of this portion of the sample. Such a spectrogram is shown in Fig. 62.

Using the proportionality constants indicated above and the measured optical densities at 4.00 and 7.05 μ, such spectrograms were used to evaluate the ratio of sulfuryl chloride to sulfur dioxide concentration for each sample. This value and a knowledge of the composition and total flowrate of the reactants feed stream allowed calculation of the percentage conversion to and the rate of production of sulfuryl chloride.

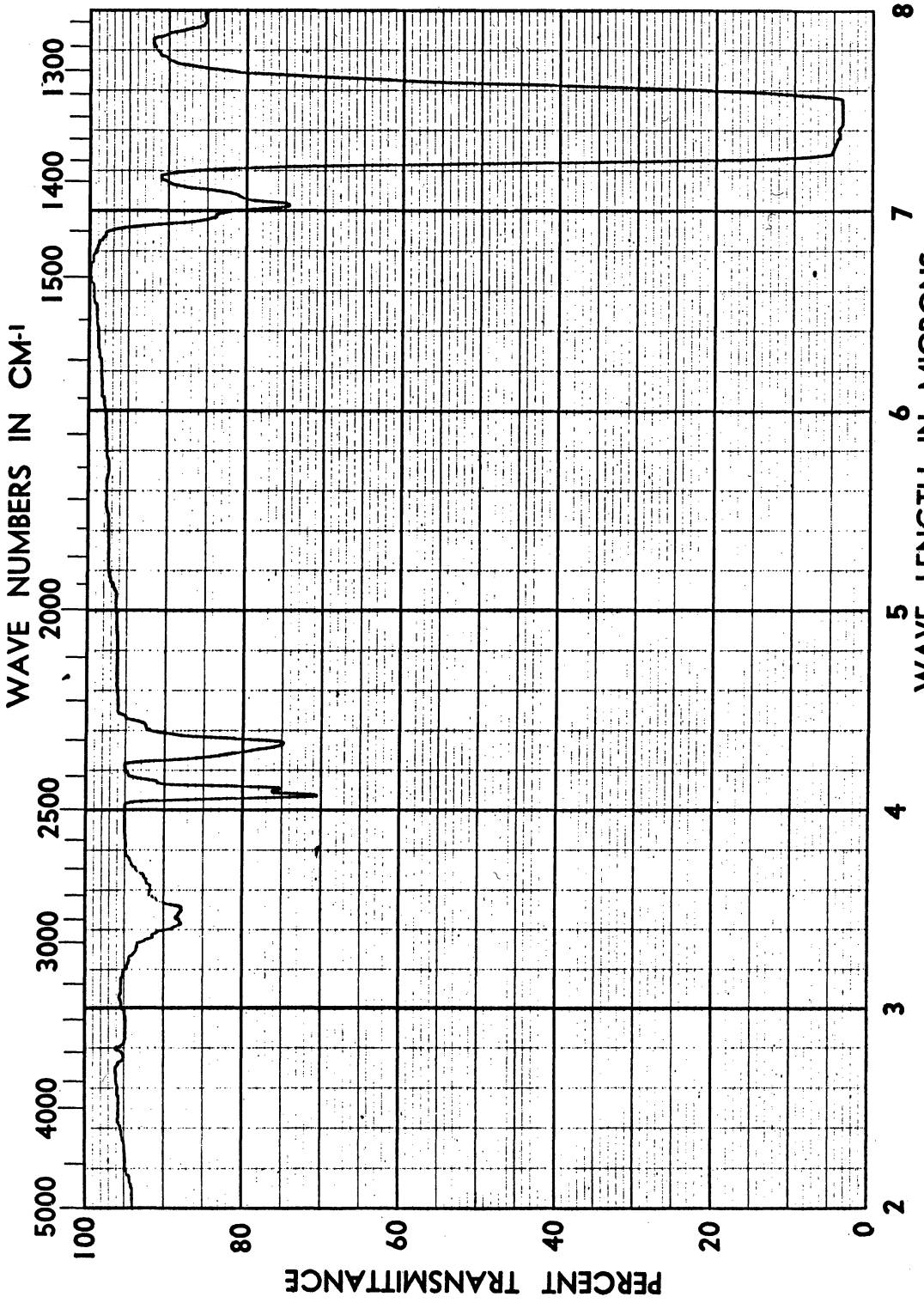

Fig. 62. Typical infrared spectrogram of the product stream.

APPENDIX V

METHODS FOR ANALYZING EXPERIMENTAL DATA

V.1 DIFFERENTIAL METHOD OF ANALYSIS

Assuming plug flow, the design equation for the photochemical reactor is given by:

$$\left(\frac{\partial x}{\partial z}\right)_{G_o} = \frac{(1+a)Ar}{G_o} \qquad (V.1)$$

The differential method of data analysis assumes that changes in reactor length at constant molar flowrate are equivalent to changes in the inverse of the molar flowrate at constant reactor length. This can be expressed mathematically as:

$$\left(\frac{\partial x}{\partial (1/G_o)}\right)_z = (1+a)Azr \qquad (V.2)$$

In order to determine what restrictions are placed on the form of the rate of reaction by the assumptions inherent in the differential method of data analysis, consider the mixed partial derivatives:

$$\frac{\partial^2 x}{\partial z(1/G_o)} = (1+a)\left[r + \frac{1}{G_o}\frac{\partial r}{\partial (1/G_o)}\right] \qquad (V.3)$$

$$\frac{\partial^2 x}{\partial (1/G_o)\partial z} = (1+a)A\left[r + z\frac{\partial r}{\partial z}\right] \qquad (V.4)$$

Equating the expressions for the mixed partial derivatives indicates that the differential method of data analysis assumes the following about the rate of reaction:

$$\frac{1}{G_o}\frac{\partial r}{\partial(1/G_o)} = z\frac{\partial r}{\partial z} \qquad (V.5)$$

In general this expression is valid if and only if the rate is independent of molar flowrate and position, or if the rate of reaction is a function only of the ratio of reactor length to molar flowrate, z/G_o.

For the photochemical reactor considered in this report, it is valid to assume that the light intensity enters into the rate expression. Since the light intensity is unrelated to the inverse molar flowrate and is a function only of position, it is unreasonable to expect that the rate will be of the form:

$$r = r(z/G_o) \qquad (V.6)$$

This shows that differentiation of the exit conversion versus inverse molar flowrate data is not a valid method of data analysis for this investigation.

V.2 INTEGRAL METHOD OF ANALYSIS

The alternative to the differential method of data analysis is known as the integral method. In the integral approach, a rate equation is assumed, and then the design expression is integrated over the length of the reactor. This integration yields a relationship between the exit conversion and the reciprocal flowrate, which may then be compared with the experimental data. The final step is the choice of the rate equation which gives the best agreement with the experimentally

determined curves off exit conversion versus reciprocal flowrate for all combinations of reactants ratios, inlet temperature, dye solution, and pressure. This is the approach which was used in the development described earlier in this report.

APPENDIX VI

EXPERIMENTAL DATA

TABLE VIII

DATA SETS NOS. 1-8

Data Set No. 1

Reaction System: Reactants inlet temperature = room temperature (approx. 25°C)
Dye solution = .05N potassium iodide
Reactor pressure = 1.0 atm
Argon diluent pressure = 0.0 atm
Power input to arc = 3.84 kw

Molar Feed Rate (gmol/hr)	Composition: $\frac{2}{3}$ Cl_2, $\frac{1}{3}$ SO_2		Composition: $\frac{1}{2}$ Cl_2, $\frac{1}{2}$ SO_2		Composition: $\frac{1}{3}$ Cl_2, $\frac{2}{3}$ SO_2	
	Exit Conversion (%)	Rate of SO_2Cl_2 Production (gmol/hr)	Exit Converstion (%)	Rate of SO_2Cl_2 Production (gmol/hr)	Exit Conversion (%)	Rate of SO_2Cl_2 Production (gmol/hr)
12.0	1.53	.0611	1.01	.0605	.66	.0532
6.0	2.31	.0463	1.64	.0492	1.11	.0449
4.0	2.96	.0395	1.94	.0388	1.40	.0372
3.0	3.42	.0342	2.39	.0359	1.76	.0352
2.4	4.26	.0341	2.90	.0348	2.04	.0327
2.0	4.91	.0327	3.55	.0355	2.50	.0334

Data Set No. 2

Reaction System: Dye solution = 1.5N potassium nitrate
Reactor pressure = 1.0 atm
Argon diluent pressure = 0.0 atm
Sulfur dioxide pressure = 0.5 atm
Chlorine pressure = 0.5 atm
Power input to arc = 3.84
Molar feed rate = 8.0 gmol/hr

Inlet Temperature (°C)	Exit Conversion (%)	Rate of SO_2Cl_2 Production (gmol/hr)
25.1	1.04	.0415
26.0	.96	.0383
26.3	.98	.0394
26.4	.96	.0384
26.8	.97	.0387
27.1	.99	.0394
29.1	.99	.0397
33.4	.91	.0363
35.1	.88	.0353
35.1	.87	.0347
36.1	.89	.0357
36.2	.87	.0347
36.3	.85	.0341
41.4	.85	.0341
41.4	.85	.0339
41.5	.77	.0307
41.5	.87	.0349
41.7	.91	.0363

Data Set No. 3

Reaction System: Dye solution = 1.5N potassium nitrate
Reactants inlet temperature = room temperature
Sulfur dioxide pressure = 0.5 atm
Chlorine pressure = 0.5 atm
Power to arc = 3.84 kw

Molar Feed Rate (gmol/hr)	Reactor Pressure (atm)	Argon Diluent Pressure (atm)	Exit Conversion (%)	Rate of SO_2Cl_2 Production (gmol/hr)
2.25	1.5	.5	2.90	.0218
2.25	1.5	.5	2.96	.0222
3.0	2.0	1.0	2.74	.0206
3.0	2.0	1.0	2.41	.0181
3.0	2.0	1.0	2.38	.0179
4.0	2.0	1.0	2.29	.0229
4.0	2.0	1.0	2.24	.0224
6.0	2.0	1.0	1.79	.0268
6.0	2.0	1.0	1.57	.0235
12.0	2.0	1.0	1.14	.0342
12.0	2.0	1.0	1.12	.0337

Data Set No. 4

Reaction System: Dye solution = 1.5N potassium nitrate
Reactants inlet temperature = room temperature
Reactor pressure = 1.0 atm
Argon diluent pressure = 0.0 atm
Sulfur dioxide pressure = 0.5 atm
Chlorine pressure = 0.5 atm
Power input to arc = 3.84 kw

Molar Flowrate (gmol/hr)	Exit Conversion (%)	Rate of SO_2Cl_2 Production (gmol/hr)
12.0	.76	.0457
6.0	1.16	.0348
6.0	1.03	.0309
4.0	1.47	.0293
3.0	1.64	.0246
3.0	1.85	.0277
2.0	2.31	.0231
1.5	2.56	.0192
1.5	2.84	.0213
1.5	2.98	.0224

Date Set No. 5

Reaction System: Dye solution = 1.5N potassium nitrate
Reactor pressure = 1.0 atm
Argon diluent pressure = 0.0 atm
Sulfur dioxide pressure = 0.5 atm
Chlorine pressure = 0.5 atm
Power input to arc = 3.84 kw

Molar Feed Rate (gmol/hr)	Inlet Temperature (°C)	Exit Conversion (%)	Rate of SO_2Cl_2 Production (gmol/hr)
1.0	15.4	3.52	.0176
1.0	15.4	3.28	.0164
1.0	15.5	2.49	.0124
1.0	24.8	3.40	.0170
1.0	25.9	3.78	.0189
1.0	26.5	3.85	.0192
1.0	32.4	3.34	.0167
1.0	32.7	3.90	.0195
1.0	33.0	3.93	.0197
8.0	15.3	1.17	.0467
8.0	15.5	1.08	.0432
8.0	15.5	1.13	.0452
8.0	23.8	1.03	.0413
8.0	23.8	1.11	.0449
8.0	24.1	1.11	.0443
8.0	32.0	1.02	.0410
8.0	33.3	1.06	.0426
8.0	33.6	1.03	.0411

Data Set No. 6

Reaction System: Reactants inlet temperature = room temperature
Dye solution = 1.5N potassium nitrate
Reactor pressure = 1.0 atm
Argon diluent pressure = 0.0 atm
Sulfur dioxide pressure = 2/3 atm
Chlorine pressure = 1/3 atm
Power input to arc = 3.84 kw

Molar Feed Rate (gmol/hr)	Exit Conversion (%)	Rate of SO_2Cl_2 Production (gmol/hr)
6.0	.94	.0377
6.0	.79	.0316
3.75	.99	.0248
3.0	1.39	.0278
3.0	1.19	.0239
2.73	1.33	.0241
2.4	1.48	.0236
2.14	1.38	.0198
1.76	1.60	.0188
1.5	2.12	.0212
1.5	1.97	.0201

Data Set No. 7

Reaction System: Reactants inlet temperature = room temperature
Dye solution = 1.5N potassium nitrate
Reactor pressure = 1.0 atm
Argon diluent pressure = 1/2 atm
Sulfur dioxide pressure = 1/6 atm
Chlorine pressure = 1/3 atm
Power input to arc = 3.84 kw

Molar Feed Rate (gmol/hr)	Exit Conversion (%)	Rate of SO_2Cl_2 Production (gmol/hr)
8.0	1.79	.0239
8.0	1.99	.0266
6.0	2.33	.0233
4.8	2.81	.0225
4.37	2.81	.0204
4.0	2.90	.0194
3.43	3.46	.0197
3.0	4.48	.0224
3.0	3.23	.0162
3.0	3.97	.0199
3.0	3.65	.0182

Data Set No. 8

Reaction System: Reactants inlet temperature = room temperature
Dye solution = 1.5N potassium nitrate
Reactor pressure = 1.0 atm
Chlorine pressure = 1/3 atm
Power input to arc = 3.84 kw

Molar Feed Rate (gmol/hr)	Argon Diluent Pressure (atm)	Sulfur Dioxide Pressure (atm)	Exit Conversion (%)	Rate of SO_2Cl_2 Production (gmol/hr)
12.0	.333	.333	.77	.0307
8.0	.167	.500	.89	.0355
4.36	.333	.333	1.54	.0336
3.0	.333	.333	1.96	.0294
3.0	.204	.463	1.86	.0258
3.0	.327	.340	2.13	.0218
3.0	.406	.261	3.22	.0252
3.0	.461	.206	3.60	.0222
3.0	.204	.463	1.64	.0227
3.0	.327	.340	2.14	.0218
3.0	.406	.261	2.52	.0197
3.0	.461	.206	3.04	.0188
2.67	.333	.333	2.44	.0217
1.5	.333	.333	3.16	.0158

NOMENCLATURE

A	area—cm^2
$A(\lambda)$	current output of photomultiplier—amp
$\bar{A}$	area per unit length—cm
c_p	heat capacity—cal/gmol-°C
c_2	second Planck constant—Å-°K
d	optical path length—cm
D	diffusion coefficient—cm^2/sec
D_o^o	bond dissociation energy--kcal/gmol
E	volumetric radiation emission rate
E	activation energy—kcal/gmol
G_o	molar feed rate--gmol/hr
G'	feed rate variable (def. by Eq. (8.13))—gmol/hr
G''	feed rate variable (def. by Eq. (8.17'))—gmol/hr-atm
H	enthalpy—Kcal/gmol
H_c	spectrographic slit height—cm
I, I_o	intensity of radiation
J	volumetric rate of light absorption—gmol/liter-hr
J_m	mean rate of light absorption—gmol/liter-hr
k_o	pre-exponential rate constant—$(sec)^{-1/2}$
$k, k', k'', k_2, k_2', k_1', k_3, k_4$	rate constants
K_2	equilibrium constant—liters/gmol

NOMENCLATURE (Continued)

k_m	mean rate constant
L	length—cm
M	spectrographic image magnification
P	pressure—atm
Q	spectral radiance—gmol/hr-cm-Å
r_w	effective thickness—cm
$R(\lambda)$	spectrographic calibration factor—gmol/hr-amp-cm^2-Å-ster
R	gas constant
r	reaction rate—gmol/liter-hr
R_o, R_1, r	radius--cm
S	entropy—e.u.
S	area—cm^2
T, T_o	temperature--°K-°C
W	rate of internal heat generation—cal/liter-hr
W_c, W	spectrographic slit width—cm
x	conversion—percent
x_{eff}	effective conversion (def. by Eq. (8.9))—percent
x_o	exit conversion—percent
x'	conversion variable (def. by Eq. (8.12))--percent
x'_{eff}	effective conversion variable (def. by Eq. (8.16))—percent
x''_{eff}	effective conversion variable (def. by Eq. (8.21))—percent

NOMENCLATURE (Concluded)

x	position—cm
y	position—cm
z	length—cm

Miscellaneous Symbol:

$(1+a)$	ratio of total concentration to sulfur dioxide concentration

Greek Symbols:

ϵ	molecular extinction coefficient—liters/gmol-cm
θ	angle—ster
λ	wavelength—Å
ν	wave number—cm^{-1}
Φ	quantum yield—molecules/photon
ϕ	angle—ster

REFERENCES

1. Papp, C. A., "Plasma and Photochemistry," Ind. Eng. Chem., 55, 48-9 (1963).

2. Papp, C. A., "Vortex Stabilized Radiation Source," Plasmadyne Corporation Report PRE-106, 1962.

3. Papp, C. A., "Plasma Technology in Chemical Processing," Chem. Eng. Prog., 59, No. 6, 51-3 (1963).

4. Anderson, J. E., R. C. Eschenbach, and H. H. Troue, "Performance Study of a Vortex-Stabilized Arc Radiation Source," Applied Optics, 4, 1435 (1965).

5. Regnault, V., Ann. Chim. Phys., 71, 445 (1839).

6. Regnault, V., J. Pr. Ch., 19, 243-4 (1840).

7. Schumacher, H. J. and C. Schott, "Die photochemische Bildung von Sulfurylchlorid in der Gasphase aus Schwefeldioxyd und Chlor und sein durch Chlor sensibilisierter Zerfall," Z. phys. Ch., 193, 343-66 (1944).

8. Londergan, M. C., "The Photochemistry of the Formation of Sulfuryl Chloride," Iowa State Coll. J. Sci., 17, 95-7 (1942-43).

9. Bonhoeffer, K. F., Z. Phys., 13, 94-105 (1923).

10. LeBlanc, M., K. Andrich, and W. Kangro, Z. Elektroch., 25, 229-51 (1919).

11. Trautz, M., Z. Elektroch., 21, 329-42 (1915).

12. Benson, S. W., The Foundations of Chemical Kinetics, McGraw-Hill Book Co., Inc., New York, 1960.

13. Chiltz, G., R. Eckling, P. Goldfinger, G. Huybrechts, G. Martins, and G. Simoens, Bull. Soc. Chim. Belg., 71, 747-58 (1962).

14. Bader, L. W. and E. A. Ogryzlo, "Recombination of Chlorine Atoms," Nature, 201, (4918), 491-2 (1964).

15. Taylor, H. S., A Treatise on Physical Chemistry, D. Van Nostrand Co., Inc., New York, 1924.

REFERENCES (Continued)

16. Walsh, A. D., "The Electronic Orbitals, Shapes, and Spectra of Polyatomic Molecules," J. Chem. Soc., 2260-2331 (1953).

17. Mulliken, R. S., Rev. Mod. Phys., 14, 204 (1942).

18. Calvert, J. G. and J. N. Pitts, Photochemistry, John Wiley and Sons, New York, 1966.

19. von Halban, H. and K. Siedentopf, Z. Phys. Chem., 103, 71-90 (1922).

20. von Halban, H. and K. Siedentopf, Z. Elektrochem., 28, 496-9 (1922).

21. Jones, F. W. and W. Spooner, Trans. Far. Soc., 31, 811-3 (1935).

22. Aickin, R. G. and N. S. Bayliss, Trans. Far. Soc., 31, 811-3 (1935).

23. Gibson, G. E. and N. S. Bayliss, Phys. Rev., 44, 188 (1933).

24. Dignam, M. J. and D. J. Leroy, J. Chem. Phys., 26, 964-5 (1957).

25. Goldfinger, P., M. Heunehomme, and G. Martens, J. Chem. Phys., 29, 456-8 (1958).

26. Noyes, R. M., J. Am. Chem. Soc., 73, 3039 (1951).

27. McAdams, W. H., Heat Transmission, McGraw-Hill Book Co., Inc., New York, 1954.

28. Darmois, J., Comptess Rendus, 223, 616-18, 663-5 (1946).

29. Villars, D. S., J. Am. Chem. Soc., 49, 326 (1927).

30. Jortner, J., R. Levine, M. Ottolenghi, and G. Stein, J. Phys. Chem., 65, 1232 (1961).

31. Szabó, Z. G. and T. Bérces, "Der Mechanismus des thermischen Zerfalls von Sulfurylchlorid," Z. für Phys. Chem., 12, 168-95 (1957).

32. Szabó, Z. G., T. Bérces, and P. Huhn, "Vollständige kinetische Analyse des Mechanismus des thermischen Sulfurylchloridzerfalls," Z. für Phys. Chem., 23, 70-83 (1960).

33. DeVos, J. C., Physics, 20, 690 (1954).

REFERENCES (Concluded)

34. Engelhard Industries, "Optical Fused Quartz," Brochure No. 6583N-Ex.

35. Griem, H. R., Plasma Spectroscopy, McGraw-Hill Book Co., Inc., New York, 1964.

36. U.S. National Bureau of Standards, "Selected Values of Chemical Thermodynamic Properties," Circular 500 (1952).

37. U.S. National Bureau of Standards, "Tables of Thermal Properties of Gases," Circular 564 (1955).

38. Dow Chemical Company, JANAF Thermochemical Tables, ARPA Proj. AF 04(611)-7554, Midland, Michigan (1965).

39. Samuel, R. and R. K. Asundi, Pr. Phys. Soc., 48, 28-34 (1936).

40. Samuel, R. and R. K. Asundi, Rev. Modern Phys., 18, 103-47 (1946).

41. Samuel, R. and L. Lorenz, Z. Phys. Ch., B14, 219-31 (1931).

42. Smith, D. F., J. Am. Chem. Soc., 47, 1862-75 (1925).

43. Howerton, M. T., Engineering Thermodynamics, Van Nostrand Co., Inc., New York, 1962.